Sorption Modelling of Np(IV), Np(V), and Pd(II) on Illite and Montmorillonite Under High Ionic Strength Conditions

SORPTION MODELLING OF NP(IV), NP(V), AND PD(II) ON ILLITE AND MONTMORILLONITE UNDER HIGH IONIC STRENGTH CONDITIONS

BY

JARED GOGUEN, B.Eng.

A THESIS

SUBMITTED TO THE DEPARTMENT OF ENGINEERING PHYSICS

AND THE SCHOOL OF GRADUATE STUDIES

OF MCMASTER UNIVERSITY

IN PARTIAL FULFILMENT OF THE REQUIREMENTS

FOR THE DEGREE OF

MASTER OF APPLIED SCIENCE

Master of Applied Science (2017) McMaster University

(Engineering Physics) Hamilton, Ontario, Canada

TITLE: Sorption Modelling of Np(IV), Np(V), and Pd(II) on Illite and Montmorillonite Under High Ionic Strength Conditions

AUTHOR: Jared Goguen

B.Eng. (Engineering Physics)

McMaster University, Hamilton, Canada

SUPERVISOR: Dr. Shinya Nagasaki

NUMBER OF PAGES: xxi, 156

For Those to Come

Abstract

A database is being developed by the NWMO that will be capable of predicting sorption for key elements of interest onto crystalline and sedimentary rocks in the highly saline groundwaters and porewaters at DGR depths in Ontario, Canada. Pd(II), Np(IV), and Np(V) have all been identified as elements of interest by the NWMO. Sorption experiments of Pd(II) were conducted on illite, bentonite, and shale to investigate the effects that ionic strength (*I*), and pH have on sorption. *Na-Ca-Cl* solutions ranging from 0.01 – 6.0 M *I* with pH values between 3 and 9 were considered under aerobic conditions at 25°C for sorption testing conditions. Sorption data for Pd(II), Np(IV), and Np(V) was used with 2SPNE SC and 2SPNE SC/CE models developed in PHREEQC to model sorption onto illite and montmorillonite at different values of *I* and pH. These models were also used to test proposed reaction constants from various sources in the existing literature, and to establish and propose optimized surface complexation constants of our own. Optimized reaction constants were compared with the LFER to determine its validity across all test conditions. The LFER was found to not adequately describe sorption of Pd(II), Np(IV), or Np(V) on either illite or montmorillonite. The JAEA TDB, R04, and R07 THEREDA were all tested along with the Davies, Debye-Hückel, SIT, and Pitzer computational methods in order to determine their overall accuracy. The JAEA TDB using the SIT computational method was found to not be capable of modelling Np(IV) onto illite or montmorillonite in 4.0 M *I*.

Acknowledgements

I would like to thank my supervisor, Dr. Shinya Nagasaki, our collaborating researcher, Dr. Satoru Tsushima, and my colleague, Andrew Walker, for all of their help and guidance throughout my time at McMaster and abroad. I would also like to thank all other colleagues, and my friends and family for their continued support throughout my research and writing of this thesis; I greatly appreciate it.

Abbreviations

ACC	American Colloid Company
BGS	below ground surface
DLM	double-layer model
FRC	formation reaction constant
HCB	highly-compacted bentonite
HLW	high-level waste
ILW	intermediate-level waste
IUPAC	International Union of Pure and Applied Chemistry
JAEA	Japan Atomic Energy Association
LFER	Linear Free Energy Relationship
LLW	low-level waste
NEA	Nuclear Energy Agency
NEM	non-electrostatic model
NWMO	Nuclear Waste Management Organization

PHREEQC	PH REdox EQuilibrium in C
RSA	regional study area
RSD	relative standard deviation
SCC	surface complexation constant
SCM	surface complexation model
SDB	sorption database
SIT	Specific-ion Interaction Theory
SR-270-PW	reference pore-water solution for sedimentary rock with a TDS of 270 g/L
SSA	specific surface area
TDB	thermodynamic database
TDS	total dissolved solids
THEREDA	THErmodynamic REference DAtabase
TLM	triple-layer model
UFC	used-fuel container
2SPNE SC/CE	2-site protolysis non-electrostatic surface complexation and cation exchange

Nomenclature

a_i	aqueous phase activity of ion *i* in solution
a_m	aqueous phase activity of master species *m* in solution
C_b	concentration of ion under study in solution in "blank" sample not containing any sorbent(s)
C_{eq}	equilibrium concentration of ion under study in solution
C_i	initial concentration of ion *i* in solution
$c_{m,I}$	stoichiometric coefficient of master species *m* for species *i*
ε_{ik}	interaction coefficient between ions *i* and *k*
E_h	redox potential
γ_i	aqueous phase activity coefficient for ion *i*
I	ionic strength
K_c	concentration quotient used for selectivity coefficients
K_d	distribution coefficient
K_i	equilibrium constant for species *i* in solution

L	volume of liquid
M_{aq}	total number of aqueous master species
Me^{+z}	fictitious metal of charge z
m_i	molality of ion i in solution
M_i	molarity of ion i in solution
n_i	number of moles of ion i in solution
pH_C	pH as calculated by the experimenter
pH_M	pH as measured by the pH probe
R^-	a molar equivalent of negative surface charge
${}^{A}R_d$	distribution ratio of element A
S	mass of solid
W_{aq}	mass of solvent water used for aqueous solution
X_{Me}	exchanger species concentration in mole fraction equivalents of Me surface charge
z_i	ionic charge of aqueous species i

Contents

List of Tables

List of Figures

Chapter 1

Introduction

1.1 Background

In 2002 the Canadian federal government passed the Nuclear Fuel Waste Act requiring all nuclear energy corporations in Canada to establish a waste management organization, and to remain a member and shareholder of it. The two purposes of the waste management organization outlined in the act are to propose long-term approaches for the management of nuclear fuel waste to the Government of Canada, and to implement the approach selected by the Governor in Council on the recommendation of the Minister. In the same year the Nuclear Waste Management Organization (NWMO) was established and tasked under the act with the completion of a three-year study for submission to the Minister that sets out its proposed approaches for the management of nuclear fuel waste, and its recommendation as to which of its proposed approaches should be adopted. Of the approaches proposed by the NWMO, at least three of them were required to be a deep geological disposal in the Canadian Shield, storage at nuclear reactor sites, and either above- or below-ground centralized storage (NFWA, 2002).

In June 2007, after the three-year study, Adaptive Phased Management (APM), was selected as the long-term management plan for used nuclear fuel. Under APM, storage and containment of nuclear waste materials from Ontario Power Generation (OPG), New Brunswick Power Corporation (NB Power), Hydro-Québec, and Atomic Energy of Canada Limited (AECL), will be achieved through the implementation of both a technical method and a management system. The used nuclear fuel from these bodies is being held in above-ground dry-storage facilities at different locations as seen in Figure 1.1, where currently, there are just under 2.6 million used nuclear fuel bundles in Canada (NWMO, 2016). For the technical solution, a deep geological repository (DGR), will be used for centralized containment and isolation of used fuel, and a transportation system will be developed to move the fuel waste from the existing storage facilities to the site location of the DGR. The management solution is broken up into six phases of technical implementation, which include the following (in sequential order): site selection and regulatory approval, site preparation and construction, operations, extended monitoring, decommissioning and closure, and post-closure monitoring. Currently, the NWMO is still in the first phase of site selection and regulatory approval, which was initiated in May 2010.

During the process of this initial phase, the NWMO is engaged in safety assessments that consider both the pre-closure and post-closure periods of the DGR. For the pre-closure period, the safety assessments are conducted primarily for construction, operation, and decommissioning of the facility at the DGR, as well as fuel transportation. Safety assessments for the post-closure period focus on the long-term safety and protection of the DGR, with generic case studies focusing on hypothetical sites prior to the finalization of the site-selection process. Currently, the NWMO is in the third step of the site selection process, which entails a set of preliminary assessments of suitability for the site. As part of the preliminary assessments, the NWMO is working on a number of progressively more detailed impact studies of the potential siting areas that identify the potential effects of the

DGR on such things as groundwater quality, soil and geology, terrestrial and aquatic environment, and human health. Two types of rock formations have been identified in the preliminary assessment as being potentially suitable for the DGR: crystalline and sedimentary. Both types of rock formation have been subjected to a separate pre-closure and post-closure safety assessment. As of December 2015 the site-selection process had narrowed the number of potential DGR host communities down to 9 for further preliminary assessments as seen in Figure 1.2.

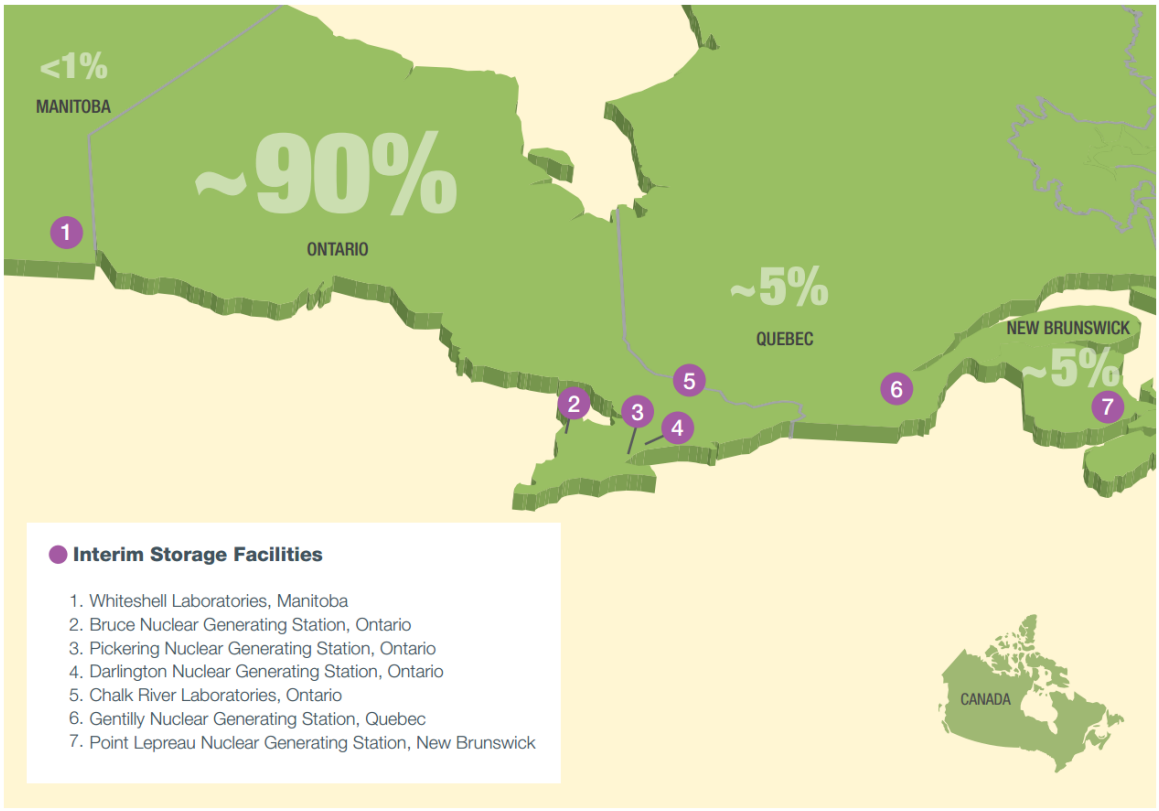

Figure 1.1: Nuclear fuel waste interim storage locations (NWMO, 2016).

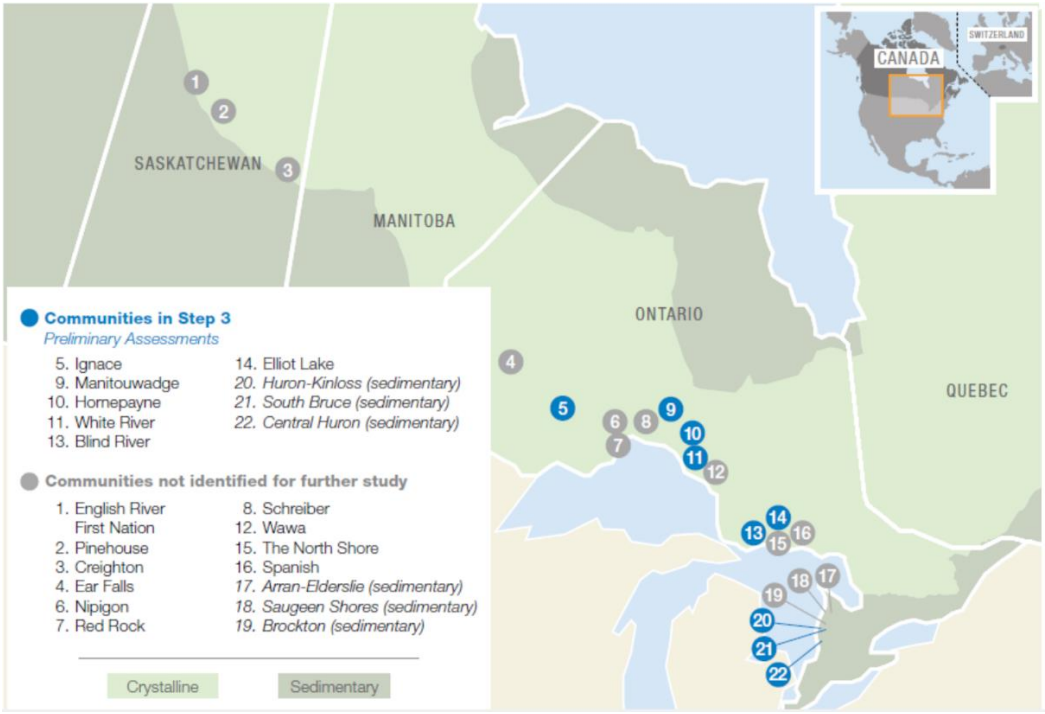

Figure 1.2: Remaining communities in the site-selection process as of December 31, 2015 (Jensen, 2017).

The DGR has been designed to implement a multi-barrier system for the fuel waste in order to help retard waste fuel from contaminating the biosphere, which for high-level waste (HLW), consists of at least 5 barriers: ceramic fuel pellet, Zircaloy fuel element, copper-coated steel used-fuel container (UFC), highly-compacted bentonite (HCB) clay block, and the geosphere. In the current design, fuel bundles containing the ceramic pellets and Zircaloy elements are placed into the UFC, which measures approximately 2.5 m in length, and 0.6 m in diameter, and has two hemispherical domes that are welded shut. Each UFC holds 48 used fuel bundles, which are contained within a steel basket inside the carbon steel pipe, as seen in Figure 1.3 below. The steel core in the UFCs are designed to provide structural strength in order to withstand pressures up to 45 MPa from glaciation. In addition to the carbon steel core, the UFCs will have a 3mm copper coating to assist in heat transfer and provide corrosion resistance for up to 2.3 million years. Each UFC is then placed inside

a HCB buffer box made of a rectangular two-piece assembly with a machined cavity to contain the UFC, as seen in Figure 1.4 below. The buffer boxes are then placed and stacked inside excavated caverns located more than 500 m below ground surface (BGS), as illustrated in Figure 1.5 and Figure 1.6 below, and backfilled with bentonite-sand mixtures (Noronha, 2016).

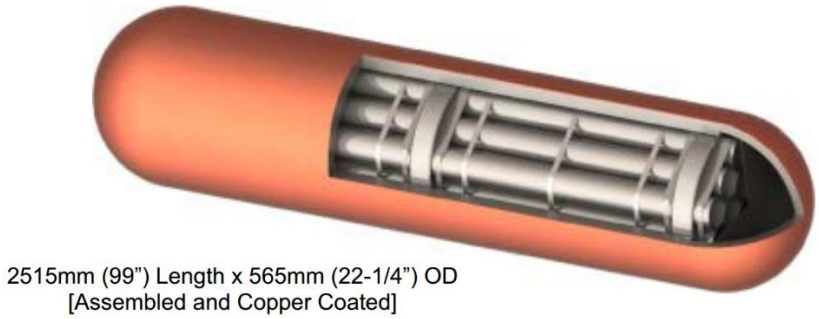

Figure 1.3: Illustration of a Mark II UFC with internal fuel baskets, a carbon steel core, and an external copper coating (Crowe, 2016).

Figure 1.4: Shaping trial of a full-sized HCB clay buffer block (Crowe, 2016).

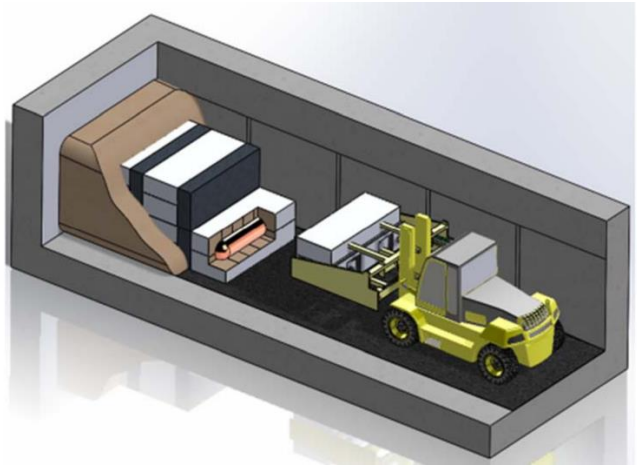

Figure 1.5: Illustration of HCB buffer block stacking underground in DGR (Crowe, 2016).

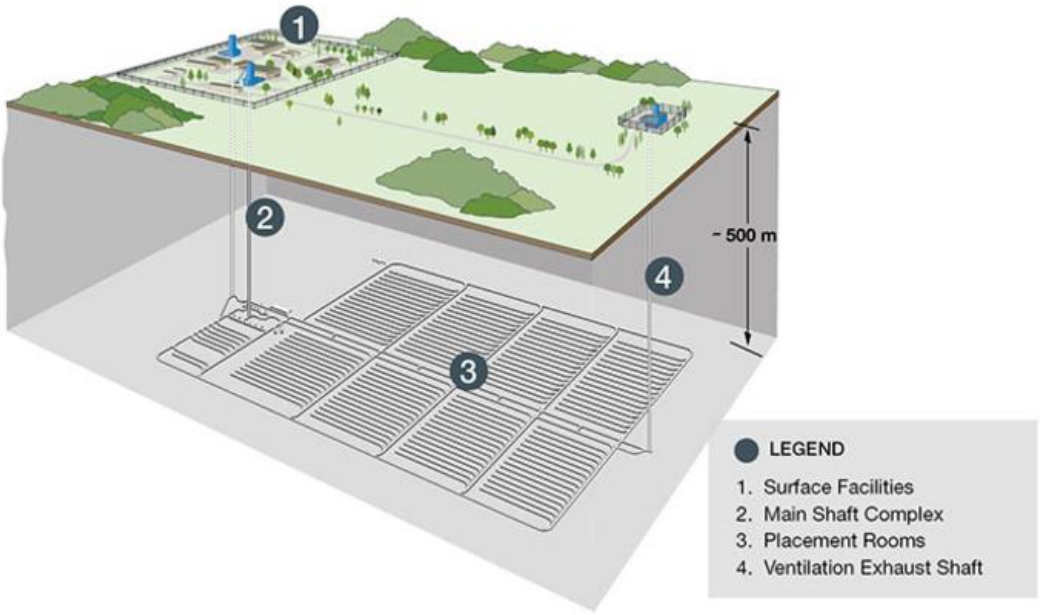

Figure 1.6: Illustration of the NWMO's DGR (NWMO, 2017).

As mentioned earlier, crystalline and sedimentary rock are the two types of host rock being considered for the geospheric barrier. A reference geosphere is being used in the safety assessments for crystalline rock settings that has attributes closely matching

that of a typical Canadian Shield site. The reference sedimentary geosphere assumes that the DGR will be placed inside a thick layer of argillaceous limestone (a chemical sedimentary rock), underneath a thick layer of shale (a clastic sedimentary rock); both having low permeability (Noronha, 2016). OPG has proposed a location for a DGR intended to contain low- and intermediate-level waste (LLW, ILW), at the site of the Bruce Power Generating Station in Kincardine, Ontario. A geological map of Southern Ontario showing the different stratigraphic systems around the Bruce nuclear site can be seen with the marked regional study area (RSA), in Figure 1.7 below. A stratigraphic map of RSA from *A* to *A'* can be seen from left to right in Figure 1.8 below, where the proposed repository horizon can be seen as being just shy of 700 mBGS. In Figure 1.8 the layer of limestone for the DGR host rock can be seen largely as the blue layer, denoting the mid-Ordovician period, with the shale cap as a natural barrier in grey, denoting the late-Ordovician period. Also shown in this figure are the various boreholes drilled for core-sampling the proposed site location. At the depth of borehole DGR1, groundwaters were found to range from freshwaters to brackish waters with total dissolved solids (TDS), of up to 5.0 g/L. Below 170 mBGS, highly saline and brine groundwaters and porewaters were found with TDS as high as 371 g/L in the Guelph Formation (Golder, 2011).

The primary purpose of the natural barrier provided by the geosphere is retarding the migration of nuclear waste products in the event that the first four barrier layers are insufficient in their role of containment. One of the primary mechanisms through which the geosphere is capable of retarding radionuclide transport from a DGR to the surrounding environment and biosphere is a process called sorption. Sorption is a term used to describe any removal of a compound from solution to a solid phase (Thompson, 2012). In order to improve the predictions of the safety assessments for how nuclear waste products will migrate through the geosphere, accurate sorption data needs to be collected for a variety of different conditions. These different conditions include each different

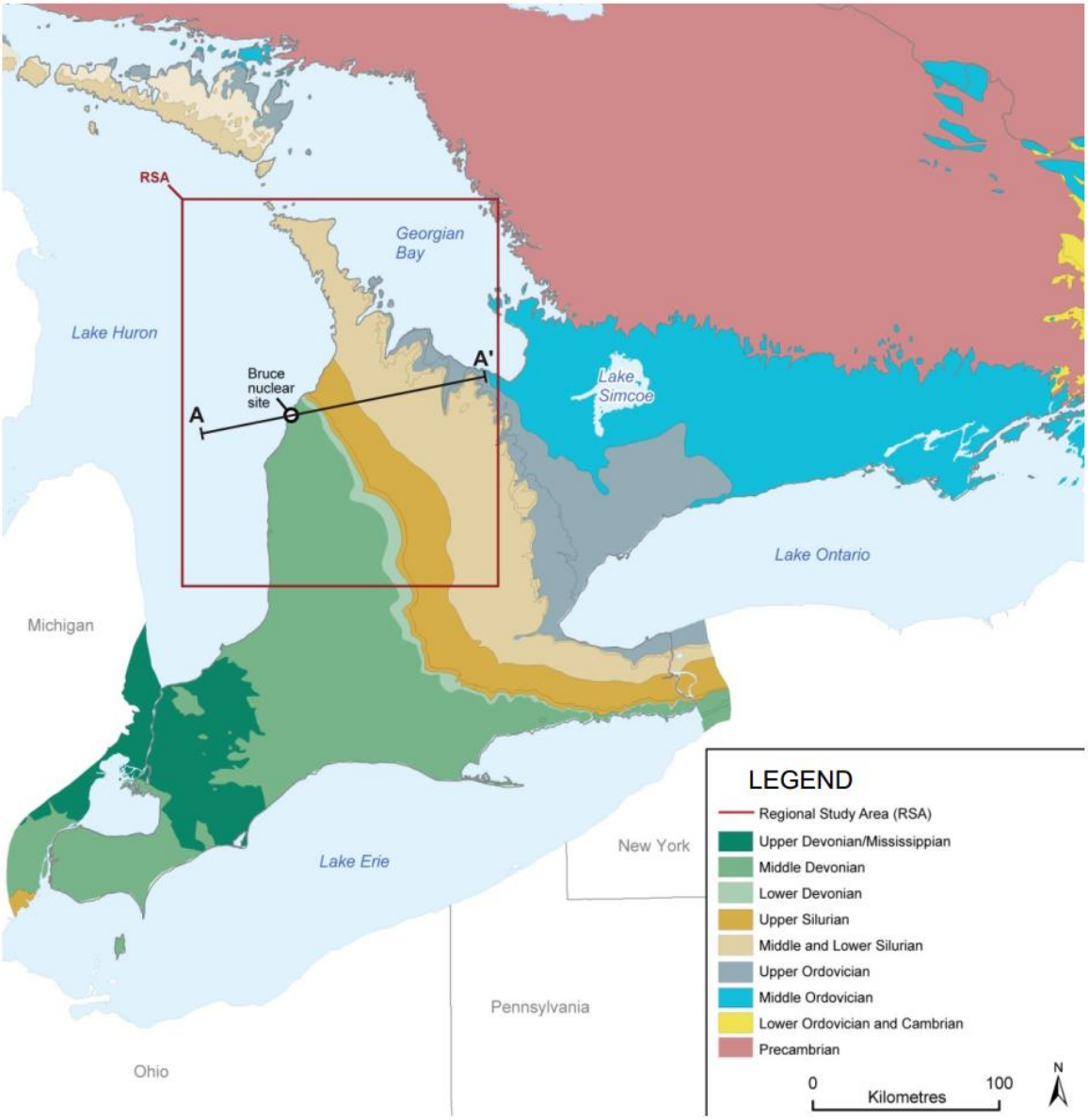

Figure 1.7: Geological map near OPG's proposed DGR at Bruce Power site (Golder, 2011).

element of interest, different host rocks (including the HCB buffer box and bentonite backfill), and the conditions of the groundwaters and porewaters that the waste elements are carried in. The NWMO has identified a number of elements of interest for which sorption coefficient (K_d), values are being measured and determined experimentally. These

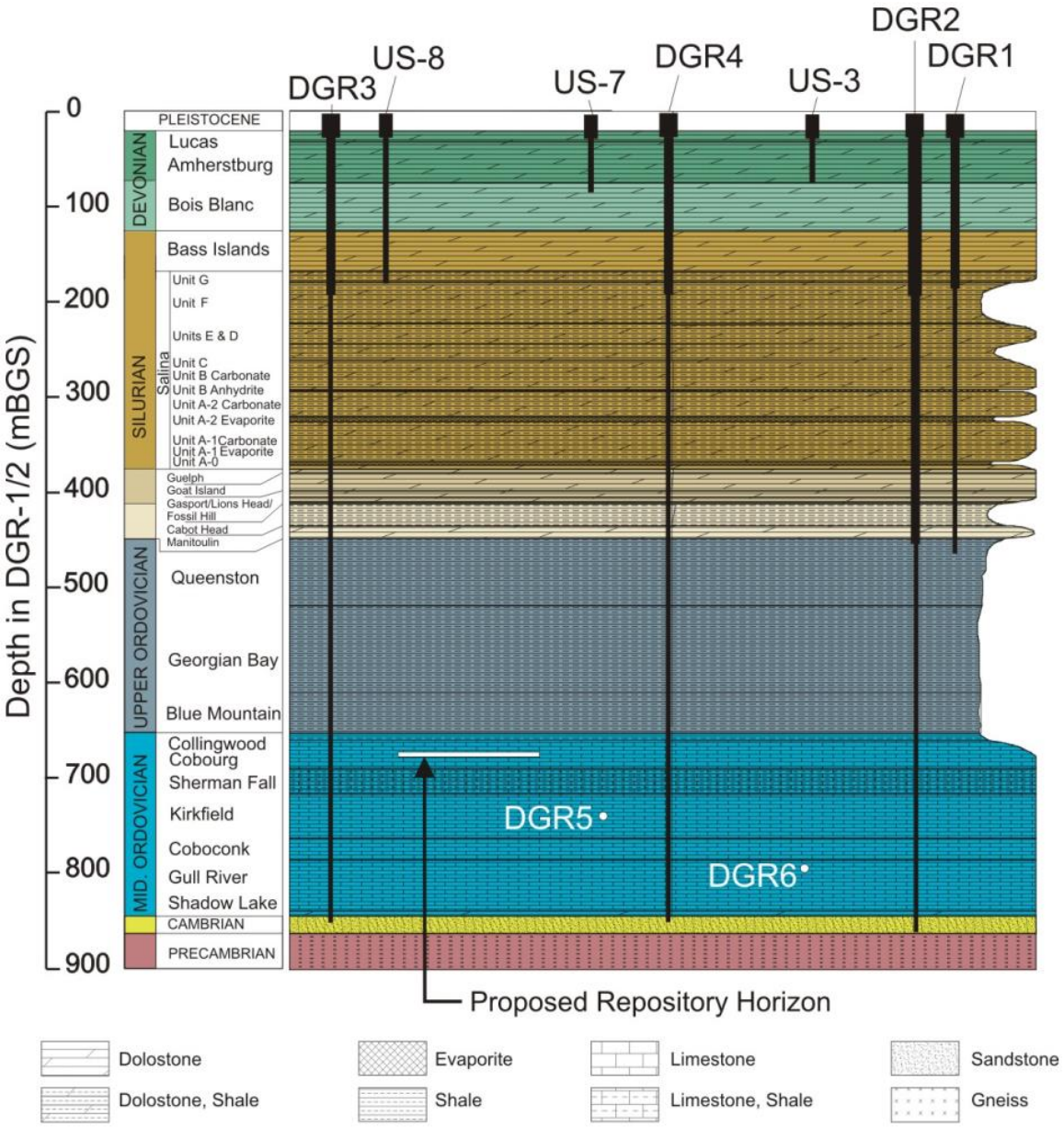

Figure 1.8: Stratigraphy encountered during drilling at Bruce nuclear site. White dots indicate approximate depth of penetration for angled boreholes DGR-5 and DGR-6 (Golder, 2011).

specified elements of interest have been selected based on the contents of the fuel waste that will be placed in a potential DGR, and what elements are produced further down the decay chain of the existing radioisotopes in the waste. Two of these specified elements are

palladium and neptunium, which are studied in this work. Palladium was selected as an element of interest by the NWMO due to the long half-life of Pd-107 (6.5×10^6 a (Tachi, 1999)), and its presence in HLW making up almost 1% by weight of CANDU fuel waste after 10^6 a (Tait, 1989). Neptunium was selected despite only being a minor constituent of HWL also due to the long half-life of its main isotope Np-237 (2×10^6 a), and its high solubility and mobility (Marsac, 2015). Specifically, the redox state of +II for Pd was studied, as it is the dominant redox state in solution, and +IV and +V for Np, as +IV is the dominant redox state in the reference groundwater at DGR depths and +V dominates when the solution is open to the atmosphere at ground surface (Vilks, 2016). In addition to the K_d values , the NWMO has also initiated the development of a Canadian sorption database capable of modelling sorption in the conditions found in the groundwaters and porewaters at DGR depths (Crowe, 2016). It was also shown in Marsac (2015), that the overall uptake of redox-sensitive actinides can be predicted by combining the uptake of each individual redox state. This allows for the study of sorption for the separate Np redox states, which can be used to predict overall sorption for Np in a solution with a given redox potential.

Recently, sorption experiments have been conducted in high ionic strength (I), *Na-Ca-Cl* solutions at various levels of pH onto illite, bentonite, and shale for Pd(II) (Riddoch, 2016), and onto illite and bentonite for Np(IV) (Nagasaki, 2017), and Np(V) (Nagasaki, 2015). Laboratory sorption experiments have been conducted for Pd(II) onto Na-illite, Na-bentonite MX-80, and Ordovician-age Queenston shale in order to build off work completed in Riddoch (2016), and further determine the dependence of K_d values on the pH, and I of solution. The pH values considered range from 3 – 9, and the values of solution I considered range from 0.01 – 6.0 M. The experiments were carried out at 25°C under aerobic conditions.

In order to develop a more detailed understanding of the sorption process, experimentally-derived K_d values for a given element across the pH spectrum and in solutions with different *I* need to be modelled. Once the processes by which sorption occurs are determined, modelling those processes allows for the determination of reaction constants through drawing on the well-established fundamentals of chemistry and thermo-dynamics. Establishing the reaction constants for the various sorption processes allows for the accurate prediction of sorption in varying conditions over time and space, which can be used to improve the dispersion models in the post-closure safety assessments. A sorption model was developed using a geochemical code called PHREEQC (Version 3.3.12), which stands for PH REdox EQuilibrium in the language C (Parkhurst, 2013). The model in PHREEQC makes use of a thermo-dynamic database (TDB), as a source of reference values in order to make all of the necessary calculations. This work makes use of multiple databases in order to compare their accuracy, completeness, and functionality. These databases include the Japan Atomic Energy Agency Thermodynamic DataBase (JAEA TDB), and different releases of the THErmodynamic REference DAtabase (THEREDA). The functional utility provided by the use of the JAEA TDB is that it allows for the implementation of the Specific-ion Interaction Theory (SIT), in calculating the single-ion activity coefficients by utilizing the epsilon values contained within. The SIT model and ensuing computational method account for the electrostatic interactions of all other ions in solution with the one ion of interest. This is necessary for accuracy when computing activity coefficients in solutions of high *I* as these interacting electrostatic forces assert a greater influence. SIT was sought out for use in this work (and therefore the JAEA TDB), as the groundwaters and porewaters at DGR depths have been found to range as high as 7.2 M (Vilks, 2016). However, SIT has only been demonstrated to have an acceptable degree of accuracy for solutions up to an *I* value of 4 M (Grenthe, 1997). In order to model solutions at higher *I*, a more rigorous model called the Pitzer aqueous model was tested during the

sorption modelling. The set of Pitzer equations require a number of database values called Pitzer parameters for calculating the single-ion activity coefficients, which are contained within the THEREDA. Although the Pitzer model is more rigorous than the SIT and can be more accurate, the required Pitzer parameters are more difficult to determine experimentally than the epsilon values required in the SIT. Due to this, the Pitzer computational method could not be used for sorption modelling of Pd(II), but was able to be used in the modelling of Np(IV) and Np(V). For species that did not contain any epsilon values or Pitzer parameters in the TDB, PHREEQC defaults to the use of the empirical Davies and WATEQ Debye-Hückel equations for calculations of charged and uncharged species respectively (Parkhurst, 1999). Sorption was also modelled with the use of the Davies and WATEQ Debye-Hückel equations individually for comparative purposes. However, since the Davies equation is only effective at calculating sorption up to a maximum of 0.5 M (Raton, 1986), this comparison could only be done at low *I*.

1.2 Literature Review

1.2.1 Review of Available Sorption Data

As discussed in Riddoch (2016), there is a very limited amount of sorption data available for Pd(II), providing the impetus for their work as well as what is presented in this thesis. The only sorption data in the JAEA sorption database (SDB), for Pd(II) that meets the requirements of the NWMO for the DGR projects in Canada is a set of 24 data points presented in Tachi (1999). However, the sorption data presented in Tachi (1999), for Pd(II) on bentonite in 0.01 and 0.1 M *I* solution does not contain Ca^{+2} ions. These sample solutions are only varying concentrations of *NaCl*, which may not adequately reproduce a close approximation to the reference brine defined by the NWMO (Vilks, 2016). Some

valuable findings in Tachi (1999), are the conclusions that in the presence of a solid, sorption of Pd(II) onto the test-tube wall is insignificant, and that using a Pd initial concentration of 4.7×10^{-7} M might have led to the production of a precipitate at a solution pH of 8. The latter finding was remediated in Riddoch (2016), and in this work by reducing the initial concentration down to 1×10^{-7} M for sorption tests.

Experimental sorption data for Pd(II) that does come close to approximating the reference brine set out by the NWMO (Vilks, 2016), was for bentonite, shale, and limestone in Vilks (2016), and illite, bentonite, and shale in Riddoch (2016). A summary of the results from the Pd(II) sorption experiments in Vilks (2016), and Riddoch (2016), can be seen in Table 1.1 and Table 1.2 below. In both Vilks (2016), and Riddoch (2016), Pd(II) sorption experiments were conducted in the reference pore-water for sedimentary rock with a *Na-Ca-Cl* TDS of 270 g/L (SR-270-PW), and dilutions thereof to reach the desired *I*. Tests from the two sources were of batch sorption, but under aerobic conditions in Riddoch (2016), and in an N_2-controlled atmosphere in Vilks (2016). Sorption durations in Vilks (2016), ranged from 8 – 17 days, whereas in Riddoch (2016), all tests had a duration of 14 days. One major difference between the sorption values reported from the two sources is that the K_d values presented in Vilks (2016), are almost twice those presented in Riddoch (2016), for shale, and almost six-times as large for bentonite. Riddoch (2016), found that sorption of Pd(II) is highly dependent on pH and *I* for all soils, and only dependent on the initial concentration (C_i) of Pd(II) for shale.

Table 1.1: Summary of Pd(II) sorption coefficients in Vilks (2016).

Solid	*I* (mol/L)	pH	K_d (m^3/kg)
Bentonite	6.0	5.7 – 6.4	0.14 – 14.5
Shale	6.0	5.6 – 6.4	0.042 – 14.3
Limestone	6.0	5.7 – 6.4	0.05 – 22

Table 1.2: Summary of Pd(II) sorption coefficients in Riddoch (2016).

Solid	I (mol/L)	pH	K_d (m^3/kg)
Illite	0.1 – 4.0	5 – 9	0.01 – 3.73
Bentonite	0.1 – 4.0	5 – 9	0.02 – 2.50
Shale	0.1 – 4.0	5 – 9	0.01 – 7.39

1.2.2 Review of Sorption Modelling

Outside of Riddoch (2016), sorption of Pd(II) has not been modelled extensively. Some modelling of Pd(II) on montmorillonite and shale was conducted in Vilks (2017), but this was only done for SR-270-PW and freshwater, with experimental K_d values for only one pH of each. Additionally, no reaction constants were proposed in Vilks (2017), through fitting the sorption model to the experimental data. It was found in Vilks (2017), that the model greatly under-predicted the K_d values from the experimental data, and proposed that the discrepancy may have been due to not accounting for chloride species in the possible sorption processes.

In Riddoch (2016), it was found that aqueous speciation of Pd(II) was highly dependent on *I*, but that the surface site speciation was not, however, they both had a strong dependence on pH. As *I* increased, the aqueous speciation of Pd(II) changed such that the $Pd(OH)_2$ species became less dominant, and the $PdCl_2$ species became more dominant. In acidic solutions $PdCl_4^{-2}$ was found to be the dominant species, while in more alkaline solutions the $Pd(OH)_2$ species became dominant, and the $Pd(OH)^+$ became dominant in solution at even higher levels of pH. The number of hydrogens on the oxygen surface sites were found to decrease as pH increases, starting from the $S\text{-}OH_2^+$ dominating at low pH, and $S{-}O^-$ dominating at high pH. Surface complexation was successfully modeled onto montmorillonite in 0.1, 1.0, and 4.0 M *I* solutions, onto illite in 0.1 M *I* solutions, and only in 1.0 and 4.0 M *I* solutions after shifting the model lower by 2 units of pH. The dominant

surface complexes forming were found to be the $S{-}OPd(OH)$, $S{-}OPd(OH)_2^-$, and $S{-}OPdCl_4^{-3}$ surface species. There were also improvements that were able to be made to the sorption model onto illite by modifying the protonation and deprotonation constants and reducing the region where the $S{-}OH$ surface species is dominant. It was also concluded in Riddoch (2016), that using a single-layer sorption model for Pd(II) is justified, given that the sorption isotherms for illite and montmorillonite had a slope of one, meaning that inner- and outer-sphere complexes were being formed inside the Stern Layer. Furthermore, it was concluded that specific chemical sorption in the form of surface complexation was the dominant sorption mechanism.

A 2-site protolysis non-electrostatic surface complexation and cation exchange (2SPNE SC/CE), model was used for modelling Np(IV) onto illite in Marsac (2015), with estimated surface complexation constants (SCCs), affected by large uncertainties. The estimated Log K_d values had an error of +/-1.1 through the propagation of the uncertainties in the SCCs through the model, which can be seen in Figure 1.9 below. This model wasn't directly compared with any experimental K_d values, however, the SCCs were optimized through fitting to experimental K_d values (Marsac, 2015). It was suggested that the $S{-}ONp(OH)_4^-$ surface species was expected to be the dominant surface complex onto illite in alkaline solutions as a result of an analogous comparison to the sorption of Th(IV). However, this work was only conducted for 0.1 M $NaClO_4$, which does not match the environmental conditions in the Michigan basin at proposed DGR depths, and doesn't provide a wide range of I in order to validate the accuracy of the model and reaction constants used. Outside of this work, sorption of Np(IV) has not been modelled extensively.

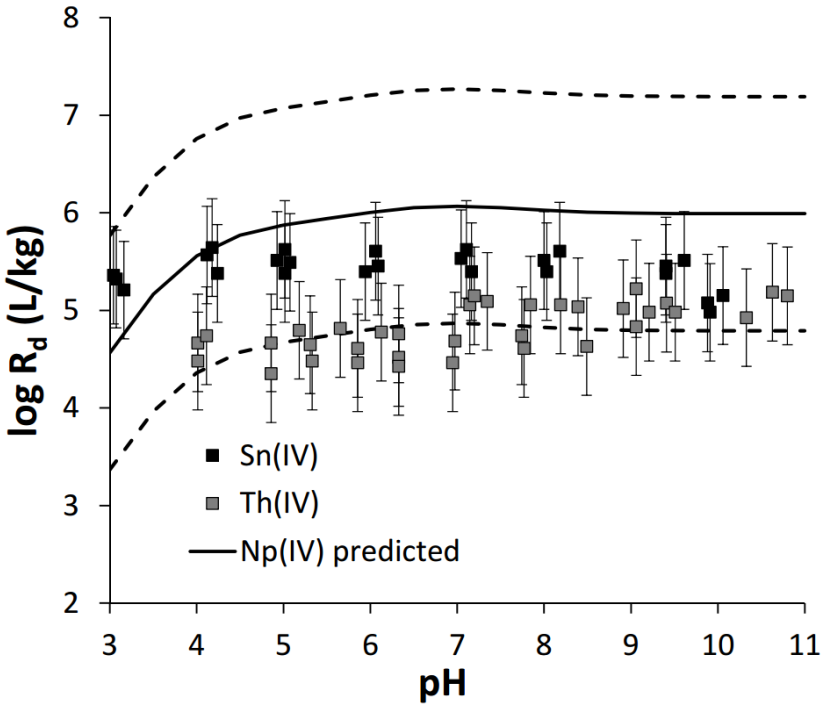

Figure 1.9: The predicted sorption of Np(IV) with the 2 SPNE SC/CE model, plotted with experimental sorption K_d values for Sn(IV) and Th(IV) onto illite in 0.1 M $NaClO_4$ versus pH. Dashed lines show the confidence interval on the surface complexation constants of Np(IV) (Marsac, 2015).

Sorption of Np(V) onto Na-illite, Na-smectite, and Na-SAz-1 was modelled using a 2SPNE SC/CE model in Bradbury (2009b), and Bradbury (2005b), and plotted against experimental data from Gorgeon (1994), for illite and Na-smectite, and data from Turner (1998), for Na-SAz-1. The sorption plots from Bradbury (2009b, 2005b), can be seen in Figure 1.10 and Figure 1.11 below. However, these models were for 0.025 and 0.1 M $NaClO_4$ for illite and Na-smectite respectively, and 0.1 M $NaNO_3$ for Na-SAz-1, which do not match the environmental conditions in the Michigan basin at proposed DGR depths or provide a wide range of I in order to validate the accuracy of the model and reaction constants used. Reasonably accurate fits were able to be obtained for all models of Np(V) from Bradbury (2009b, 2005b). It was identified in Bradbury (2009b), that the sorption of

Np(V) onto Na-illite was dominated by cation exchange in the region of the sorption edge with a pH < 5. Outside of this work, sorption of Np(V) has not been modelled extensively.

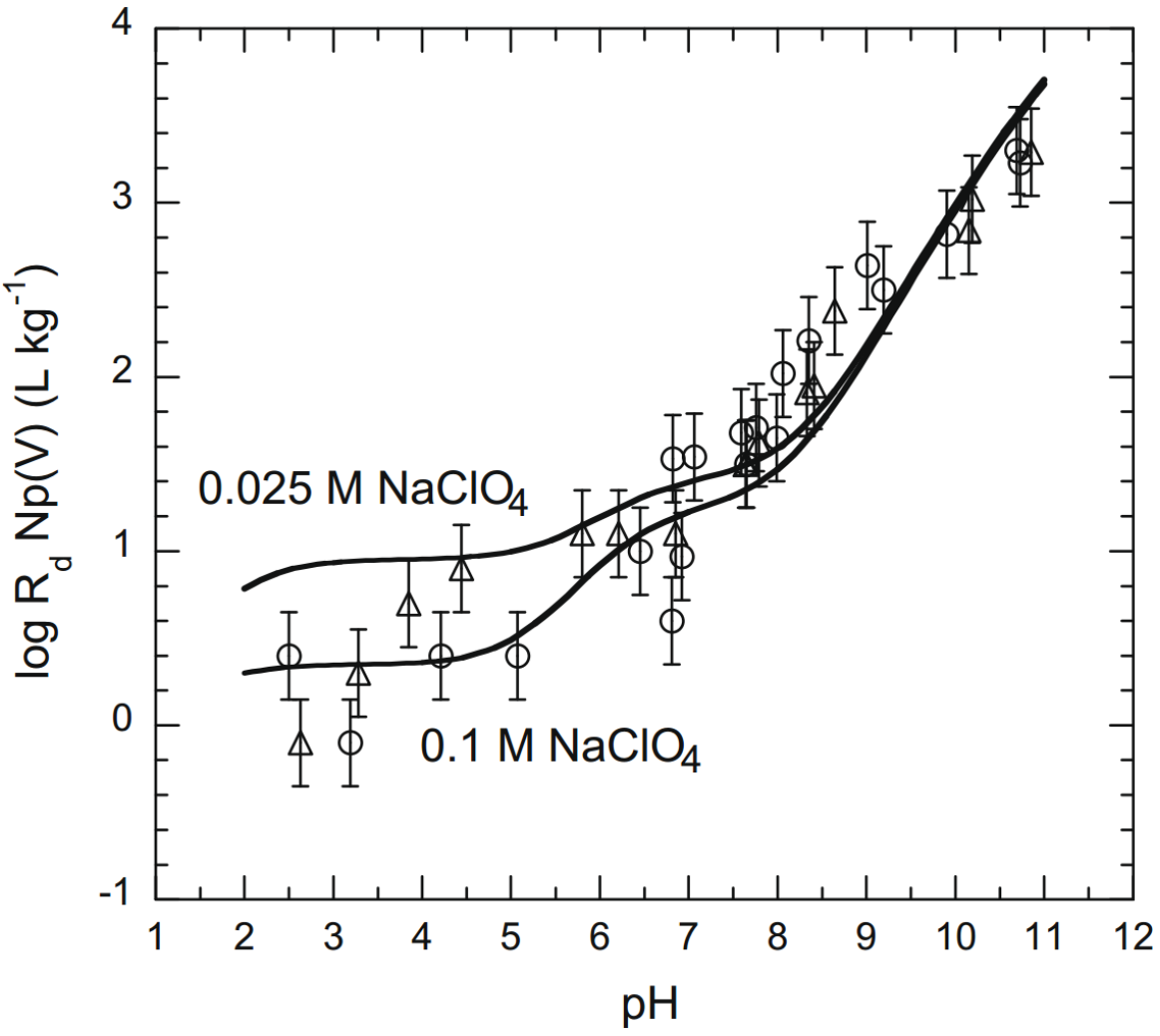

Figure 1.10: Experimental sorption data of Np-237 on Na-illite in 0.025 and 0.1 M *$NaClO_4$* (Gorgeon, 1994), plotted with results from the 2SPNE SC/CE model (Bradbury, 2009b).

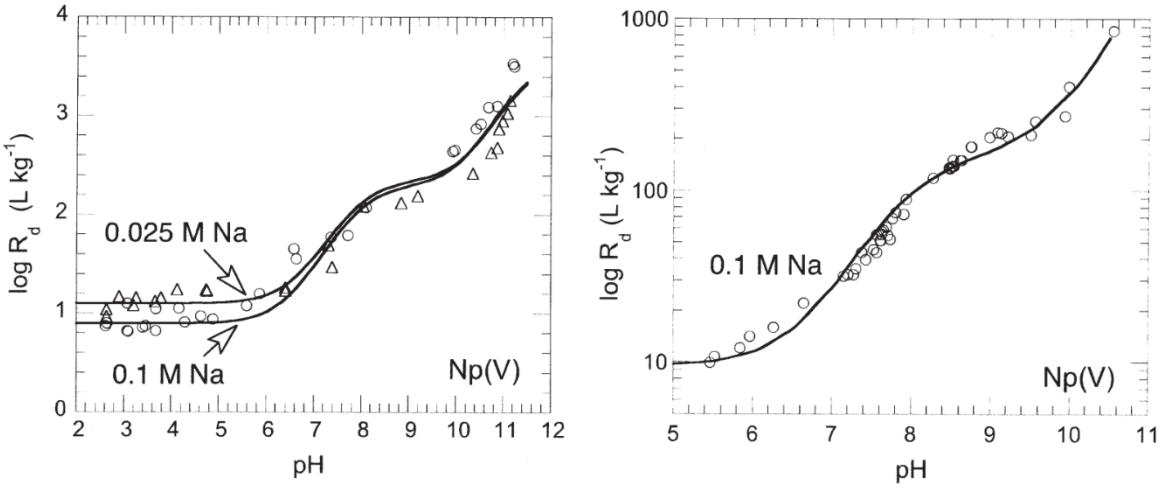

Figure 1.11: Experimental sorption data of Np-237 on Na-smectite (left), in 0.025 and 0.1 M *$NaClO_4$* (Gorgeon, 1994), and on Na-SAz-1 (right), in 0.1 M $NaNO_3$ (Turner, 1998), plotted with results from the 2SPNE SC/CE model (Bradbury, 2005b).

1.3 Purpose

The purpose of this thesis is to expand upon the available sorption data for Pd(II) (particularly that presented in Riddoch (2016)), by testing additional experimental conditions. Focus will be directed toward Pd(II) sorption conditions that have a higher and lower *I* than those presented in Riddoch (2016), a lower pH in order to expand on the pH dependence, and in particular, a lower pH at low *I* so that cation exchange constants can be determined. Sorption experiments will be conducted on three soils; Na-illite, Na-bentonite MX-80, and Queenston shale. Sorption modelling of Pd(II) will focus on determining reaction constants for various sorption processes with the use of experimental results from the tests previously described. Sorption modelling of Np(IV) and Np(V) will be used for the same purposes as the Pd(II) modelling. Neptunium models will use recently published sorption data (Nagasaki 2017, 2015), from experiments tailored to the NWMO DGR project conditions. Additional modelling work will be conducted in order to make

comparisons between different TDBs and computational methods for all experimental conditions. Optimized metal-binding SCCs will also be used with their respective hydrolysis constants in order to determine the validity and accuracy of the LFER.

Chapter 2

Theory

2.1 Sorption

Following Sposito (2008), sorption is defined in Thompson (2012), as describing any removal of a compound from a solution to a solid phase, which according to Tinsley (2004), this can occur irrespective of any specific mechanism, of which there are many. The reverse process of sorption is called desorption, where ions, atoms, or molecules are released from the bulk phase back into solution. In Thompson (2012), the accumulation of atoms, ions, or molecules within existing solids is referred to as absorption, the accumulation of those at the solid-liquid interface is referred to as adsorption (IUPAC, 1987), and the incorporation of substances within an expanding three-dimensional solid as precipitation. In the sorption process, the solid phase that is doing the absorbing or adsorbing is called a sorbent, the constituents that accumulate on or within the sorbent are called sorbates, and the aqueous solutes that could potentially sorb are called sorptives, which can be seen graphically in Figure 2.1 below (Thompson, 2012). Absorption can also occur to sorptives and sorbates that are in the liquid or gaseous phase if the sorbent is in a

solid bulk phase, or sorptives and sorbates that are in the gaseous phase only if the sorbent is in a liquid bulk phase (McMurry, 2003). However, in this work sorption will always refer to processes involving sorbents in the solid bulk phase, and sorptives and sorbates that are fully-dissolved solvents.

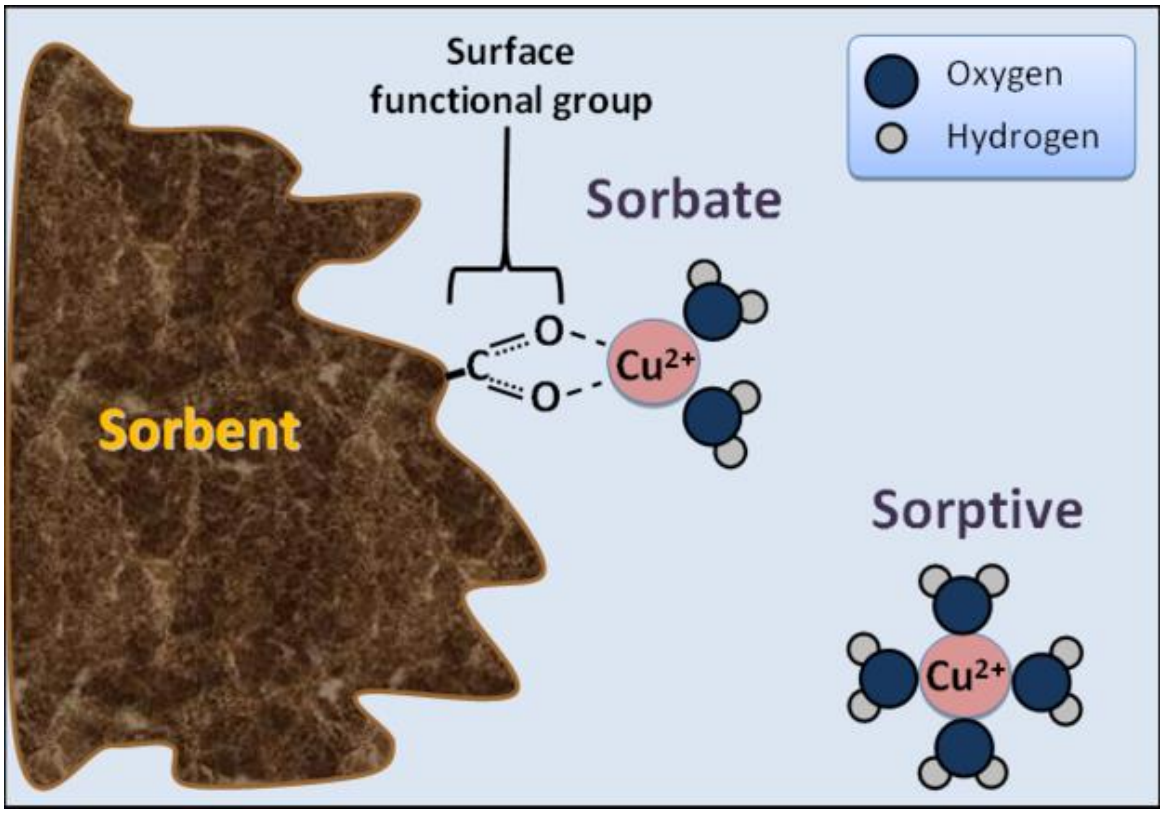

Figure 2.1: Sorptive, sorbate, and sorbent (Thompson, 2012).

2.1.1 Sorption Mechanisms

There are a number of different sorption mechanisms that can occur during sorption depending on the different environmental properties which sorption is occurring within. The two main sorption mechanisms focused on in this work are specific chemical sorption, and non-specific Coulombic sorption, or an ion-exchange reaction. Other sorption

mechanisms include structural penetration, isotopic exchange, and physical sorption. Structural penetration is a very slow process that can occur for dehydrated cations with a radius no larger than 0.74 angstroms. The sorptive can become permanently incorporated in the sorbent after penetration of a hole in the tetrahedral layer of a clay, and re-hydrating (Vilks, 2016). Given that Th(IV), Pd(II), Np(IV), and Np(V) all have an ionic radius greater than 0.74 angstroms, structural penetration was not considered for any models in this work (Shannon, 1976). Although not strictly a sorption process, isotopic exchange occurs when a radioisotope exchanges with its stable isotopes that are sorbed onto solids through Coulombic attraction (Vilks, 2016). Sorption experiments involving Pd used a non-radioactive stock solution with an isotopic abundance equal to naturally occurring Pd in nature. Because of this, isotopic exchange would have no effect on the concentration of the Pd isotope being used to calculate sorption (Pd-105), and the process was therefore not considered in the modelling of Pd(II). Np is a radioactive actinide element with no stable isotopes, and therefore isotopic exchange was also not considered in the modelling of Np(IV) or Np(V). Physical sorption is caused by non-specific long-range forces of attraction (such as Van der Waal's forces), that can occur for neutral metal hydrolysis complexes (such as $Pd(OH)_2$), on solid surfaces that are also neutral (*S-OH*). Since this is a rapid and reversible weak process, it was also not considered in any of the sorption models in this work (Vilks, 2016).

Specific Chemical Sorption

Specific chemical sorption is an adsorption mechanism, and was defined in Jenne (1977), as "that quantity adsorbed from micro concentrations of the trace element in the presence of macro concentrations of alkaline earth or alkali cations, and which is largely desorbable by chemically similar elements". As shown in Figure 2.2 below, different

cations of roughly the same charge exhibit a sharp increase in sorption onto a ferric oxide surface at different levels of solution pH (Stumm, 1996).

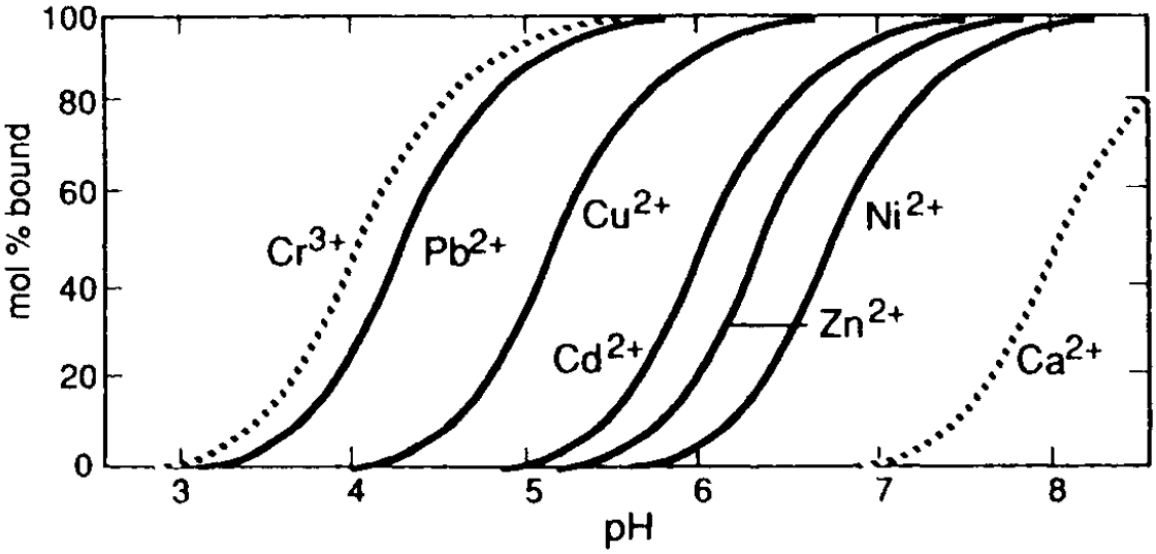

Figure 2.2: pH dependence of metal sorption on iron oxide (Stumm, 1996).

The sorbent surface contains hydroxyl species at the phase boundary that become negatively charged oxygen adsorption sites as the protons are stripped off the surface with an increasing solution pH. If sorption of these cations was dependent on charge alone, then one would expect the sharp rise in uptake by the sorbent to occur at the same pH for all cations. Since this does not occur, something other than Coulombic attraction must be responsible. Cations that have stronger hydrolysis constants are found to have sorption spikes that occur at a lower pH than cations that hydrolyze more weakly (Vilks, 2016). One explanation is that despite having the same charge, the cations range in terms of electronegativity (the tendency to bond with an electron). The difference in electronegativity results in each cation having different hydrolysis constants, which are measures of the propensity of a cation to bond or dissociate from a hydroxyl species (OH^-). If a cation has a larger hydrolysis constant (resulting from a larger electronegativity),

then it would follow that a rise in sorption would begin to occur when there is a smaller negative surface charge on the sorbent (which occurs at a lower pH). Surface complexation is the most common concept used to explain specific chemical sorption, which involves the formation of metal complexes on surface oxygen sites. Since metal cations sorb onto surface oxygen sites of a sorbent through the displacement of bonded H^+ ions, it can be treated as a coordination reaction with a surface ligand (Vilks, 2016).

Non-Specific Coulombic Sorption & Ion Exchange

Coulombic sorption and ion-exchange are processes that are dependent on charge. Charged mineral sorbent surfaces can produce what is called a diffuse layer in solution caused by the attractive Coulombic forces between the ion and the charged surface. This causes a higher concentration of ions than in the rest of the solution to collect closely to the sorbent surface, with a decreasing concentration further away from the interface in accordance with the Boltzmann function (Parks, 1967). It was proposed in Stern (1924), that between the diffuse layer and the sorbent, there was a monolayer of adsorbed ions, which can be seen in Figure 2.3 below. Part of the surface charge that creates the diffuse layer is neutralized by the Stern Layer, which slightly decreases the ion concentration in the diffuse layer. Coulombic sorption is a reversible process because no chemical bonds are formed, but sorption occurs quickly since the only impediment is diffusion. This sorption mechanism is dependent on *I* since the increased concentration of cations in solution displaces sorptives that could sorb through exchange with another Coulombically-sorbed cation. Due to this dependence on *I*, Coulombic sorption is only a significant sorption process in low *I*.

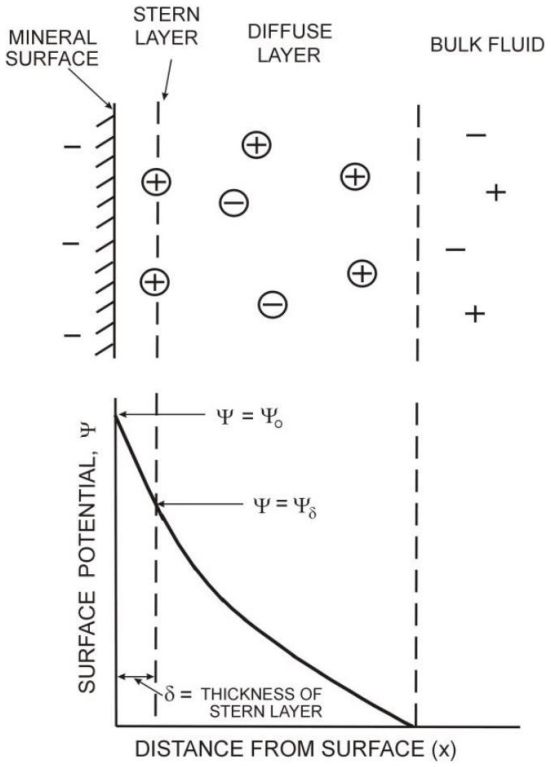

Figure 2.3: Illustration of the electric potential inside the Stern & diffuse layers (Stern, 1924).

Coulombic sorption is modelled with cation exchange reactions whose equilibrium constants are called selectivity coefficients (K_c). Applying mass-action laws to an exchange reaction shown for two cationic species of any charge *x* and *z* in Equation 2.1 below, the concentration of exchanger species (X_{Me}), (written as mole fraction equivalents of surface charge), can be seen in Equation 2.2 and 2.3, where R^- represents one molar equivalent of negative surface charge. The selectivity coefficient (K_c), can be seen in Equation 2.4, and simplified in Equation 2.5 using mass balance for exchanger ions: $1 = X_{Me} + X_{Me'}$ (Bidoglio, 1994).

$$z/x\,(R^-)_x Me'^{+x} + Me^{+z} \leftrightarrow (R^-)_z Me^{+z} + z/x\,Me'^{+x} \tag{2.1}$$

$$X_{Me} = \frac{(z[R^-{}_z Me^{+z}])}{x[R^-{}_x Me^{+'x}] + z[R^-{}_z Me^{+z}]} \tag{2.2}$$

$$X_{Me\prime} = \frac{(x[R^{-}{}_{x}Me'^{+x}])}{x[R^{-}{}_{x}Me'^{+x}]+z[R^{-}{}_{z}Me^{+z}]} \tag{2.3}$$

$$K_c = \frac{X_{Me}}{X_{Me\prime}^{z/x}} \cdot \frac{\{Me'^{+x}\}^{z/x}}{\{Me^{+z}\}} \tag{2.4}$$

$$K_c = \frac{X_{Me}}{(1-X_{Me})^{z/x}} \cdot \frac{\{Me'^{+x}\}^{z/x}}{\{Me^{+z}\}} \tag{2.5}$$

2.1.2 Measuring Sorption Experimentally

There are two main ways to experimentally measure sorption. The most common method (making up the largest portion of known sorption data), is called batch sorption. The second is a set of methods called mass-transport experiments, which include diffusion, advection, and a combination of the two. Batch sorption is the most commonly used method due to the experimental simplicity, low cost, and absence of complicating factors associated with the mass transport set of methodologies. The latter set of methods are less commonly used, as the experimental testing duration is most often multiple times longer than that of batch, and in some cases up to an order of magnitude longer (Vilks, 2016).

In batch sorption experiments, the sorbate(s), sorptive(s), and sorbent(s) are all contained within the same vessel (often a test tube). Parameterization of batch sorption experiments include: the mass, composition, and physical form of the sorbent; the volume and chemical composition of the solution including the *I*, pH, E_h, and the concentration of sorptive(s) and complexing ligands; the atmospheric composition (oxidizing, reducing, carbonate rich or free, etc.); and the temperature. Sorption duration is not considered part of the parameterization as measurements of sorption coefficients can only be measured once the system has reached equilibrium. Once reaching a steady-state, the bulk solid and liquid phases can be separated through centrifugation or filtration, and either the liquid is

analyzed for the remaining sorptive concentration, or the sorbent is analyzed for the net amount of sorbate concentration. This method can be used for either sorption or desorption experiments (Vilks, 2016). An illustration of a batch sorption experiment can be seen in Figure 2.4 (a) below from Riddoch (2016).

Diffusion experiments consist of two separate solution reservoirs on both sides of a single bulk solid sorbent, with one solution containing a test concentration of the sorptive under study, and the other containing a very low concentration. Once the concentration of sorptive is the same in both solutions, then the sorption process through means of diffusion is considered to be complete. Once the amount of sorbate is determined (often through calculating the net change in sorptives in solution by using concentration measurements), then the sorption coefficients can be calculated in a similar manner as with batch sorption techniques. Measured values such as that of porosity and tortuosity can be used in combination with the measured sorption data and mass transport calculations to obtain a set of simulated results that can help with improving the understanding of the sorption process (Vilks, 2016). An illustration of a diffusion experiment can be seen in Figure 2.4 (b) below from Riddoch (2016).

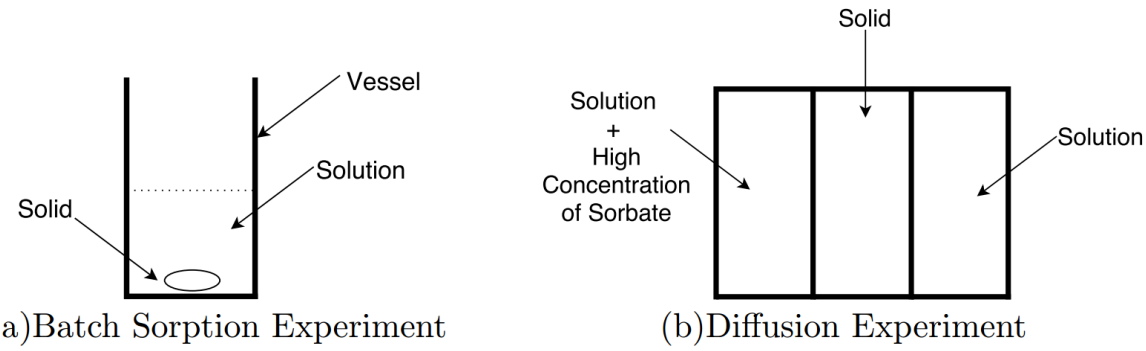

Figure 2.4: Batch and diffusion (transport), sorption experiments (Riddoch, 2016).

Calculating K_d Values

The most common way to quantify sorption is with the use of a value called a distribution coefficient (K_d). K_d values are a measure of the ratio between the amount of sorbate and sorbent, with a correction factor for the ratio of solution volume to the mass of sorbent (L/S). One method of determining the amount of sorbate experimentally is to dissolve the sorbent using some form of acid (like aqua regia), and to then measure the amount of sorbate in solution. This can then be used with the known initial amount of sorptive in solution to calculate the K_d value. This is a less common method of measuring K_d values, as it requires additional processes and introduces more error. However, this is a viable solution for overcoming problems associated with attempting to measure sorptive concentrations in solutions of high *I*, as detection limit problems arise from dilution requirements of the device measuring concentration.

The other method of determining K_d values involves knowing the initial (C_i), and final concentration (C_{eq}), of sorptive in solution. Additionally, the concentration of sorptive in solution in the absence of a sorbent can be measured to account for loss of sorptive from solution through processes other than sorption onto the desired sorbent (such as sorption onto the vessel wall). This can be done by running a parallel "blank" experiment with the sorption experiment with the same conditions in the absence of a sorbent, and then measuring the sorptive solution concentration (C_b), at the end of the sorption period. However, this method was determined to be a misapplication of a correction method for the sorption of Pd(II) in Tachi (1999), as sorption of Pd(II) onto a vessel wall is only significant in the absence of a sorbent. Due to this finding, Equation 2.6 can be simplified down to Equation 2.7 as seen below. Solution concentrations are often measured with the use of an inductively-coupled plasma mass spectrometer (ICP-MS).

$$K_d = \frac{C_b - C_{eq}}{C_{eq}} \frac{L}{S} \quad (2.6)$$

$$K_d = \frac{C_i - C_{eq}}{C_{eq}} \frac{L}{S} \quad (2.7)$$

2.1.3 Modelling Sorption

Although PHREEQC (Version 3.3.12), was used to model sorption in this work, some other codes that can be used include MINTEQA2 (Allison, 1991), and MINSORB (Bradbury, 1997). For each aqueous species *i*, PHREEQC has to calculate the corresponding activity (a_i), activity coefficient (γ_i) , molality (m_i), and number of moles in solution (n_i). These four unknowns can be related to each other using Equations 2.8 and 2.9, where W_{aq} is the mass of solvent water used for the aqueous solution. These two equations can be combined to produce Equation 2.10, reducing the number of unknowns (Parkhurst, 1999).

$$a_i = \gamma_i m_i \quad (2.8)$$

$$n_i = m_i W_{aq} \quad (2.9)$$

$$n_i = W_{aq} \frac{a_i}{\gamma_i} \quad (2.10)$$

To further reduce the number of unknowns, PHREEQC relates all a_i values to the activities of the master species *m* (a_m), which can be defined in the source code or database. This relationship can be seen in Equation 2.11 below, where K_i is the temperature-dependent equilibrium constant (also defined in the source code or database), M_{aq} is the total number of aqueous master species, and $c_{m,i}$ is the stoichiometric coefficient of master species *m* for species *i*. If the aqueous species $CaSO_4$ is considered then the formation

reaction can be seen in Equation 2.12, and the equilibrium constant can be seen for the mass-action expression shown in Equation 2.13.

$$a_i = K_i \prod_m^{M_{aq}} a_m^{-c_{m,i}} \tag{2.11}$$

$$Ca^{+2} + SO_4^{-2} \leftrightarrow CaSO_4 \tag{2.12}$$

$$K_{CaSO_4} = \log_{10} \frac{a_{CaSO_4}}{a_{Ca^{+2}} \cdot a_{SO_4^{-2}}} \tag{2.13}$$

Combining Equation 2.10 and 2.11 yields the mass-action expression shown in Equation 2.14, which is used to calculate the number of moles in solution of an aqueous species *i*. PHREEQC uses the Newton-Raphson method to iteratively solve for the equilibrium state (Parkhurst, 1999).

$$n_i = \frac{K_i W_{aq} \prod_m^{M_{aq}} a_m^{c_{m,i}}}{\gamma_i} \tag{2.14}$$

To calculate the number of moles in solution for each aqueous species, the corresponding activity coefficients must be determined. There are four main computational methods that can be used to calculate the activity coefficients: Davies (Davies, 1962), WATEQ Debye-Hückel (Truesdell, 1974), Specific-ion Interaction Theory (Grenthe, 1997), and Pitzer (Pitzer, 1991). PHREEQC defaults to using the empirical Davies equation and WATEQ Debye-Hückel equation for charged and uncharged species respectively, shown in Equations 2.15 and 2.16 below (Parkhurst, 1999). The linear term in Equation 2.16 is added to the original Debye-Hückel equation to account for inaccuracies at higher concentrations (Bretti, 2004). Since the WATEQ Debye-Hückel equation is used in PHREEQC by default for uncharged species, and *b* is assumed to be 0.1 for all uncharged

species unless otherwise specified (Parkhurst, 1999), Equation 2.16 simplifies to Equation 2.17.

$$\log(\gamma_i) = -z_i^2 A\left(\frac{\sqrt{I}}{1+\sqrt{I}} - 0.3I\right) \tag{2.15}$$

$$\log(\gamma_i) = -\frac{z_i^2 A\sqrt{I}}{1+Ba_i^0\sqrt{I}} + b_i I \tag{2.16}$$

$$\log(\gamma_i) = 0.1I \tag{2.17}$$

In these equations, z_i is the ionic charge of aqueous species i, A and B are constants dependent on temperature only (Equation 2.18 & 2.19 (Sipos, 2008)), and I is the ionic strength of the solution calculated using Equation 2.20 below. The a_i^0 and b_i parameters in the WATEQ Debye-Hückel equation are ion-specific parameters fitted from mean-salt activity-coefficient data.

$$A = 0.509\sqrt{kg/mol}\ @\ 25°C \tag{2.18}$$

$$1 \leq B \leq 1.5 \tag{2.19}$$

$$I = \frac{1}{2}\sum_i^N n_i z_i^2 \tag{2.20}$$

Although PHREEQC defaults to using the empirical Davies and WATEQ Debye-Hückel equations, it has the ability to use other computational methods for determining the activity coefficients like SIT and Pitzer. This makes PHREEQC a better sorption modelling program, since MINSORB can only use the Davies equation (Bradbury, 1997), and MINTEQA2 can only use the WATEQ Debye-Hückel equation (Allison, 1991). SIT is a more accurate computational method than the Davies or WATEQ Debye-Hückel methods in solutions of higher I as SIT takes into account the electrostatic interactions of all other

ions in solution on the ion of interest (Robinson, 1968). SIT modifies the base Debye-Hückel equation by adding linear terms according to oppositely-charged ions shown in Equation 2.21 where ε_{ik} are the interaction coefficients between ions *i* and *k*. This equation assumes that ions of the same charge have no effect ($\varepsilon = 0$), and that triple-interactions are negligible (Bretti, 2004).

$$\log(\gamma_i) = \frac{-z_i^2 A\sqrt{I}}{1+B\sqrt{I}} + \sum_k \varepsilon_{ik} \cdot m_i \tag{2.21}$$

PHREEQC can be commanded to use Equation 2.21 when a SIT data block is read off an input file while compiling, but with the JAEA TDB the data block does not need to be explicit in the input file because it is already present in the TDB. In the SIT data block contained in the JAEA TDB, single ε values are defined per ion pair. ε values are dependent on ionic strength, but many electrolytes were found to be constant between 0.5 – 3.5 m *I* in Ciavatta (1980). The Pitzer aqueous model used in PHREEQC is derived from the excess of Gibbs energy in a solution containing many electrolytes. The Pitzer computational method is much more rigorous than the previous models mentioned, and could possibly calculate activity coefficients more accurately. This method requires a large number of constants, which have to be determined empirically. These are more difficult to determine than epsilon values for the SIT, and are therefore not established for as many ions. The derivation is omitted in this work for brevity, but the full equation for the single-ion activity coefficient is shown in Equation 2.22 below (Pitzer, 1991). Supporting formulas for the *F* and Z_M values can be seen in Equation 2.23 and 2.24 below.

$$\ln(\gamma_M) = Z_M^2 F + \sum_a m_a(2B_{Ma} + ZC_{Ma}) + \sum_c m_c(2\Phi_{Ma} + \sum_a m_a \Psi_{Mca}) \tag{2.22}$$
$$+ \sum_a \sum_{a'} m_a m_{a'} \Psi_{Maa'} + Z_M \sum_c \sum_a m_c m_a C_{ca} + 2\sum_n m_n \lambda_{Mn}$$

$$F = f^{\gamma} + \sum_c \sum_a m_c m_a B'_{ca} + \sum_{c<} \sum_{c'} m_c m_{c'} \Phi'_{cc'} + \sum_{a<} \sum_{a'} m_a m_{a'} \Phi'_{aa'} \quad (2.23)$$

$$Z_M = \sum_i m_i |z_i| \quad (2.24)$$

β, C^{φ}, α, θ, λ, and ψ values are tabulated in the THEREDA for many ion pairings and groups. The use of the Pitzer computational method in PHREEQC requires the use of a PITZER data block in either the input file or the database used. Similar to SIT, if Pitzer cannot determine an activity coefficient, it will default to using the Davies and WATEQ Debye-Hückel equations. The use of SIT and PITZER in PHREEQC are mutually exclusive, and cannot be used in the same simulation (Parkhurst, 1999).

Surface Complexation & Cation Exchange

Surface complexation and cation exchange are the two components used in modelling sorption as they are used to accurately describe specific chemical sorption and non-specific Coulombic sorption respectively. There are several types of equilibria that are taken into consideration in the model, which can be seen in Equations 2.27 – 2.35 below (Stumm, 1996). These equations are shown considering a fictitious metal Me^{+z}. In addition to the surface complexation reactions, acid-base equilibria reactions describing the pH dependence of surface-site speciation are shown in Equation 2.25 and 2.26 below.

Acid-Base Equilibria

$$S - OH + H^+ \leftrightarrow S - OH_2^+ \quad (2.25)$$

$$S - OH \leftrightarrow S - O^- + H^+ \quad (2.26)$$

Metal Binding

$$\mathrm{S-OH + Me^{+z} \leftrightarrow S-OMe^{+(z-1)} + H^{+}} \quad (2.27)$$

$$\mathrm{S-OH + \ Me^{+z} + H_2O \leftrightarrow S-OMeOH^{+(z-2)} + 2H^{+}} \quad (2.28)$$

$$\mathrm{S-OH + \ Me^{+z} + 2\ H_2O \leftrightarrow S-OMe(OH)_2{}^{+(z-3)} + 3H^{+}} \quad (2.29)$$

Ligand Exchange

$$\mathrm{S-OH + L^{-y} \leftrightarrow SL^{+(1-y)} + OH^{-}} \quad (2.30)$$

Ternary Complex Formation (Type A)

$$\mathrm{S-OH + L^{-y} + \ Me^{+z} \leftrightarrow S-OMeL^{+(z-y-1)} + H^{+}} \quad (2.31)$$

$$\mathrm{S-OH + 2L^{-y} + \ Me^{+z} \leftrightarrow S-OMeL_2^{+(z-2y-1)} + H^{+}} \quad (2.32)$$

$$\mathrm{S-OH + 3L^{-y} + \ Me^{+z} \leftrightarrow S-OMeL_3^{+(z-3y-1)} + H^{+}} \quad (2.33)$$

Ternary Complex Formation (Type B)

$$\mathrm{S-OH + L^{-y} + \ Me^{+z} + H^{+} \leftrightarrow S-MeL^{+(z-y+1)} + H_2O} \quad (2.34)$$

Cation Exchange

$$z/x\,(R^{-})_x Me'^{+x} + Me^{+z} \leftrightarrow (R^{-})_z Me^{+z} + z/x\,Me'^{+x} \quad (2.35)$$

Chapter 3

Experimental Methods

All materials used (including software and experimental equipment), and experimental procedures conducted in this work were the same as those summarised in Riddoch (2016). This chapter outlines the difference between the work performed for this thesis and that outlined in Riddoch (2016).

3.1 Saline Sample Solution Preparation

Sample solutions were made saline with the addition of $NaCl$ and $CaCl_2$ in a molar ratio of Na/Ca equal to 2.7, as defined by the SR-270-PW reference groundwater brine solution in Vilks (2017). The composition of the two salts used in combination with deionized water is $NaCl$ and $CaCl_2{\cdot}2H_2O$. The mass of each salt per liter of deionized water for each ionic strength solution used in the experiments of this work can be seen in Table 3.1 below.

Table 3.1: Salt masses used in preparation of saline sample solutions.

I	***NaCl*** **(g/L)**	***$CaCl_2 \cdot 2H_2O$*** **(g/L)**
0.01	0.277	0.258
0.1	2.768	2.579
1.0	15.380	14.329
4.0	92.278	85.973
5.0	138.417	128.960
6.0	166.101	154.752

3.2 pH Calibrations for *Na-Ca-Cl* Solutions

Acid-base titrations were conducted using the same Metrohm titrator used in Riddoch (2016). The experimental procedure for this work includes the testing of six solutions in total: 0.01, 0.1, 1.0, 4.0, and 6.0 M *Na-Ca-Cl* solutions, and one solution of deionized (DI) water. The initial solution volume and pH remained unchanged, but solutions were placed in 250 mL beakers. To account for the reduction in beaker volume, tests were only done to a maximum pH_M of 11 instead of 12.

3.3 ICP-MS Measurement Procedures

Although the ICP-MS used in in this work is designed to be able to measure samples with an *I* up to 0.75 M (Agilent Technologies, 2013), the relative standard deviation (RSD), stated in the output files of sample measurements was found to be higher when the *I* approaches this limit. In addition, higher *I* samples result in a greater buildup of material on the copper cone in the ICP-MS. In order to remediate these issues, all samples were diluted by a factor of 10 after centrifugation and before sample measurements. Due to the

larger dilution, the volume of supernatant removed from the centrifuge tube was less than that stated in Riddoch (2016).

3.4 Ionic Strength Effects on Sorption of Pd(II)

Pd sorption experiments were conducted in two additional *I* solutions of *Na-Ca-Cl* (with an unadjusted pH), above those conducted in Riddoch (2016); 5.0 and 6.0 M. This was done on Na-illite, Na-bentonite (MX-80), and Queenston shale in order to further investigate the dependence of K_d on *I*.

3.5 pH Effects on Sorption of Pd(II)

Pd sorption experiments were conducted on Na-illite and Na-bentonite (MX-80), in 0.01 M *I Na-Ca-Cl* solutions with a pH_C of 3, 4, 5, and 6; 0.1, 1.0, and 4.0 M *I* with a pH_C of 3 and 4; and 6.0 M *I* with a pH_C of 3, 4, 5, 6, 7, 8, and 9. They were also conducted on Queenston shale on 6.0 M *I Na-Ca-Cl* solutions with a pH_C of 5, 6, 7, 8, and 9. This was done following the same experimental procedure outlined in Riddoch (2016), in order to further determine and expand upon the dependence of K_d on pH at various levels of *I*.

3.6 Materials

In addition to the materials described in Riddoch (2016), titration tests were conducted with the use of a Metrohm 916 Ti-Touch, and element concentration

measurements were conducted with a Triple Quad 8800 ICP-MS from Agilent Technologies (model number G3663A).

Chapter 4

Modelling Methods

A *2-site protolysis non-electrostatic surface complexation and cation exchange* (2SPNE SC/CE), model was used with the program PHREEQC (version 3.3.12), to model the sorption of Pd(II), and a 2SPNE SC model for Np(IV), and Np(V), all individually onto Na-illite, and Na-montmorillonite. The model was first confirmed and validated against known sorption model results for Th(IV) onto illite and montmorillonite. Strong and weak-binding surface sites were considered in this model despite low sorbate concentrations, which results in weak sites having a negligible effect compared to the strong sites which dominate sorption processes despite a lower specific surface site capacity, as they form much stronger metal complexes. Very few weak surface complexation constants were considered in the model, as they are not well established in literature. Surface complexation and cation exchange were the only sorption mechanisms considered in all models, as there is likely no physical incorporation of or structural penetration by Pd(II), Np(IV), or Np(V) into illite or montmorillonite due to ionic radii constraints. The electric double layer was not accounted for, and therefore a single layer model was used, as the thickness data required for implementing the double-layer model is not known. The diffuse layer model

was turned off in PHREEQC by using the *–no_edl* flag in the *SURFACE* data block (see Appendix B). The cation exchange component of the model was added for the modelling of Pd(II) in order to help account for acidic sorption edge features at low ionic strength.

4.1 Thermodynamic Data

The initial aqueous master species concentrations of brine salt ions, and elements under study, defined in the *SOLUTION* data blocks can be seen in Table 4.1 below for the solution ionic strengths of 0.1 & 1.0 M $NaClO_4$ used in the sorption model confirmation of Th(IV) outlined in Bradbury (2005b, 2009b). These parameters are also shown in Table 4.2 for solution ionic strengths of 0.01, 0.1, 1.0, 4.0, & 6.0 M *Na-Ca-Cl* (molar ratio of 2.7 Na/Ca), used in the sorption modelling of Pd(II), Np(IV), and Np(V). Th(IV), Pd(II), Np(IV), and Np(V) are listed with their initial concentrations only for the ionic strengths of solution that they were modelled in. The Th(IV) sorption model reference results were for 0.1 & 1.0 M brine solutions for sorption onto illite, and only 1.0 M for montmorillonite to match the reference cases obtained from Bradbury (2005b, 2009b). Sorption of Pd(II) was found to be dependent on *I*, so all brine concentrations were modelled (with the exception of 6.0 M). Pd(II) was modelled using the specific-ion interaction theory (SIT), computational method, which is only accurate up to a maximum solution ionic strength of 4.0 M (Grenthe, 1997). No database containing Pitzer parameters was known to be publicly available at the time of modelling so the 6.0 M experimental results were therefore not modelled. In Nagasaki (2017), it was found that the K_d values for the sorption of Np(IV) were dependent on *I*; therefore, the experimental data from the same source were modelled for each concentration of solution salinity: 0.1, 4.0, and 6.0 M. It was found in Nagasaki (2015), that K_d values for Np(V) sorption on both illite and montmorillonite were

independent of solution ionic strength above 0.10 M. The K_d values were still modelled at the same I as the experimental conditions: 4.6 M. These solutions were also defined in the data block to have an E_h of -200 mV at a nominal pH of 6.0 in accordance with the SR-270-PW reference groundwater brine as defined by the NWMO in Vilks (2017).

Table 4.1: Aqueous species defined in solution data blocks for Th(IV).

Initial Concentration (M) at I =	0.1 M	1.0 M
Na^{+}	0.1	1.0
ClO_4^{-}	0.1	1.0
Th^{+4}	1×10^{-9}	1×10^{-9}

Table 4.2: Aqueous species defined in solution data blocks for Pd(II), Np(IV), and Np(V).

C_i (M) at I =	0.01 M	0.1 M	1.0 M	4.0 M	4.6 M	6.0 M
Na^{+}	0.004737	0.04737	0.4737	1.89474	2.17895	2.84211
Ca^{+}	0.001754	0.01754	0.1754	0.70175	0.80701	1.05263
Cl^{-}	0.008246	0.08246	0.8246	3.29824	3.79298	4.94974
Pd^{+2}	1×10^{-7}	1×10^{-7}	1×10^{-7}	1×10^{-7}		-
Np^{+4}	-	1×10^{-11}	-	1×10^{-11}		1×10^{-11}
Np^{+5}	-	-	-		1×10^{-5}	-

For the model confirmation with Th(IV), the referenced C_i value used in Bradbury (2005b, 2009b), was 10^{-9} M, so the same value was chosen for this work and defined in the code. In Riddoch (2016), it was found that the Freundlich isotherms for Pd(II) had a slope equal to 1 for solution ionic strengths of 0.1, 1.0, and 4.0 M for both illite and MX-80. This indicates that Pd(II) forms inner-sphere and outer-sphere complexes inside the Stern Layer and that sorption is independent from the initial concentration of Pd(II) in solution for those ionic strengths. However, since the C_i used in the experimental procedures (10^{-7} M), was close to the solubility limit (1.9×10^{-6} M – 5.9×10^{-5} M for 0.1 – 4.0 M I), and sorption in

additional ionic strengths to those tested were modelled, the C_i used was chosen to be the same as that used in the experimental procedures: 10^{-7} M. Due to the low solubility of Np(IV), isotherm tests were not able to be conducted in Nagasaki (2017), and therefore the same C_i used in the experimental procedures was used in the sorption modelling in this work: 10^{-11} M. The plotted Freundlich isotherms of Np(V) sorption in the SR-270-PW reference brine solution were found to be linear on Log-Log plots with slopes approximately equal to 1 for both illite and MX-80, indicating that the experimental results could be modelled at any C_i below the solubility limit (Nagasaki, 2015). A C_i of 10^{-5} M was used for the modelling in this work, as the solubility limit of Np(V) was found to be approximately 10^{-4} M in diluted neutral pH solutions in Itagaki (1992).

Based on the aqueous master species included in the PHREEQC input files listed in the tables above, the resulting aqueous species and their formation reactions can be seen in Table 4.3 below, divided up between the three databases used: the JAEA TDB (version 140331s0.tdb), and the THEREDA release number 4 and 7 for Np(V) and Np(IV) respectively (THEREDA R04, 2015 & R07, 2013). In order for PHREEQC to include the perchlorate aqueous species in the Th(IV) model confirmation, the +VII redox state had to be manually entered into the *SOLUTION_MASTER_SPECIES* data block in the JAEA TDB.

Table 4.3: Formation reactions of relevant species.

Formation Reaction	Log *K*	Error
JAEA TDB:		
$H^+ + OH^- \leftrightarrow H_2O$	-14.00	0.015
$4H^+ + 4e^- - 2H_2O \leftrightarrow O_2$	83.09	0.010
$Ca^{2+} + H_2O - H^+ - 2e^- \leftrightarrow CaOH^+$	-12.85	0.50
$Cl^- + H_2O - H^+ - 2e^- \leftrightarrow HClO$	-50.51	0.109
$Cl^- + 2H_2O - 3H^+ - 4e^- \leftrightarrow HClO_2$	-105.91	0.708
$Cl^- + H_2O - 2H^+ - 2e^- \leftrightarrow ClO^-$	-57.93	0.708
$Cl^- + 2H_2O - 4H^+ - 4e^- \leftrightarrow ClO_2^-$	-107.87	0.708

Formation Reaction	Log *K*	Error
JAEA TDB:		
$Cl^- + 3H_2O - 6H^+ - 6e^- \leftrightarrow ClO_3^-$	-146.24	0.236
$Cl^- + 4H_2O - 8H^+ - 8e^- \leftrightarrow ClO_4^-$	-187.78	0.108
$Th^{+4} + H_2O - H^+ \leftrightarrow ThOH^{+3}$	-2.50	0.50
$Th^{+4} + 2H_2O - 2H^+ \leftrightarrow Th(OH)_2^{+2}$	-6.20	0.50
$Th^{+4} + 3H_2O - 3H^+ \leftrightarrow Th(OH)_3^+$	-	-
$Th^{+4} + 4H_2O - 4H^+ \leftrightarrow Th(OH)_4$	-17.40	0.70
$Pd^{+2} + H_2O - H^+ \leftrightarrow PdOH^+$	-	-
$Pd^{+2} + 2H_2O - 2H^+ \leftrightarrow Pd(OH)_2$	-3.49	-
$Pd^{+2} + 3H_2O - 3H^+ \leftrightarrow Pd(OH)_3^-$	-15.48	0.35
$Pd^{+2} + Cl^- \leftrightarrow PdCl^+$	5.00	0.24
$Pd^{+2} + 2Cl^- \leftrightarrow PdCl_2$	8.42	0.31
$Pd^{+2} + 3Cl^- \leftrightarrow PdCl_3^-$	10.93	0.38
THEREDA (R07):		
$Np^{+4} + H_2O - H^+ \leftrightarrow NpOH^{+3}$	0.55	-
$Np^{+4} + 2H_2O - 2H^+ \leftrightarrow Np(OH)_2^{+2}$	0.35	-
$Np^{+4} + 3H_2O - 3H^+ \leftrightarrow Np(OH)_3^+$	-2.80	-
$Np^{+4} + 4H_2O - 4H^+ \leftrightarrow Np(OH)_4$	-8.30	-
$Np^{+4} + 5H_2O - 5H^+ \leftrightarrow Np(OH)_5^-$	-	-
$Np^{+4} + Cl^- \leftrightarrow NpCl^{+3}$	1.50	-
THEREDA (R04):		
$NpO_2^+ + H_2O - H^+ \leftrightarrow NpO_2OH$	-11.30	-
$NpO_2^+ + 2H_2O - 2H^+ \leftrightarrow NpO_2(OH)_2^-$	-23.60	-

In order to calculate the aqueous solution concentrations of the various species listed in Table 4.3 above, the mass-action equation (2.14), is used in combination with the corresponding activity coefficient (γ_i), and Log *K* values. In order to calculate the activity coefficient for each aqueous species listed for the JAEA TDB, the computational method of the SIT is used in PHREEQC with the *SIT* keyword data block contained in the database. The *SIT* data block in the JAEA TDB contains epsilon values for a number of the aqueous species listed for the database, and can be seen in Table 4.4. For the species that do not have epsilon values, PHREEQC defaults to the Davies equation (2.15), for charged species and the WATEQ Debye-Hückel equation (2.16), for neutral species. However, of the species listed for a simulation of Pd that does not have an epsilon value in the database,

only one has an a^o and b value for the WATEQ Debye-Hückel equation: $CaOH^+$. Since $CaOH^+$ is a charged species, the Davies equation is used. Therefore, the WATEQ Debye-Hückel equation is not used at all in calculating the activities when simulating Pd sorption.

Table 4.4: SIT parameters for select species of Pd(II) from the JAEA TDB (Kitamura, 2014).

Species 1	Species 2	Epsilon Value	Error
H^+	Cl^-	0.12	0.01
H^+	ClO_4^-	0.14	0.02
OH^-	Na^+	0.04	0.01
Ca^{2+}	Cl^-	0.14	0.01
Ca^{2+}	ClO_4^-	0.27	0.03
Cl^-	Na^+	0.03	0.01
ClO_3^-	Na^+	-0.01	0.02
ClO_4^-	Na^+	0.01	0.01
Pd^{+2}	ClO_4^-	0.22	-
$PdCl^+$	ClO_4^-	0.25	0.02
$PdCl_3^-$	Na^+	0.03	0.01
$PdCl_4^{-2}$	Na^+	-0.044	-
$PdCl_3OH^{-2}$	Na^+	-0.044	-
$Pd(OH)_3^-$	Na^+	-0.11	-
$Np(OH)_3^+$	Cl^-	0.35	0.10
$Np(OH)_3^+$	ClO_4^-	0.29	0.15
$Np(OH)_2^{+2}$	ClO_4^-	0.35	0.11
$NpOH^{+3}$	ClO_4^-	0.5	0.05
$NpOH^{+3}$	ClO_4^-	0.49	0.15
$NpCl^{+3}$	ClO_4^-	0.81	0.09
$Th(OH)_3^+$	Cl^-	0.06	0.15
$Th(OH)_3^+$	ClO_4^-	0.15	0.1
$Th(OH)_3^+$	NO_3^-	0.05	0.15
$Th(OH)_2^{+2}$	Cl^-	0.13	0.05
$Th(OH)_2^{+2}$	ClO_4^-	0.33	0.1
$Th(OH)_2^{+2}$	NO_3^-	0.1	0.15
$ThOH^{+3}$	Cl^-	0.19	0.05
$ThOH^{+3}$	ClO_4^-	0.48	0.08
$ThOH^{+3}$	NO_3^-	0.2	0.15
$ThCl^{+3}$	Cl^-	0.62	0.11
$ThCl^{+3}$	ClO_4^-	0.62	0.11

The aqueous species listed in Table 4.3 under the JAEA TDB that form as a result of the salts contained in the solution master species (all but Th & Pd), are not listed for the two THEREDAs because they do not contain the formation reaction constants, and were not required. To calculate the activity coefficients when using the THEREDAs, the Pitzer computational method was used, which does not require the use of formation reaction constants but does utilize a number of parameters listed in Table 4.5 and Table 4.6. The rows in Table 4.5 that are greyed-out are not contained in the R04 THEREDA (2015), used for modelling Np(V).

Table 4.5: Pitzer Parameters for select species of Np(IV) and Np(V) from the THEREDA.

Ion 1	**Ion 2**	β_0	β_1	β_2	C^ϕ	α_1	α_2	θ	λ
H^+	Cl^-	0.176	0.300	-	-	2	-	-	-
Na^+	Cl^-	0.075	0.277	-	0.001	2	-	-	-
Na^+	OH^-	0.104	0.125	-	0.002	2	-	-	-
Ca^{2+}	Cl^-	0.307	1.708	-	0.002	2	-	-	-
Ca^{+2}	OH^-	-0.110	-0.230	-5.72	-	2	50	-	-
$Ca_4(Np(OH)_8)^{+4}$	Cl^-	0.58	8.9	-	0.07	2	-	-	-
Np^{+4}	Cl^-	1.32	13.5	-	-	2	-	-	-
NpO_2^+	Cl^-	0.142	0.281	-	-	2	-	-	-
$Np(OH)_2^{+2}$	Cl^-	0.23	1.9	-	-	2	-	-	-
$NpOH^{+3}$	Cl^-	0.6	5.9	-	-	2	-	-	-
$Np(OH)_3^+$	Cl^-	0.1	0.4	-	-	2	-	-	-
Ca^{+2}	H^+	-	-	-	-	-	-	0.097	-
Na^+	Ca^{+2}	-	-	-	-	-	-	0.058	-
Na^+	H^+	-	-	-	-	-	-	0.035	-
$NpO_2(OH)_2^-$	Cl^-	-	-	-	-	-	-	-0.24	-
OH^-	Cl^-	-	-	-	-	-	-	-0.055	-
NpO_2OH	Cl^-	-	-	-	-	-	-	-	-0.19

*All values rounded to 3 decimal places. Greyed-out ion pairs are not contained in the R04 THEREDA (2015).

Table 4.6: Pitzer Parameter Psi for select species from the THEREDA.

Ion 1	Ion 2	Ion 3	ψ
Ca^{+2}	Cl^-	OH^-	-0.038
Ca^{+2}	H^+	Cl^-	-0.012
Na^+	Ca^{+2}	Cl^-	-0.001
Na^+	Ca^{+2}	OH^-	0.255
Na^+	H^+	Cl^-	-0.003
Na^+	Cl^-	OH^-	-0.004

4.2 Surface Definitions

To define the surface properties of the soil being modelled, PHREEQC requires parameters to be outlined in a *SURFACE* data block in the input file(s). The quantitative values include the total number of surface sites (in moles), the specific surface area (in m^2/g) , and the total mass of solid (in grams). The qualitative parameters are whether or not the electrostatic diffuse second layer is being considered in the model (and if so, the specified thickness), and whether the surface charge will be counterbalanced in the diffuse layer with counter-ions only. The electrostatic double layer was not considered in this model, and was turned off using the *-no_edl* flag in the data block. The total number of sites are calculated using the equation below.

$$\text{Total Sites} = \text{Specific Surface Site Capacity} \times \text{Total Mass of Solid} \qquad (4.1)$$

The specific surface site capacity used in calculating the total number of strong-bonding sites was that recommended in Bradbury (2009b, 2005b) for both illite and montmorillonite: 2×10^{-3} mol/kg. In all models the total solution volume used was 1 L and the total mass of solid used was 1 g, resulting in a liquid-to-solid ratio of 1.0 m^3/kg, or 1.0 g/L. These values were used in combination with equation 4.1 to obtain a total number of

strong sites equal to 2×10^{-6} moles. The illite used by Bradbury (2005b, 2009b) in the development of the LFER was collected from the Le Puyen-Velay (Haute-Loire), region in France, and has a specific surface area of 97 m^2/g, whereas the illite used in this research for Pd and Np sorption was collected from Silver Hill in Montana, USA, and has a SSA of 70 m^2/g (Pivovarov, 2004). The differences in illite soil properties were accounted for by modifying the total number of sites in the model by a factor of 70/97, so that the models could be compared to the experimental results obtained in this work. This modification made to the number of surface sites for illite was not done in the Th(IV) model confirmation, as there are no experimental results in this work to compare against. The specific surface area for the Na-bentonite MX-80 used in experiments (acquired from the American Colloid Company, ACC), was obtained from Bertetti (2016), with a value of 26.2 m^2/g. The soil properties of both illite sources, and bentonite can be seen in Table 4.7, and the soil parameters contained in the PHREEQC input files can be seen in Table 4.8 below. The same process was followed using weak 1 (W_1) and weak 2 (W_2) surface site capacities for illite and montmorillonite (4×10^{-2} mol/kg), obtained from Bradbury (2009b, 2005b), and can be seen in Table 4.9 below.

Table 4.7: Soil properties.

Solid	Site Capacity (mmol/kg)	Surface Area (m^2/g)	Ion-Exchange Capacity (meq/kg)
Illite (France)	2	97.0	225
Illite (Montana)	1.44	70.0	210
Bentonite (MX-80)	2	26.2	1021

Table 4.8: Soil parameters entered into PHREEQC input file.

Solid	Total Sites (mol)	Surface Area (m^2/g)	Solid Mass (g)	Exchange Capacity (mmol)
Illite	1.44×10^{-6}	70.0	1	0.21
Montmorillonite	2.00×10^{-6}	26.2	1	1.021

Table 4.9: Weak surface site properties and parameters entered into PHREEQC input file.

Solid	W_1 Site Cap. (mmol/kg)	W_2 Site Cap. (mmol/kg)	W_1 Total Sites (mol)	W_2 Total Sites (mol)
Illite	28.9	28.9	2.89×10^{-5}	2.89×10^{-5}
Montmorillonite	40	40	4.00×10^{-5}	4.00×10^{-5}

For Pd(II) only, cation exchange parameters were added to the sorption model to improve the fit of the sorption edge to the experimental data. Cation exchange capacities were obtained from Bradbury (2009b), Pivovarov (2004), and Villa-Alfageme (2014) for the French illite, American illite, and MX-80 respectively, and are shown in Table 4.7 above. Ion-exchange capacities are defined for PHREEQC in the *EXCAHNGE* data block in the input file in units of moles, which can be seen in the right-most column of Table 4.8 above. Selectivity coefficients for H^+, K^+, Mg^{+2}, Ca^{+2}, and Al^{+3} were all obtained from Bradbury (2009a), for illite, and were also adopted for montmorillonite due to their absence in the existing literature (sorption-edge sensitivity to these parameters is low). The selectivity coefficient for Ca^{+2} was estimated to have a value of 6.0 from Aku Itälä (2012), and can be seen along with other selectivity coefficient values in Table 4.10 below.

Table 4.10: Selectivity coefficients of cation exchange reactions.

Cation Exchange Reaction	Selectivity Coefficient (K_c)	
	Na-illite	Na-Montmorillonite
$S\text{-}ONa + H^+ \leftrightarrow S\text{-}OH + Na^+$	1.0	1.0
$S\text{-}ONa + K^+ \leftrightarrow S\text{-}OK + Na^+$	12.9	12.9
$2S\text{-}ONa + Mg^{+2} \leftrightarrow S\text{-}O_2Mg + 2Na^+$	11.0	11.0
$2S\text{-}ONa + Ca^{+2} \leftrightarrow S\text{-}O_2Ca + 2Na^+$	11.0	6.0
$3S\text{-}ONa + Al^{+3} \leftrightarrow S\text{-}O_3Al + 3Na^+$	10.0	10.0
$2S\text{-}ONa + Pd^{+2} \leftrightarrow S\text{-}O_2Pd + 2Na^+$	-	-
$S\text{-}ONa + PdOH^+ \leftrightarrow S\text{-}OPdOH + Na^+$	-	-

Surface hydroxyl groups can behave as an acid or base and have associated reaction constants for each soil called protonation and deprotonation surface complexation constants. These constants for strong and weak surface sites were obtained from Bradbury (2009b, 2005b), and can be seen for illite and montmorillonite in Table 4.11 below.

Table 4.11: Protonation and deprotonation reactions for illite and montmorillonite.

Surface Complexation Reaction	Log^{S} K_I	Log^{S} K_M	Log^{W1} K_I	Log^{W1} K_M	Log^{W2} K_I	Log^{W2} K_M
Acid-Base:						
$S\text{-}OH + H^+ \leftrightarrow S\text{-}OH_2^+$	4.0	4.5	4.0	4.5	8.5	6.0
$S\text{-}OH - H^+ \leftrightarrow S\text{-}O^-$	-6.2	-7.9	-6.2	-7.9	-10.5	-10.5

4.3 Surface Complexation Reactions

Given the possible aqueous species of Th(IV), Pd(II), Np(IV), and Np(V) listed in Table 4.3, the corresponding surface complexes and cation exchanges were determined according to the metal binding, ternary surface complex, and exchange species formation theories outlined in Equations 2.27 – 2.29, Equations 2.31 – 2.34, and Equation 2.35 respectively. These surface complexes can be seen with their corresponding aqueous species and formation reaction constants in Table 4.12, Table 4.13, Table 4.14, and Table 4.15 for Th(IV), Pd(II), Np(IV), and Np(V) respectively.

Table 4.12: ASFRCs for Th(IV) sorption from Neck (2000).

Surface Complex	Aqueous Species Formation Reaction	Log *K*	Error
Metal Binding:			
$S\text{-}OTh^{+3}$	$Th^{+4} + H_2O - H^+ \leftrightarrow ThOH^{+3}$	-2.20	-
$S\text{-}OThOH^{+2}$	$Th^{+4} + 2H_2O - 2H^+ \leftrightarrow Th(OH)_2^{+2}$	-6.00	-
$S\text{-}OTh(OH)_2^+$	$Th^{+4} + 3H_2O - 3H^+ \leftrightarrow Th(OH)_3^+$	-11.00	-

Surface Complex	Aqueous Species Formation Reaction	Log *K*	Error
Metal Binding:			
$S\text{-}OTh(OH)_3$	$Th^{+4} + 4H_2O - 4H^+ \leftrightarrow Th(OH)_4$	-17.50	-
$S\text{-}OTh(OH)_4^-$	$Th^{+4} + 5H_2O - 4H^+ \leftrightarrow Th(OH)_5^-$	-	-

The formation reaction constant for $Th(OH)_3^+$ was not contained in the JAEA TDB, and was therefore added to the database for the corresponding $S\text{-}OTh(OH)_2^+$ surface species. A value of -11.0 was selected from Bradbury (2009b), which was obtained originally from Neck (2001). In order to confirm the model with Th(IV) by obtaining the same results as those in Bradbury (2005b, 2009b), the formation reaction constants for all aqueous species had to be modified in the JAEA TDB to those obtained from Neck (2001). All altered values fall within the error range given by the original values contained in the JAEA database. No formation reaction constants are known for the $Th(OH)_5^-$ aqueous species; therefore, this species was excluded from the database, as illustrated in Table 4.12. The formation reaction constants between redox states did not need to be modified as Th(IV) dominates in solution by many orders of magnitude.

Table 4.13: ASFRCs for Pd(II) sorption from JAEA TDB & LFER.

Surface Complex	Aqueous Species Formation Reaction	Log *K*	Error
Metal Binding:			
$S\text{-}OPd^+$	$Pd^{+2} + H_2O - H^+ \leftrightarrow PdOH^+$	-1.85	0.29
$S\text{-}OPdOH$	$Pd^{+2} + 2H_2O - 2H^+ \leftrightarrow Pd(OH)_2$	-3.49	-
$S\text{-}OPd(OH)_2^-$	$Pd^{+2} + 3H_2O - 3H^+ \leftrightarrow Pd(OH)_3^-$	-15.48	0.35
Ternary:			
$S\text{-}OPdCl$	$Pd^{+2} + Cl^- \leftrightarrow PdCl^+$	5.00	0.24
$S\text{-}OPdCl_2^-$	$Pd^{+2} + 2Cl^- \leftrightarrow PdCl_2$	8.42	0.31
$S\text{-}OPdCl_3^{-2}$	$Pd^{+2} + 3Cl^- \leftrightarrow PdCl_3^-$	10.93	0.38
$S\text{-}OPdCl_4^{-3}$	$Pd^{+2} + 4Cl^- \leftrightarrow PdCl_4^{-2}$	13.05	0.59
$S\text{-}OPdCl_3OH^{-3}$	$Pd^{+2} + 3Cl^- + H_2O - H^+ \leftrightarrow PdCl_3OH^{-2}$	3.77	0.63

Bradbury (2005), uses formation reaction constants for the $Pd(OH)_2$ and $Pd(OH)_3^-$ aqueous species obtained from Hummel (2002), but the JAEA TDB references constants from a 2012 paper by Rai. With this discrepancy in mind, the most recent values were chosen, leaving the values in the database unchanged, although the $Pd(OH)_3^-$ species has an error range that includes the constant used in Bradbury (2005b). No formation reaction constant for the aqueous $PdOH^+$ species was listed in Bradbury (2005b), as their referenced study (Hummel, 2002), did not attempt to fit a formation reaction constant to the solubility data of Middlesworth et al. (1999), due to the species' small effect on solubility, and the large scatter of the experimental data. In addition to having no reaction constant for the aqueous species in Bradbury (2005b), there was also no surface complexation constant for the $S\text{-}OPd^+$ surface species. In Vilks (2014), a recommended surface complexation constant ($Log^S K$) for $S\text{-}OPd^+$ of 6.4 was proposed for both illite and montmorillonite, so this value was adopted for the sorption modelling in this work. In order to derive a formation reaction constant for the corresponding aqueous species from the adopted surface complexation constant, the **L**inear **F**ree **E**nergy **R**elationship (LFER), was used. The LFER developed in Bradbury (2005b, 2009), relates the two values for metal-binding complexes for illite (Bradbury, 2009b), and montmorillonite (Bradbury, 2005b), shown in equations 4.2 and 4.3 respectively. Since the surface complexation constant was the same value for both clays, equations 4.2 and 4.3 produced two different hydrolysis constants, which were averaged, and can be seen with its respective error in Table 4.13 above. In another technical report it is stated that the aqueous species formation reaction constant used in Vilks (2017), that corresponds with this surface species was -1.86, which is well within the error of the value calculated using the method described.

$$\mathrm{Log}^{\mathrm{S}}K_I = 7.9 \pm 0.4 + (0.83 \pm 0.02)\,\mathrm{Log}^{\mathrm{OH}}K \tag{4.2}$$

$$\mathrm{Log}^{\mathrm{S}}K_M = 8.1 \pm 0.3 + (0.90 \pm 0.02)\,\mathrm{Log}^{\mathrm{OH}}K \tag{4.3}$$

The LFER was developed by Bradbury (2005b, 2009), by correlating hydrolysis constants from solubility data of various elements with the surface complexation constant of the corresponding surface species for both strong and weak surface sites. These correlations, when divided up according to the solid used for the sorption constants, were found to be linear when placed on a Log-Log plot. The formation reaction constants between redox states did not need to be modified, as Pd(II) dominates in solution by many orders of magnitude.

Table 4.14: ASFRCs for Np(IV) sorption from the R07 THEREDA (2013).

Surface Complex	Aqueous Species Formation Reaction	Log *K*	Error
Metal Binding:			
$S\text{-}ONp^{+3}$	$Np^{+4} + H_2O - H^+ \leftrightarrow NpOH^{+3}$	0.55	-
$S\text{-}ONpOH^{+2}$	$Np^{+4} + 2H_2O - 2H^+ \leftrightarrow Np(OH)_2^{+2}$	0.35	-
$S\text{-}ONp(OH)_2^+$	$Np^{+4} + 3H_2O - 3H^+ \leftrightarrow Np(OH)_3^+$	-2.80	-
$S\text{-}ONp(OH)_3$	$Np^{+4} + 4H_2O - 4H^+ \leftrightarrow Np(OH)_4$	-8.30	-
$S\text{-}ONp(OH)_4^-$	$Np^{+4} + 5H_2O - 5H^+ \leftrightarrow Np(OH)_5^-$	-	-
Ternary:			
$S\text{-}ONpCl^{+2}$	$Np^{+4} + Cl^- \leftrightarrow NpCl^{+3}$	1.50	-

Although the values contained in the JAEA TDB and used in Bradbury (2005b), (Neck, 2000), for the Np(IV) formation reaction constants were both different, the values chosen for this work were those originally contained in the THEREDA, whose source reference is the **N**uclear **E**nergy **A**gency (NEA), as seen in Table 4.14 above. The formation reaction constants between redox states did not need to be modified, as Np(IV) dominates in solution by many orders of magnitude. The Np(V) reaction constants for the two aqueous species used in Bradbury (2009), were the same as those obtained from the NEA and were therefore left unchanged as seen in Table 4.15 below. In order to ensure that all Np species in solution were in the +V redox state, the formation reaction constant was set to 30, as seen in the table below.

Table 4.15: ASFRCs for Np(V) sorption from the R04 THEREDA (2015).

Surface Complex	Aqueous Species Formation Reaction	Log K	Error
Metal Binding:			
$S\text{-}ONpO_2$	$NpO_2^+ + H_2O - H^+ \leftrightarrow NpO_2OH$	-11.30	-
$S\text{-}ONpO_2OH^-$	$NpO_2^+ + 2H_2O - 2H^+ \leftrightarrow NpO_2(OH)_2^-$	-23.60	-
Redox:			
-	$H_2O + Np^{+4} - 4H^+ - e^- \leftrightarrow NpO_2^+$	30	-

The surface complexation constants used for the Th(IV) model confirmation were the same as those used for illite (Bradbury, 2009b), and montmorillonite (Bradbury, 2005b), in the reference cases, and can be seen in Table 4.16 below.

Table 4.16: SCCs used for Th(IV) sorption.

Surface Complexation Reaction	$Log^S K_I$	$Log^S K_M$
Metal Binding:		
$S\text{-}OH + Th^{+4} \leftrightarrow S\text{-}OTh^{+3} + H^+$	7.4	7.2
$S\text{-}OH + Th^{+4} + H_2O \leftrightarrow S\text{-}OThOH^{+2} + 2H^+$	2.3	2.7
$S\text{-}OH + Th^{+4} + 2H_2O \leftrightarrow S\text{-}OTh(OH)_2^+ + 3H^+$	-2.4	-2.6
$S\text{-}OH + Th^{+4} + 3H_2O \leftrightarrow S\text{-}OTh(OH)_3 + 4H^+$	-8.8	-9.1
$S\text{-}OH + Th^{+4} + 4H_2O \leftrightarrow S\text{-}OTh(OH)_4^- + 5H^+$	-15.3	-16.9

In order to determine the surface complexation constants for Pd(II), the two LFER equations for illite and montmorillonite above (4.2 & 4.3), were used with the formation reaction constants for the $Pd(OH)_2$ and $Pd(OH)_3^-$ aqueous species listed in the JAEA TDB (shown in Table 4.13 above). These values, along with the $S\text{-}OPd^+$ surface complexation constant from Vilks (2017), can be seen for the metal-binding constants in Table 4.17 below. To determine the sorption reaction constants for ternary complexes, the methodology followed in Fein (2002), for Type B ternary surface complexes (shown in Equation 2.34), with organic ligands was analogously followed for Type A (shown in Equations 2.31 – 2.33), with inorganic ligands for this work. Fein found that for Type B

complexes there is a linear correlation between the logarithm of the ternary surface complexation constant (*Log* K_T), and the sum of the logarithm of the surface complexation constant for the organic ligand-surface complex (*Log* $K_{S\text{-}L}$), with the logarithm of the formation reaction constant for the metal-organic ligand aqueous complex (*Log* $K_{M\text{-}L\ (aq)}$), as seen in Equation 4.4 below. Fein found this correlation to have a correlation coefficient of 0.992, which may be approximated as unity. For chloride species, it was determined by Vilks (2017), that the sorption of chlorine directly onto shale and bentonite without a metal did not occur. Since illite and montmorillonite are the major clay constituents of shale and bentonite respectively, it can be assumed that the inorganic ligand-surface complex reaction constant (*Log* $K_{S\text{-}L}$), is equal to zero. This reduces the Fein correlation to equating the ternary surface complexation constant (*Log* K_T), to the metal-inorganic ligand aqueous complex formation constant (*Log* $K_{M\text{-}L\ (aq)}$), as seen in Equation 4.5 below. The ternary surface complexation constants for Pd(II) can be seen listed in Table 4.17 below.

$$\text{Log}\, K_T = 0.992\left(\text{Log}\, K_{S-L} + \text{Log}\, K_{M-L\,(aq)}\right) \tag{4.4}$$

$$\text{Log}\, K_T \approx \text{Log}\, K_{M-L\,(aq)} \tag{4.5}$$

Table 4.17: Various surface complexation reactions modeled in PHREEQC for Pd(II).

Surface Complexation Reaction	**Log$^S K_I$**	**Log$^S K_M$**
Metal Binding:		
$S\text{-}OH + Pd^{+2} \leftrightarrow S\text{-}OPd^{+} + H^{+}$	6.4	6.4
$S\text{-}OH + Pd^{+2} + H_2O \leftrightarrow S\text{-}OPdOH + 2H^{+}$	4.96	5.00
$S\text{-}OH + Pd^{+2} + 2H_2O \leftrightarrow S\text{-}OPd(OH)_2^{-} + 3H^{+}$	-5.83	-4.95
Ternary:		
$S\text{-}OH + Pd^{+2} + Cl^{-} \leftrightarrow S\text{-}OPdCl + H^{+}$	5.00	5.00
$S\text{-}OH + Pd^{+2} + 2Cl^{-} \leftrightarrow S\text{-}OPdCl_2^{-} + H^{+}$	8.42	8.42
$S\text{-}OH + Pd^{+2} + 3Cl^{-} \leftrightarrow S\text{-}OPdCl_3^{2-} + H^{+}$	10.93	10.93
$S\text{-}OH + Pd^{+2} + 4Cl^{-} \leftrightarrow S\text{-}OPdCl_4^{3-} + H^{+}$	13.05	13.05
$S\text{-}OH + Pd^{+2} + 5Cl^{-} \leftrightarrow S\text{-}OPdCl_3OH^{3-} + H^{+}$	3.77	3.77

The surface complexation constants for Np(IV) were obtained from Banik (2016), for illite, and Bradbury (2005b), for montmorillonite, and can be seen in Table 4.18 below. Bradbury (2005b), is the only source that contained surface complexation constants for the weak 1 sites for any complex, so their value of 6.7 was included in this work for the *S-ONp*$^{+3}$ surface species, as seen in the table. For the one aqueous chloride species contained in the R07 THEREDA (2013), the same process for Type A ternary surface complexes was followed as that explained for Pd(II) earlier. The reaction constant for the Np(IV) ternary surface species can also be seen in the table below.

Table 4.18: Various surface complexation reactions modeled in PHREEQC for Np(IV).

Surface Complexation Reaction	$Log^{S}K_I$	$Log^{S}K_M$	$Log^{W1}K_M$
Metal Binding:			
$S\text{-}OH + Np^{+4} \leftrightarrow S\text{-}ONp^{+3} + H^{+}$	-	8.5	6.7
$S\text{-}OH + Np^{+4} + H_2O \leftrightarrow S\text{-}NpOH^{+2} + 2H^{+}$	-	8.3	-
$S\text{-}OH + Np^{+4} + 2H_2O \leftrightarrow S\text{-}ONp(OH)_2^{+} + 3H^{+}$	6.4	5.5	-
$S\text{-}OH + Np^{+4} + 3H_2O \leftrightarrow S\text{-}ONp(OH)_3 + 4H^{+}$	0.7	0.1	-
$S\text{-}OH + Np^{+4} + 4H_2O \leftrightarrow S\text{-}ONp(OH)_4^{-} + 5H^{+}$	-5.7	-	-
Ternary:			
$S\text{-}OH + Np^{+4} + Cl^{-} \leftrightarrow S\text{-}ONpCl^{+2} + H^{+}$	1.5	1.5	-

All Np(V) surface complexation constants were obtained from Bradbury (2009b), for illite (which were obtained from Gorgeon (1994)), and Bradbury (2005b), for montmorillonite. Only two surface species were found in the available literature with reaction constant values, so those were the only ones included in this work. These values can be seen in Table 4.19 below.

Table 4.19: Referenced surface complexation reactions modeled in PHREEQC for Np(V).

Surface Complexation Reaction	$Log^S K_I$	$Log^S K_M$
Metal Binding:		
$S\text{-}OH + NpO_2^+ \leftrightarrow S\text{-}ONpO_2 + H^+$	-2.0	-2.8
$S\text{-}OH + NpO_2^+ + H_2O \leftrightarrow S\text{-}ONpO_2OH^- + 2H^+$	-10.3	-12.8

Chapter 5

Results and Analysis

5.1 pH Calibrations for *Na-Ca-Cl* Solutions

In order to derive the pH correction factors for the *Na-Ca-Cl* solutions of different ionic strengths, the measured pH (pH_M), must be plotted against the calculated pH (pH_C). The titrator instrument records the pH_M and the volume of 0.1 N *HCl* and *NaOH* added ($V_{A\ add}$ & $V_{B\ add}$), which can be used in combination with the known initial volume of solution (V_i), and initial concentration of hydrogen ions ($[H^+]_i$), to calculate the concentration of hydrogen or hydroxide ions in solution. This logic is outlined in Equation 5.1. The concentration of *HCl* and *NaOH* can be directly equated to the concentration of H^+ and OH^- ions respectively. These concentrations can also linearly combine with each other as they are both a strong acid and strong base respectively, that completely dissociate into their respective ion pairs. Depending on whether or not the equation indicates a concentration of H^+ or OH^- ions, the correct form of Equation 5.2 below can be used to calculate the pH_C that corresponds with the recorded pH_M.

$$\frac{([H^+]_i \cdot V_i) + ([HCl] \cdot V_{A\,add}) - ([NaOH] \cdot V_{B\,add})}{V_i + V_{A\,add} + V_{B\,add}} = \begin{cases} [H^+], & if > 0 \\ -[OH^-], & if < 0 \end{cases} \quad (5.1)$$

$$pH_C = -\text{Log}[H^+] = 14 + \text{Log}[OH^-] \quad (5.2)$$

The pH_C values were calculated and plotted against the pH_M values recorded by the titrator for five ionic strength solutions of *Na-Ca-Cl* (with a molar ratio of 2.7 between Na and Ca): 0.01, 0.1, 1.0, 4.0, and 6.0 M. These five plots can be seen in Figure 5.1 below, where linear regression was used to produce lines of best fit for each data series.

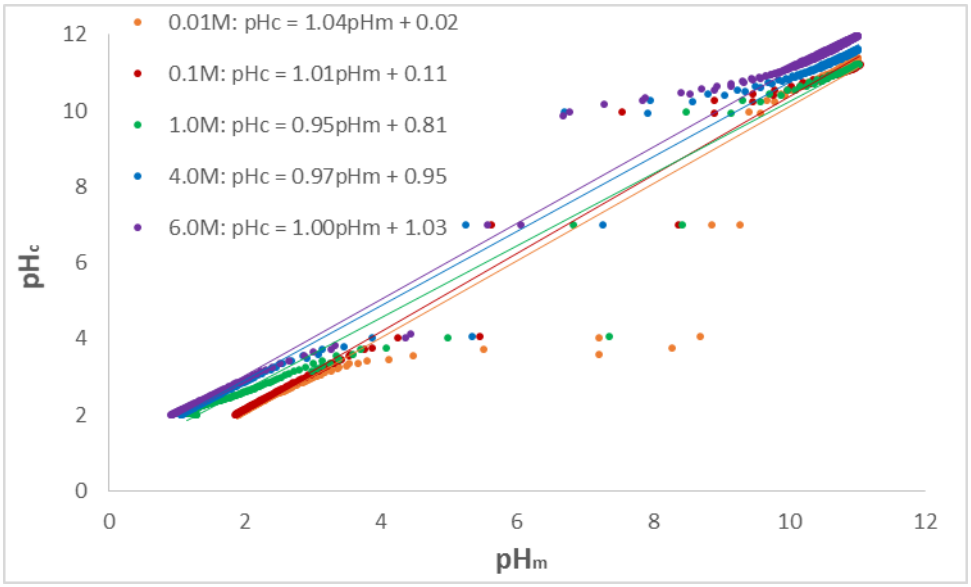

Figure 5.1: Titration curves for *Na-Ca-Cl* solutions.

The equations for the linear trend lines serve a valuable purpose for being able to convert pH_M values to pH_C values for each ionic strength solution, and were used in the experimental procedure for obtaining the correct pH when adjusting sample solutions. These formulas for pH conversion can be seen tabulated in Table 5.1 below.

Table 5.1: pH_C & pH_M relationships for aqueous *Na-Ca-Cl* solutions.

Ionic Strength (M)	Adjustment Equation
0.01	$pH_C = 1.04 \times pH_M + 0.02$
0.1	$pH_C = 1.01 \times pH_M + 0.11$
1.0	$pH_C = 0.95 \times pH_M + 0.81$
4.0	$pH_C = 0.97 \times pH_M + 0.95$
6.0	$pH_C = 1.00 \times pH_M + 1.03$
DI	$pH_C = 1.02 \times pH_M + 0.01$

After obtaining the pH conversion formulas for low ionic strength solutions of *Na-Ca-Cl*, the offset between pH_C and pH_M was still very large, so the same process was followed with DI water in order to obtain a relationship for the offset of the equipment and method. This offset was determined to follow the formula for the trend line obtained through linear regression as seen in Table 5.1 above. The plot and trend line can be seen in Figure 5.2 below.

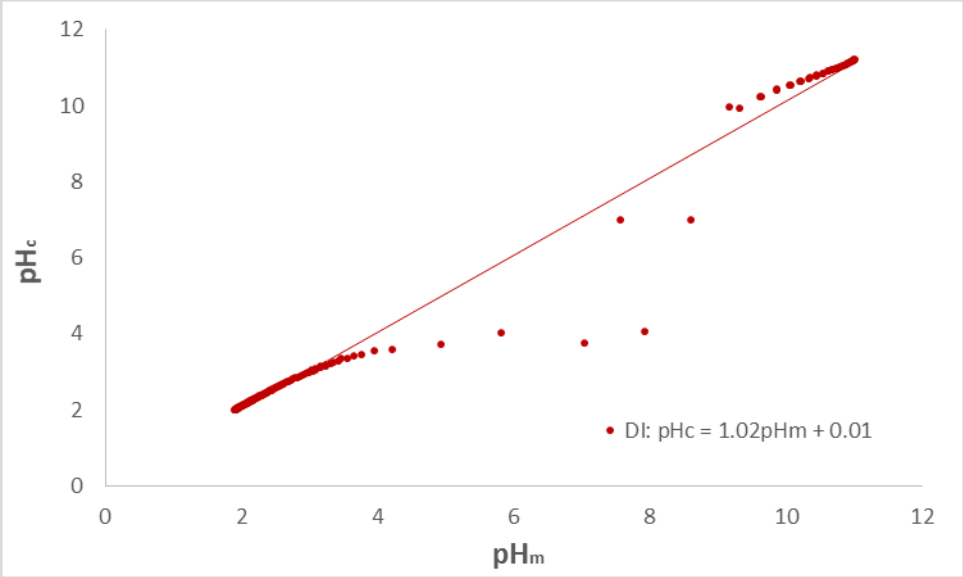

Figure 5.2: Titration curve for deionized water.

5.2 Pd(II) Sorption Experiments

5.2.1 Ionic Strength Effects on Sorption of Pd(II)

Building off of work done by Riddoch (2016), two additional ionic strengths were tested for determining the dependence of sorption on ionic strength for illite, bentonite, and shale: 5.0 and 6.0 M. The K_d values for sorption can be seen in Table 5.2 below, along with the pH_M and E_h values.

Table 5.2: Recorded data for *IS* dependence on Pd(II) sorption.

***IS* (M)**	**Soil**	**pH_M**	**E_h (mV)**	**K_d (m^3/kg)**
0.1	Illite	5.34 - 5.83	528 - 542	0.33 - 0.60
0.5	Illite	5.38 - 5.44	550 - 555	0.50 - 0.67
1.0	Illite	5.40 - 5.50	536 - 546	0.63 - 0.66
2.0	Illite	5.52 - 5.77	519 - 527	0.32 - 0.35
3.0	Illite	5.65 - 5.79	517 - 530	0.02 - 0.27
4.0	Illite	5.53 - 5.73	541 - 545	0.01 - 0.38
5.0	Illite	5.49 - 5.76	191 - 210	0.24 - 0.43
6.0	Illite	5.57 - 5.62	226 - 232	0.15 - 0.31
0.1	Bentonite	6.83 - 6.91	501 - 506	0.99 - 1.61
0.5	Bentonite	6.55 - 6.65	473 - 506	0.50 - 0.59
1.0	Bentonite	6.28 - 6.48	484 - 508	0.27 - 0.38
2.0	Bentonite	6.18 - 6.33	497 - 514	0.17 - 0.20
3.0	Bentonite	6.06 - 6.31	503 - 513	0.02 - 0.08
4.0	Bentonite	6.01 - 6.07	513 - 519	0.03 - 0.07
5.0	Bentonite	5.86 - 6.03	215 - 218	0.26 - 0.47
6.0	Bentonite	5.65 - 5.93	223 - 225	0.24 - 0.34
0.1	Shale	7.44 - 7.72	481 - 498	3.90 - 4.42
0.5	Shale	7.20 - 7.36	465 - 476	1.92 - 3.60
1.0	Shale	7.07 - 7.19	467 - 470	3.02 - 3.89
2.0	Shale	6.84 - 6.92	485 - 493	1.40 - 1.83
3.0	Shale	6.71 - 6.74	498 - 501	0.68 - 0.83
4.0	Shale	6.49 - 5.64	505 - 519	1.29 - 3.11
5.0	Shale	6.14 - 6.26	205 - 218	0.55 - 0.74
6.0	Shale	6.02 - 6.12	216 - 219	0.38 - 0.72

*Data obtained from Riddoch (2016), is highlighted in grey.

The collected data can be seen, plotted with data from Riddoch (2016), in Figure 5.3 below. The K_d for illite appears to remain constant from an I of 3 M all the way up to 6 M. The K_d measurement for shale at 4 M looks like it may be an outlier in the general trend of constant K_d values beyond an I of 3 M. K_d values for bentonite at an I of 5.0 and 6.0 M are much larger than those reported by Riddoch for 3.0 and 4.0 M, where the K_d values appear to be approaching a constant value range. Despite the large range of values reported in Riddoch (2016), for 3.0 and 4.0 M, their discrepancy with the values reported in this work for bentonite may point towards low experimental procedure tolerances or a sudden rise in sorption beyond 4.0 M.

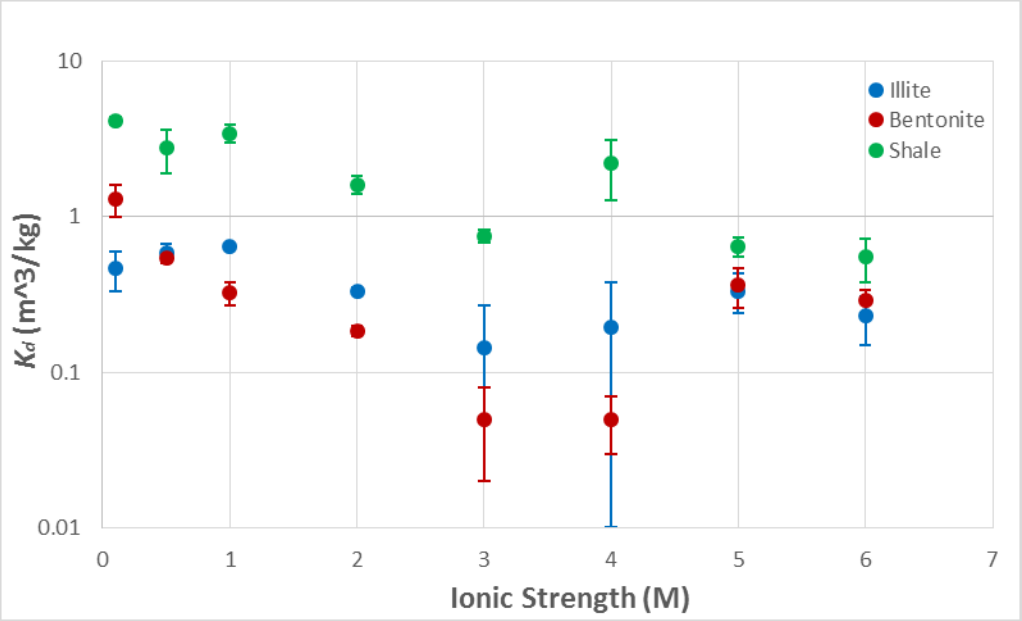

Figure 5.3: K_d for Pd sorption as a function of ionic strength for illite, bentonite, and shale.

5.2.2 pH Effects on Sorption of Pd(II)

In addition to the K_d values obtained from Riddoch (2016), sorption experiments were conducted on illite and bentonite in 0.01 M *Na-Ca-Cl* solutions at a pH_C of 3.0, 4.0, 5.0, and 6.0, and in 0.1, 1.0, 4.0, and 6.0 M *Na-Ca-Cl* solutions at a pH_C of 3.0 and 4.0. Sorption experiments were also conducted on illite, bentonite, and shale in 6.0 M *Na-Ca-Cl* solutions at a pH_C of 5.0, 6.0, 7.0, 8.0, and 9.0. The K_d values for these sorption tests can be seen in Table 5.3 below with data obtained from Riddoch (2016). A summary of the measured E_h values can also be seen in Table 5.4 below.

Table 5.3: Recorded K_d data for pH dependence on Pd(II) sorption.

IS **(M)**	**pH_C**	***K_d*** **Illite (m^3/kg)**	***K_d*** **Bentonite (m^3/kg)**	***K_d*** **Shale (m^3/kg)**
0.01	3	0.41 - 0.51	0.46 - 0.62	-
0.01	4	0.70 - 0.76	0.57 - 1.07	-
0.01	5	7.59 - 8.82	12.5 - 24.2	-
0.01	6	< 0.01 - 6.21	2.09 - 3.61	-
0.1	3	< 0.01	0.56 - 0.89	-
0.1	4	< 0.01	1.13 - 2.41	-
0.1	5	3.40 - 3.73	1.24 - 2.50	5.16 - 5.64
0.1	6	0.41 - 0.74	0.99 - 1.61	3.14 - 5.70
0.1	7	1.60 - 2.68	0.57 - 0.67	3.90 - 4.42
0.1	8	0.73 - 1.24	0.83 - 1.36	4.48 - 7.39
0.1	9	0.87 - 1.86	0.68 - 1.06	1.72 - 3.34
1.0	3	0.05 - 0.11	0.03 - 0.05	-
1.0	4	< 0.01	0.36 - 0.96	-
1.0	5	0.86 - 1.45	0.39 - 0.63	1.15 - 1.87
1.0	6	0.82 - 0.84	0.27 - 0.38	1.32 - 1.50
1.0	7	0.52 - 0.68	0.02 - 0.18	3.02 - 3.89
1.0	8	0.07 - 0.17	0.41 - 0.51	2.34 - 2.64
1.0	9	0.38 - 0.61	0.42 - 0.54	0.42 - 0.63
4.0	3	< 0.01	< 0.01	-
4.0	4	< 0.01	< 0.01	-
4.0	5	0.01 - 0.02	0.07 - 0.2	0.01 - 0.09
4.0	6	0.08 - 0.53	0.03 - 0.07	0.05 - 0.27
4.0	7	0.08 - 0.12	0.06 - 1.25	1.29 - 3.11

IS **(M)**	**pHc**	K_d **Illite** **(m^3/kg)**	K_d **Bentonite** **(m^3/kg)**	K_d **Shale** **(m^3/kg)**
4.0	8	0.13 - 0.21	0.05 - 0.06	0.28 - 0.57
4.0	9	0.01 - 0.08	0.53 - 0.80	0.04 - 0.25
6.0	3	< 0.01	< 0.01	-
6.0	4	< 0.01	< 0.01	-
6.0	5	< 0.01	< 0.01	0.29 - 0.32
6.0	6	< 0.01 - 0.05	0.01 - 0.20	0.32 - 1.01
6.0	7	< 0.01 - 0.06	0.16 - 0.24	0.13 - 0.19
6.0	8	0.05 - 0.10	0.00 - 0.25	0.09 - 0.40
6.0	9	0.06 - 0.11	0.10 - 0.18	0.29 - 0.59

*Data obtained from Riddoch (2016), is highlighted in grey.

Table 5.4: Recorded E_h data for pH dependence on Pd(II) sorption.

IS (M)	**pHc**	E_h **- Illite** **(mV)**	E_h **Bentonite** **(mV)**	E_h **Shale** **(mV)**
0.01	3	475 - 490	363 - 379	-
0.01	4	429 - 444	296 - 310	-
0.01	5	373 - 386	236 - 243	-
0.01	6	338 - 340	232 - 236	-
0.1	3	486 – 492	373 - 376	-
0.1	4	354 - 393	329 - 343	-
0.1	5	547 - 563	472 - 509	499 - 402
0.1	6	538 - 542	501 - 506	452 - 460
0.1	7	440 - 457	374 - 419	481 - 498
0.1	8	381 - 309	405 - 415	408 - 413
0.1	9	359 - 391	375 - 403	348 - 360
1.0	3	477 - 494	397 - 401	-
1.0	4	397 - 432	369 - 380	-
1.0	5	400 - 435	471 - 491	459 - 473
1.0	6	536 - 546	484 - 508	431 - 445
1.0	7	452 - 456	355 - 383	467 - 470
1.0	8	375 - 382	361 - 363	368 - 380
1.0	9	361 - 375	365 - 379	350 - 356
4.0	3	457 - 463	382 - 391	-
4.0	4	421 - 445	394 - 403	-
4.0	5	492 - 501	433 - 441	404 - 422
4.0	6	541 - 545	513 - 519	417 - 427
4.0	7	436 - 443	353 - 376	405 - 514
4.0	8	367 - 370	320 - 323	341 - 375
4.0	9	353 - 361	347 - 357	342 - 373
6.0	3	453 - 465	390 - 393	-

IS (M)	**pHC**	***E_h* - Illite (mV)**	***E_h* Bentonite (mV)**	***E_h* Shale (mV)**
6.0	4	421 - 425	382 - 405	-
6.0	5	389 - 407	375 - 390	324 - 329
6.0	6	306 - 369	305 - 347	285 - 292
6.0	7	275 - 283	269 - 298	264 - 286
6.0	8	235 - 238	233 - 252	234 - 247
6.0	9	192 - 213	193 - 220	202 - 235

*Data obtained from Riddoch (2016), is highlighted in grey.

The K_d values tabulated in Table 5.3 above from this work and Riddoch (2016), can be seen plotted for illite, bentonite, and shale in Figure 5.4, Figure 5.5, and Figure 5.6 respectively. The K_d value range shown in the plots are not error bars, but rather the range of the triplicate measurements. K_d values that were equal to, or less than, 0.01 m^3/kg are displayed in the plots as points on the horizontal axis, as the experimental methods and instruments cannot produce reliable measures of sorption below that point. For both illite and bentonite, it can be seen that the K_d values increase with increasing pH_C from 3 – 5 for all ranges of *I* (except 6.0 M), with a sharp rise from a pH of 4 – 5. Above a pH of 5, the K_d values appear to be falling for both soils in the 0.01 M ionic strength *Na-Ca-Cl* solutions. For 6.0 M *I*, the dependence of the K_d values on pH between a pH of 3 – 5 could not be determined because the K_d values could not be accurately measured below 0.01 m^3/kg. The K_d values also increased with increasing pH for illite between a pH of 5 – 8 and remained constant between 8 – 9. For bentonite, the K_d values increased from a pH of 5 – 7 and remained relatively constant from 7 – 9 for 6.0 M *I*. For shale, the K_d values increased from a pH of 5 – 6, decreased from 6 – 7, and increased again from 7 – 9.

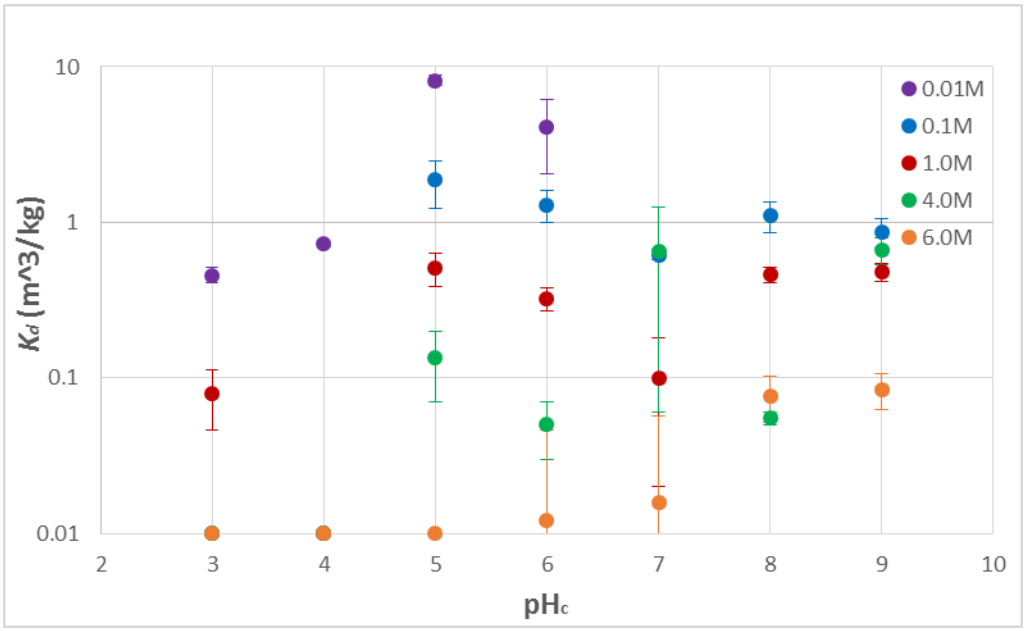

Figure 5.4: pH dependence of K_d for Pd sorption onto illite.

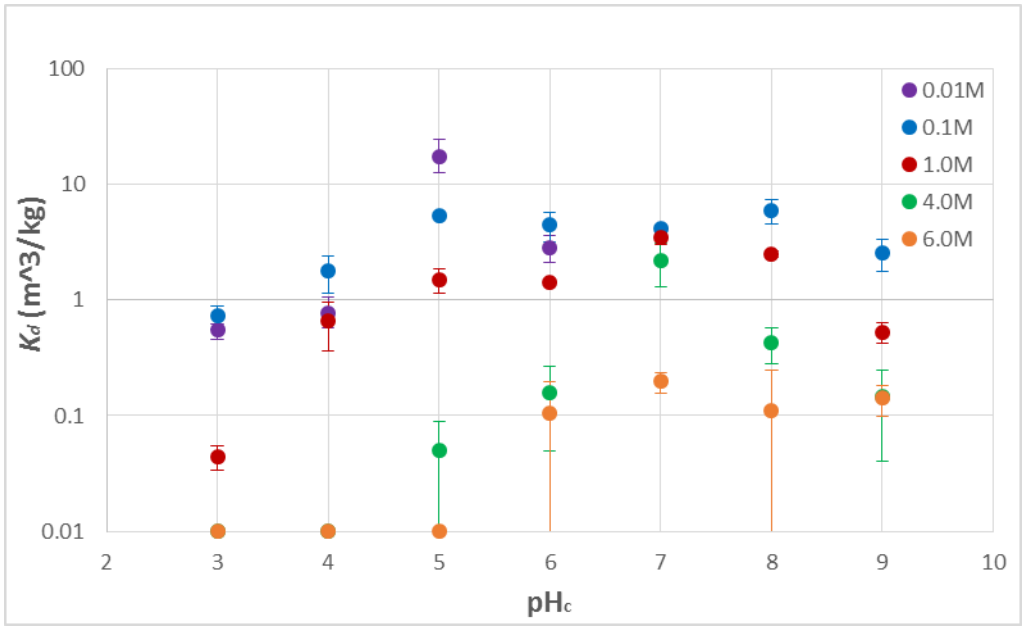

Figure 5.5: pH dependence of K_d for Pd sorption onto bentonite.

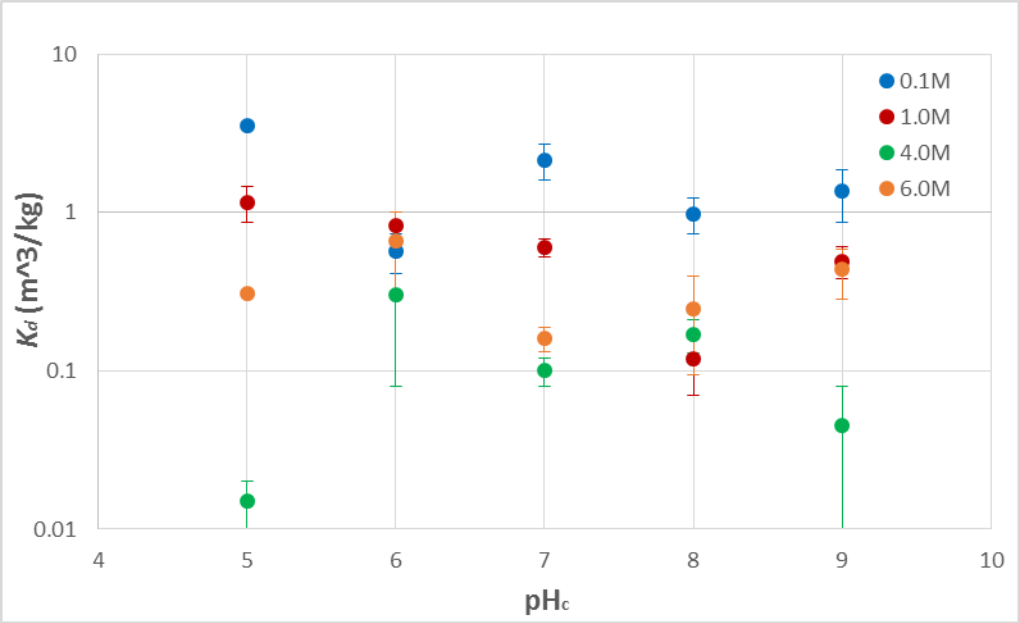

Figure 5.6: pH dependence of K_d for Pd sorption onto shale.

5.3 PHREEQC Surface Complexation Modelling

5.3.1 2SPNE SC Model Confirmation With Th(IV)

Following the changes made to the JAEA TDB outlined in Chapter 4, Th(IV) was modelled using PHREEQC (the addition of the formation reaction for the Th(OH)3 aqueous species, the addition of the Cl^{+7} redox state to the solution master species for the inclusion of ClO_4^- in the model, as well as the adjustments to all other formation reaction constants within their stated error to match those used in the reference modelling). The modelling results can be seen in Figure 5.8 and Figure 5.10 below with the corresponding reference Th(IV) sorption edge model from Bradbury (2009b, 2005b), for illite and montmorillonite in Figure 5.7 and Figure 5.9 respectively below. For both clays, K_d values were plotted in units of L kg^{-1} to match the scale of the reference plots, which plot R_d instead

of K_d. R_d is called the distribution ratio, which can be seen in Equation 5.3 below, and is equal to the distribution coefficient K_d defined in a different manner (Bradbury, 2005b).

$$R_d = \frac{Quantity\ of\ sorbate\ on\ the\ solid\ per\ unit\ mass}{Equilibrum\ sorbate\ aqueous\ concentration} \tag{5.3}$$

In the reference plot for montmorillonite, experimental results are plotted for both 0.1 and 1.0 M $NaClO_4$. Consequently, both ionic strengths were modelled in this work despite the reference only showing the 0.1 M model results. As seen in the four figures below, the 2SPNE SC model used in this work correctly reproduces the sorption edges for Th(IV) on both illite and montmorillonite in 0.1 M $NaClO_4$ solution when compared against the existing literature for the model's use.

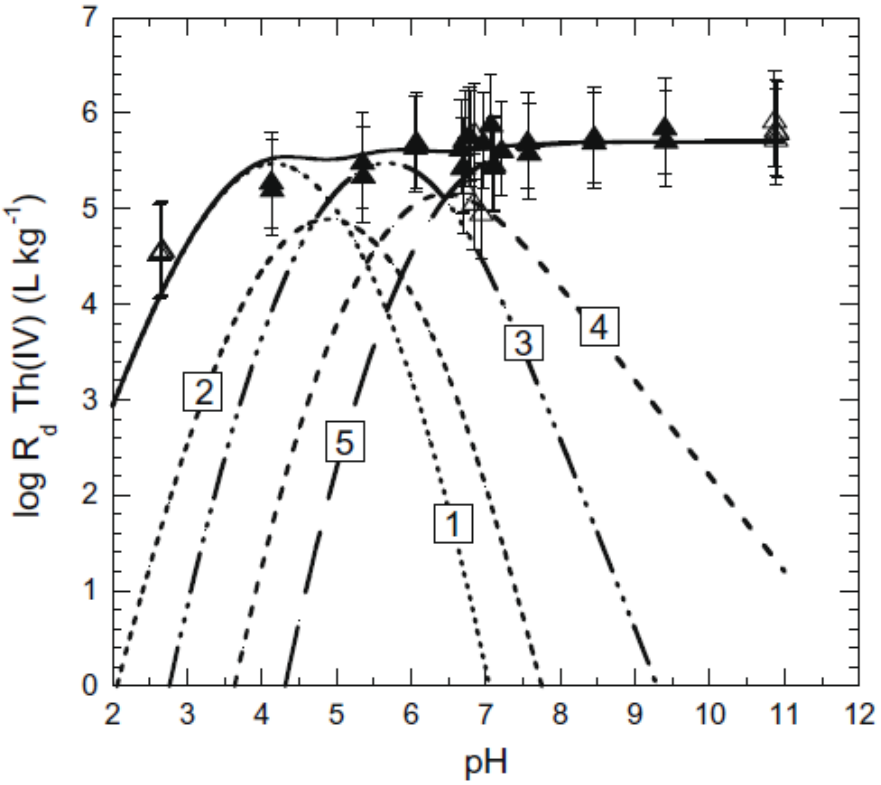

Figure 5.7: Th(IV) reference sorption edge model for illite in 0.1 M *$NaClO_4$* (Bradbury, 2009b).

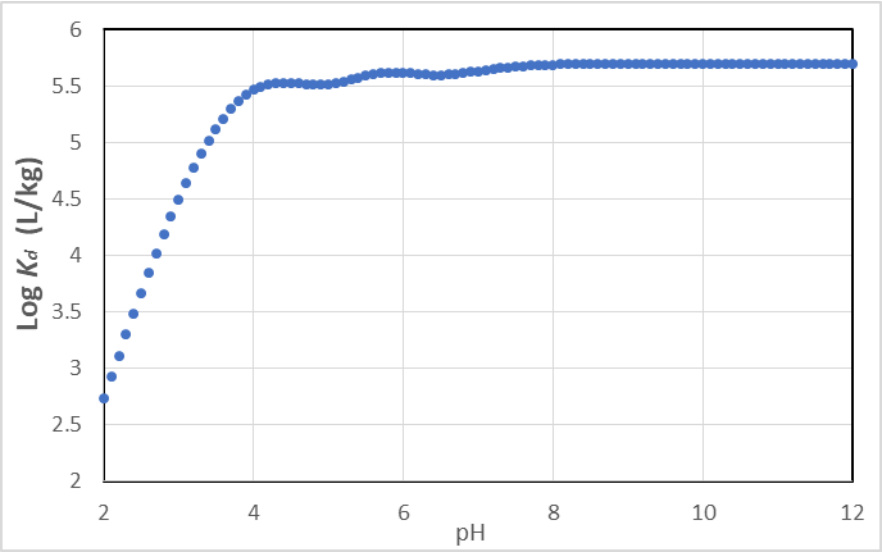

Figure 5.8: Th(IV) sorption confirmation model results for illite in 0.1 M *$NaClO_4$*.

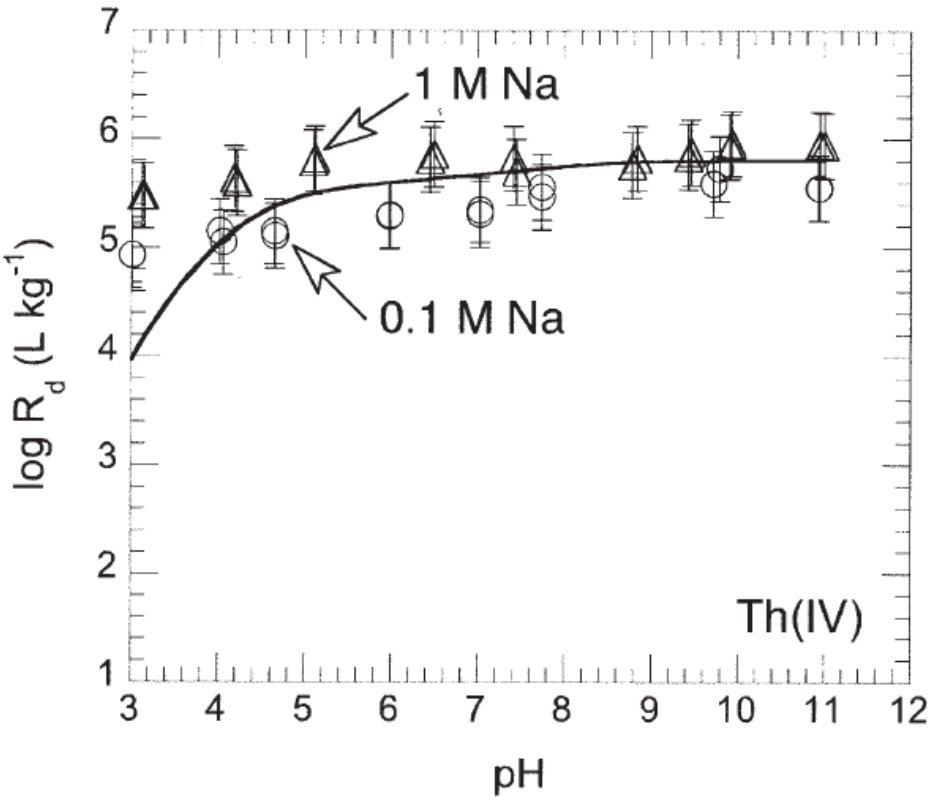

Figure 5.9: Th(IV) reference sorption edge model for montmorillonite in 0.1 M & 1.0 M *$NaClO_4$* (Bradbury, 2005b).

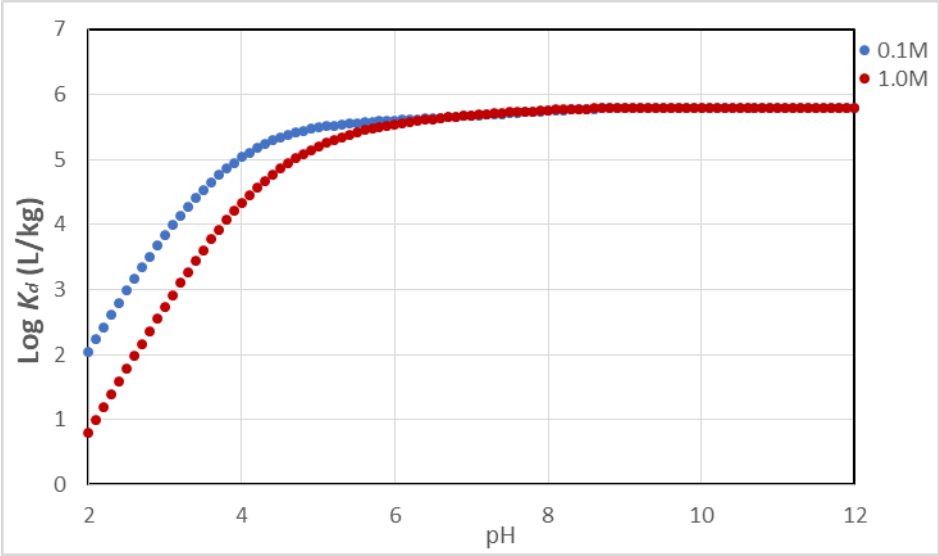

Figure 5.10: Th(IV) sorption confirmation model results for montmorillonite in *$NaClO_4$*.

5.3.2 Pd(II) Sorption Using the 2SPNE SC/CE Model

The 2SPNE SC model was initially used to calculate the sorption of Pd(II) onto illite and montmorillonite with the JAEA TDB and SIT using the *S-OPdOH* and *S-OPd(OH)$_2^-$* surface species and corresponding reaction constants shown in Table 4.17 above. These results were plotted with the experimental K_d values obtained from this work and from Riddoch (2016), for *I* values of 0.01, 0.1, 1.0, and 4.0 M, but not 6.0 M since the SIT is only accurate up to a maximum *I* of 4.0 M (Grenthe, 1997). These plots for illite and montmorillonite can be seen in Figure 5.11 and Figure 5.12 respectively below. The *S-OPd$^+$* surface species was then added to the model with the reaction constant of 6.4 for both clays, obtained from Vilks (2017), and the formation reaction constant for the corresponding aqueous species in the JAEA TDB. With the addition of this surface species there was no observable impact on the sorption edge. The surface complexation constants for the ternary chloride species seen in Table 4.17 above were added to the model for both clays, which can be seen in Figure 5.13 for illite, and Figure 5.14 for montmorillonite below. The addition of these species significantly raised the sorption edge closer to the experimental K_d values for *I* of 1.0 and 4.0 M in the mildly alkaline to acidic regions of the curve for both clays. This can mostly be attributable to the *S-OPdCl$_4^{-3}$* surface species.

Cation exchange was then added to the 2SPNE SC model in order to improve the simulation with the addition of the selectivity coefficients obtained from Bradbury (2009a). The K_c values used are listed in Table 4.10, and the cation exchange capacities used are shown in Table 4.7 and Table 4.8 above. Only cationic species were considered in this portion of the 2SPNE SC/CE model as neutral and anionic species do not contribute to sorption since charge sites on the soil surface are negatively-charged. The two exchange species, *Pd^{+2}* and *PdOH$^+$*, were considered for addition to the exchanger. In the code they are first conditioned in an identical solution as that used for sorption without palladium in

order to create the initial state before use with the solution containing the Pd(II). The selectivity coefficients for these species were then optimized to fit the sorption edge to the experimental data in the pH regions at values of *I* that could not be fitted with the surface species formed through specific chemical sorption. The *S-O₂Pd* exchange species was found to contribute to sorption at lower *I*, and mostly below a pH of 4 for illite, and peaking at less than 2 for montmorillonite at an *I* of 0.01 M. The *S-OPdOH* exchange species was also found to contribute to sorption at lower *I*, but its contribution to the sorption edge peaks around a pH of 4 and 3.75 for illite and montmorillonite respectively, at an *I* of 0.01 M. Based on preliminary calculations, the cation exchange reactions were found to not significantly contribute to sorption at an *I* of 1.0 and 4.0 M and at pH values greater than 6. The *S-OPdOH* exchange species had less of a contribution to total sorption and was not required for fitting the sorption edge to the experimental results. Therefore, the *S-OPdOH* exchange species was left out of the optimization without a recommended value for its respective selectivity coefficient. When compared to the $S\text{-}OPd^{+}$ surface species for fitting, the *S-OPdOH* exchange species contributes to the sorption edge at a lower pH, and has a wider curve; both features that produce a less-accurate fit to the experimental K_d values. The selectivity coefficient for the *S-O₂Pd* exchange species was optimized to fit the experimental data for both clays at low pH and *I*, and assigned a value of 6.75 and 5.7 for illite and montmorillonite respectively. These values are shown in Table 5.5 below. The modelling results with the addition of the selectivity coefficients obtained from Bradbury (2009a), and the optimized Pd(II) exchange species can be seen in Figure 5.15 and Figure 5.16 for illite and montmorillonite respectively.

The selectivity coefficients for the *S-O₂Pd* exchange species were then held constant while the surface complexation constants for the metal-binding surface species were optimized to best fit the experimental data, which can be seen in Figure 5.17 for illite and Figure 5.19 for montmorillonite below. It was later found for illite that at this step in

the optimization the modelling results for illite had the best fit to the experimental data. The surface complexation constants and selectivity coefficients for illite can be seen in Table 5.5. Figure 5.18 shows the contribution of each Pd surface species to the total sorption in units of L kg^{-1}. With the addition of the exchange species there was a good fit that was obtained for illite with an *I* of 0.01 M, and a reasonably good fit that was able to be obtained for 0.1 M as the calculations produced K_d values that decrease starting at a pH of 6.5 instead of approximately 5. For 1.0 M the experimental data has larger K_d values than the calculated values in the acidic region, however, the data matches well for the alkaline region. For 4.0 M the modelled sorption edge averages the experimental data well but does not produce a good fit visually due to the large variation in K_d values. The surface complexation constants for the *S-OPdOH* and $S\text{-}OPd(OH)_2^-$ surface species were reduced in order to reduce the sorption edge above a pH of 4 for 0.01 M *I*, 5 for 0.1 M *I*, and 8 for 1.0 M *I*. The reaction constant for the $S\text{-}OPd^+$ surface species was left unchanged as it did not dominate sorption for any of the *I* modelled (which would allow for optimization).

In an attempt to optimize the models further for both clays, the ternary surface species reaction constants were looked at for adjustment. The $S\text{-}OPdCl_4^{-3}$ surface species was found to dominate sorption for 1.0 and 4.0 M *I* up to a pH of 8 and 9.5 respectively for illite, and 8.75 and 9.75 respectively for montmorillonite. For these regions of the sorption models, the sorption edge needs to be increased for illite, and reduced for montmorillonite to better fit the experimental data. For illite, the surface complexation constant for the $S\text{-}OPdCl_4^{-3}$ surface species was increased from 13.05 to 13.50, the results of which can be seen in Figure 5.20 below. However, if the Fein (2002), relationship holds then the formation reaction constant for the $PdCl_4^{-2}$ aqueous species would also have to be increased to the same value in the JAEA TDB. After changing the formation reaction constant in the TDB to 13.50 (within stated error), the selectivity coefficient for the $S\text{-}O_2Pd$ exchange species also had to be increased from 6.75 to 7.05 to maintain the same fit, which is

illustrated in Figure 5.21. The effect on the sorption edge of these modifications for 1.0 and 4.0 M *I* were the opposite of the intended effect, where the K_d values were reduced above a pH value of 8, and up to a pH of 7 for 0.1 M *I*. Modifications for this surface species were not considered for the best fit for sorption of Pd(II) on illite.

For montmorillonite, the surface complexation constant for the $S\text{-}OPdCl_4^{-3}$ surface species was reduced from 13.05 to 12.46, and the results can be seen in Figure 5.22. Following the same procedure as that for illite, the formation reaction constant for the $PdCl_4^{-2}$ aqueous species was also decreased to the same value in the JAEA TDB. After changing the formation reaction constant in the TDB to 12.46 (within stated error), the selectivity coefficient for the $S\text{-}O_2Pd$ exchange species also had to be decreased from 5.9 to 5.7 to maintain the same fit, which can be seen in Figure 5.23. After these modifications, the effect on the sorption edge for all *I* was a peak shift to the left (lower pH), which slightly improved the fit for all *I* except 0.01M. This was taken to be an overall improvement, and the reaction constants for this case can be seen as the best fit for montmorillonite in Table 5.5 below. For this case, a speciation plot can be seen in Figure 5.24 where the contribution of each Pd surface species to the total sorption is plotted in units of L kg^{-1}. Sorption of Pd(II) was found to be highly dependent on *I* and pH for both illite and montmorillonite

Table 5.5: Optimized surface complexation and cation exchange constants used for Pd(II) sorption modelling.

Surface Complexation Reaction	$\text{Log}^S K_I$	$\text{Log}^S K_M$
Metal Binding:		
$S\text{-}OH + Pd^{+2} \leftrightarrow S\text{-}OPd^{+} + H^{+}$	6.4	8.2
$S\text{-}OH + Pd^{+2} + H_2O \leftrightarrow S\text{-}OPdOH + 2H^{+}$	3.2	3.0
$S\text{-}OH + Pd^{+2} + 2H_2O \leftrightarrow S\text{-}OPd(OH)_2^{-} + 3H^{+}$	-4.0	-5.5
Ternary:		
$S\text{-}OH + Pd^{+2} + Cl^{-} \leftrightarrow S\text{-}OPdCl + H^{+}$	5.00	5.00
$S\text{-}OH + Pd^{+2} + 2Cl^{-} \leftrightarrow S\text{-}OPdCl_2^{-} + H^{+}$	8.42	8.42

Surface Complexation Reaction	$Log^S K_I$	$Log^S K_M$
Ternary:		
$S\text{-}OH + Pd^{+2} + 3Cl^- \leftrightarrow S\text{-}OPdCl_3^{-2} + H^+$	10.93	10.93
$S\text{-}OH + Pd^{+2} + 4Cl^- \leftrightarrow S\text{-}OPdCl_4^{-3} + H^+$	13.05	12.46
$S\text{-}OH + Pd^{+2} + 3Cl^- + H_2O \leftrightarrow S\text{-}OPdCl_3OH^{-3} + 2H^+$	3.77	3.77
Ion-Exchange:		
$2S\text{-}ONa + Pd^{+2} \leftrightarrow S\text{-}O_2Pd + 2Na^+$	6.75	5.7
$S\text{-}ONa + PdOH^+ \leftrightarrow S\text{-}OPdOH + Na^+$	-	-

*Reaction constants highlighted in grey fall outside of the range of the LFER.

Equations 4.2 and 4.3 were also used to calculate the range of surface complexation constants that could still be described by the LFER with the use of the hydrolysis constants contained in the JAEA TDB for metal binding surface species. These values are shown in Table 5.6 below. For illite, the surface complexation constant for the $S\text{-}OPd^+$ surface species falls within the LFER range of allowable values, *S-OPdOH* is below the range by 1.3, and $S\text{-}OPd(OH)_2^-$ is above the range by only 0.2. For montmorillonite, the surface complexation constant for the $S\text{-}OPd^+$ surface species is above the LFER range of allowable values by 1.4, *S-OPdOH* is below the range by 1.6, and $S\text{-}OPd(OH)_2^-$ is above the range by only 0.3.

Table 5.6: Range of SCCs allowed for LFER based on FRCs for Pd(II) sorption.

Surface Complexation Reaction	$Log^S K_I$	$Log^S K_M$
$S\text{-}OH + Pd^{+2} \leftrightarrow S\text{-}OPd^+ + H^+$	5.93 – 6.80	6.10 – 6.77
$S\text{-}OH + Pd^{+2} + H_2O \leftrightarrow S\text{-}OPdOH + 2H^+$	4.53 – 5.47	4.59 – 5.33
$S\text{-}OH + Pd^{+2} + 2H_2O \leftrightarrow S\text{-}OPd(OH)_2^- + 3H^+$	-5.66 – -4.24	-6.44 – -5.22

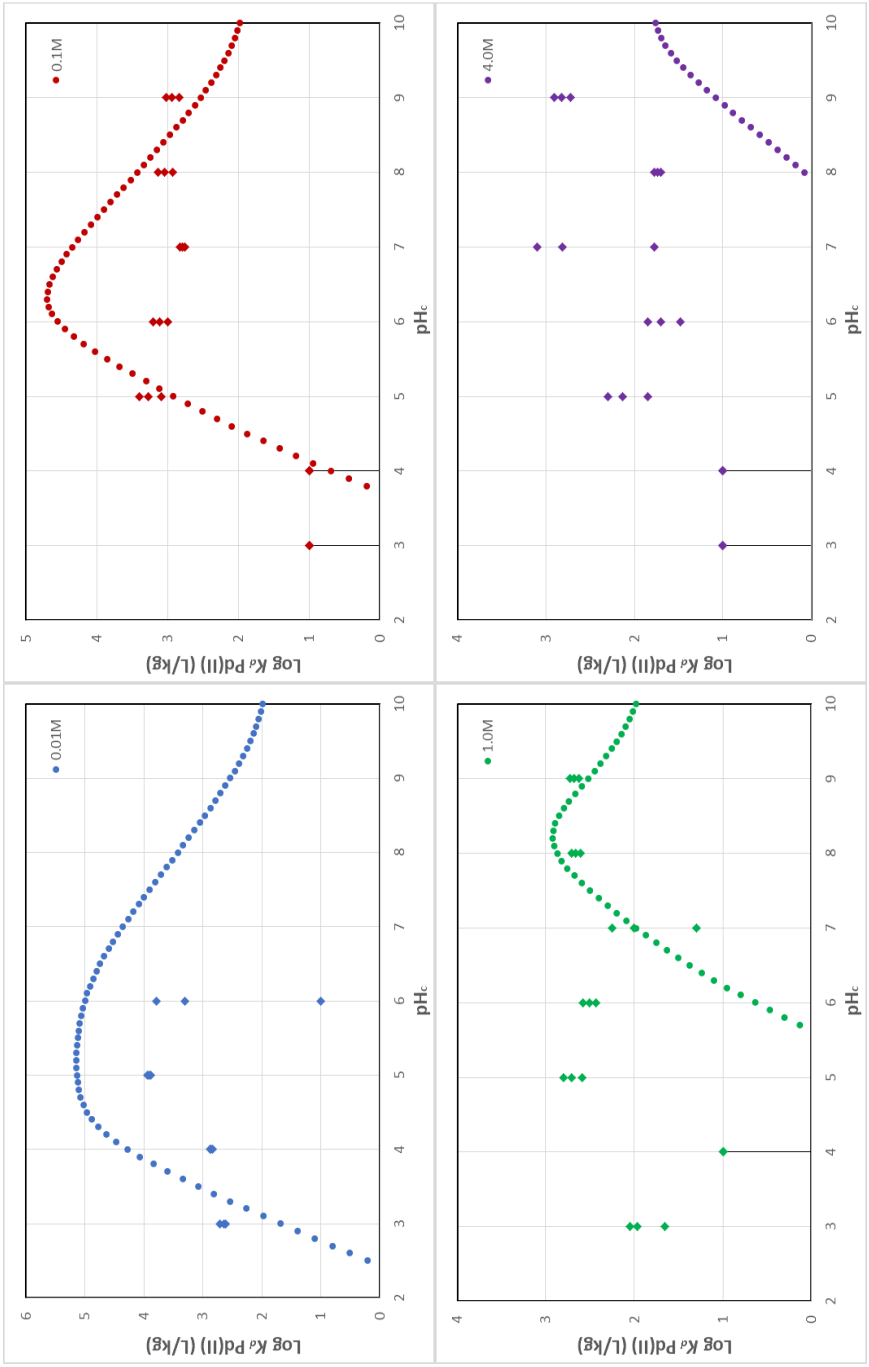

Figure 5.11: Sorption modelling results for Pd(II) onto illite with the surface species recommended in Bradbury (2005b), using surface complexation constants calculated from the formation reaction constants in the JAEA TDB with Equation 4.2. The JAEA TDB was used with the SIT and Davies computational method.

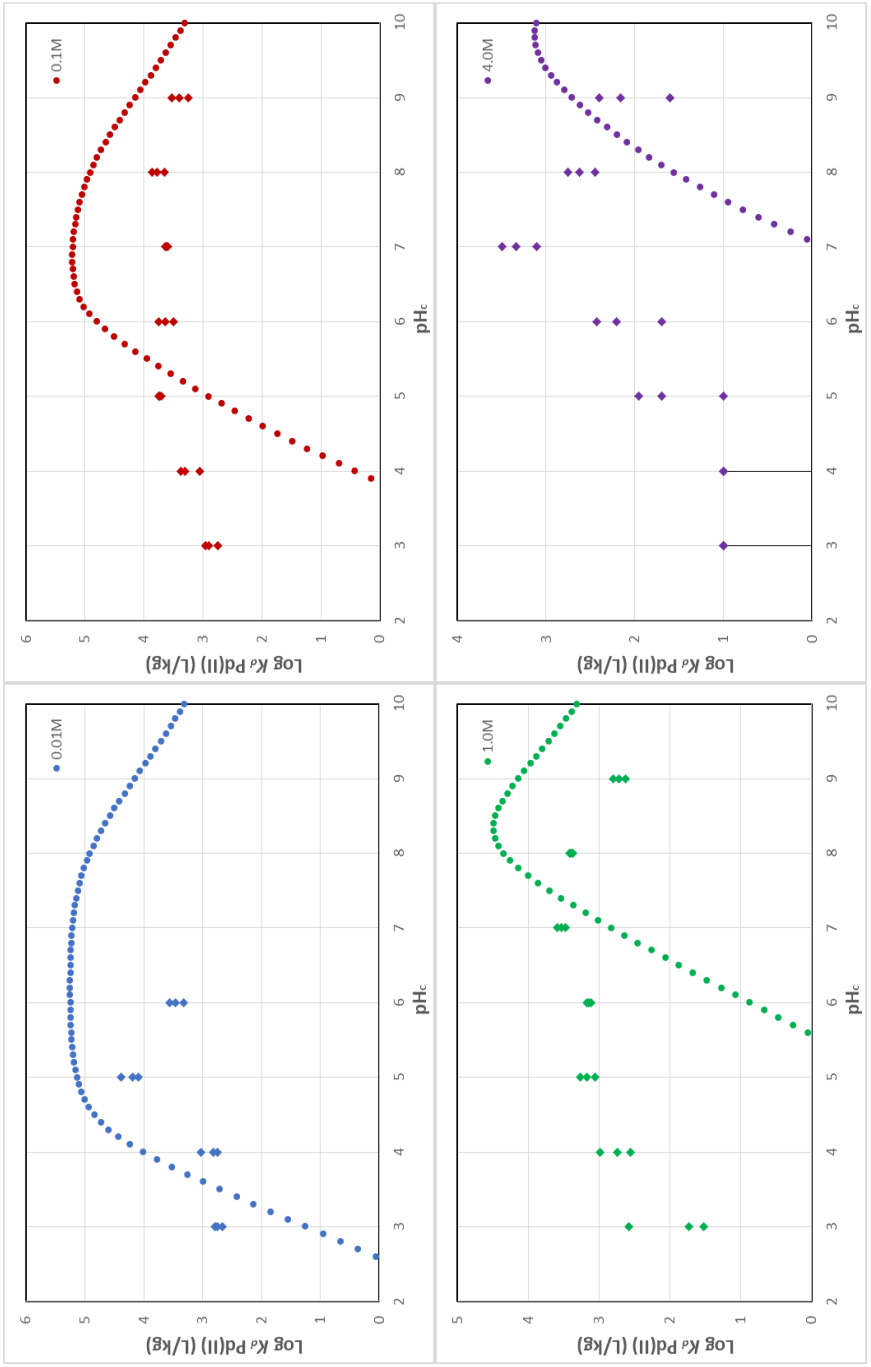

Figure 5.12: Sorption modelling results for Pd(II) onto montmorillonite with the surface species recommended in Bradbury (2005b), using surface complexation constants calculated from the formation reaction constants in the JAEA TDB with Equation 4.3. The JAEA TDB was used with the SIT and Davies computational method.

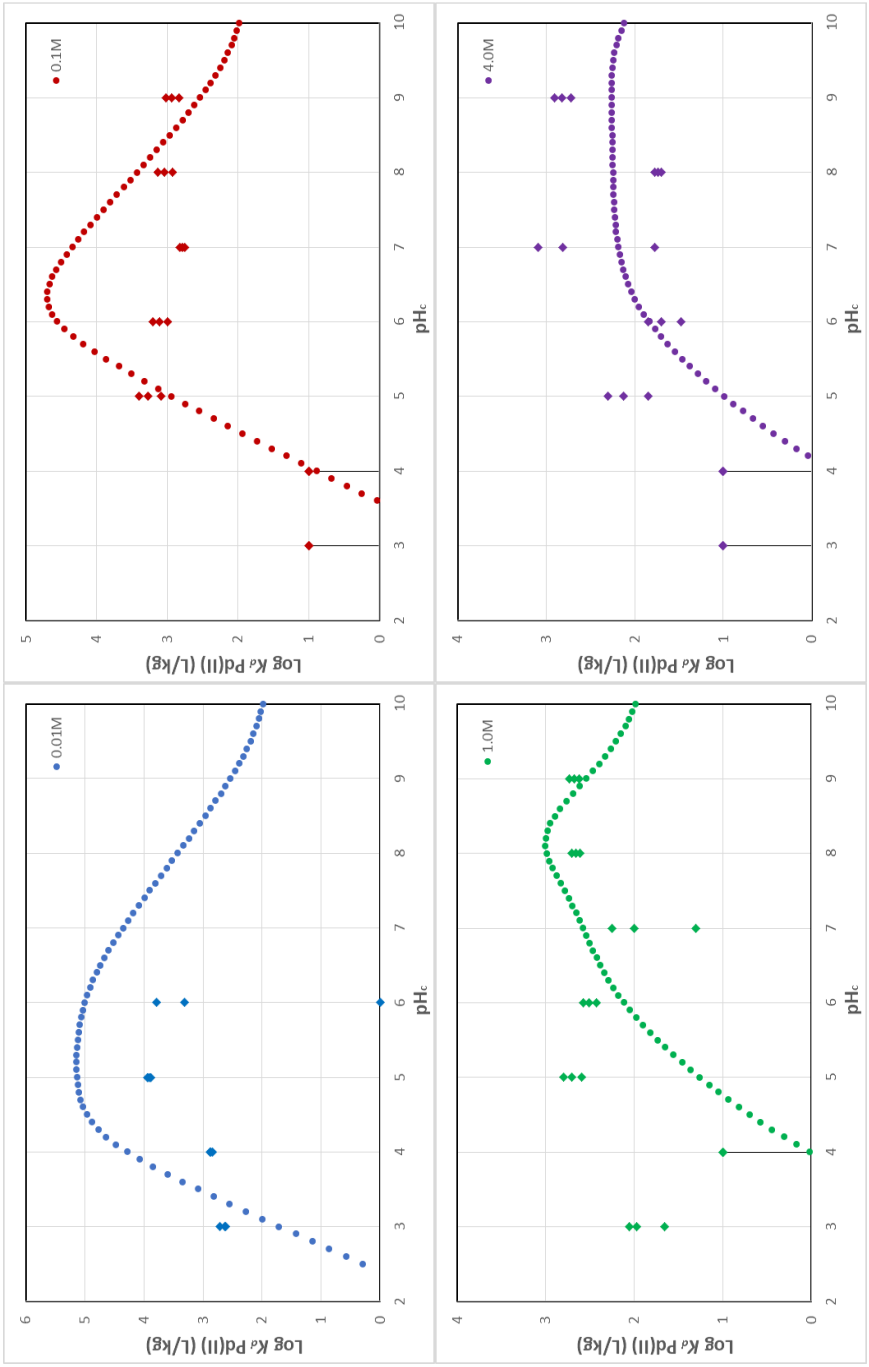

Figure 5.13: Sorption modelling results for Pd(II) onto illite using the two metal binding surface species recommended in Bradbury (2005b), the third proposed in Vilks (2017), and the addition of all ternary chloride species with formation reaction constants for the respective aqueous species contained in the JAEA TDB. The JAEA TDB was used with the SIT and Davies computational method.

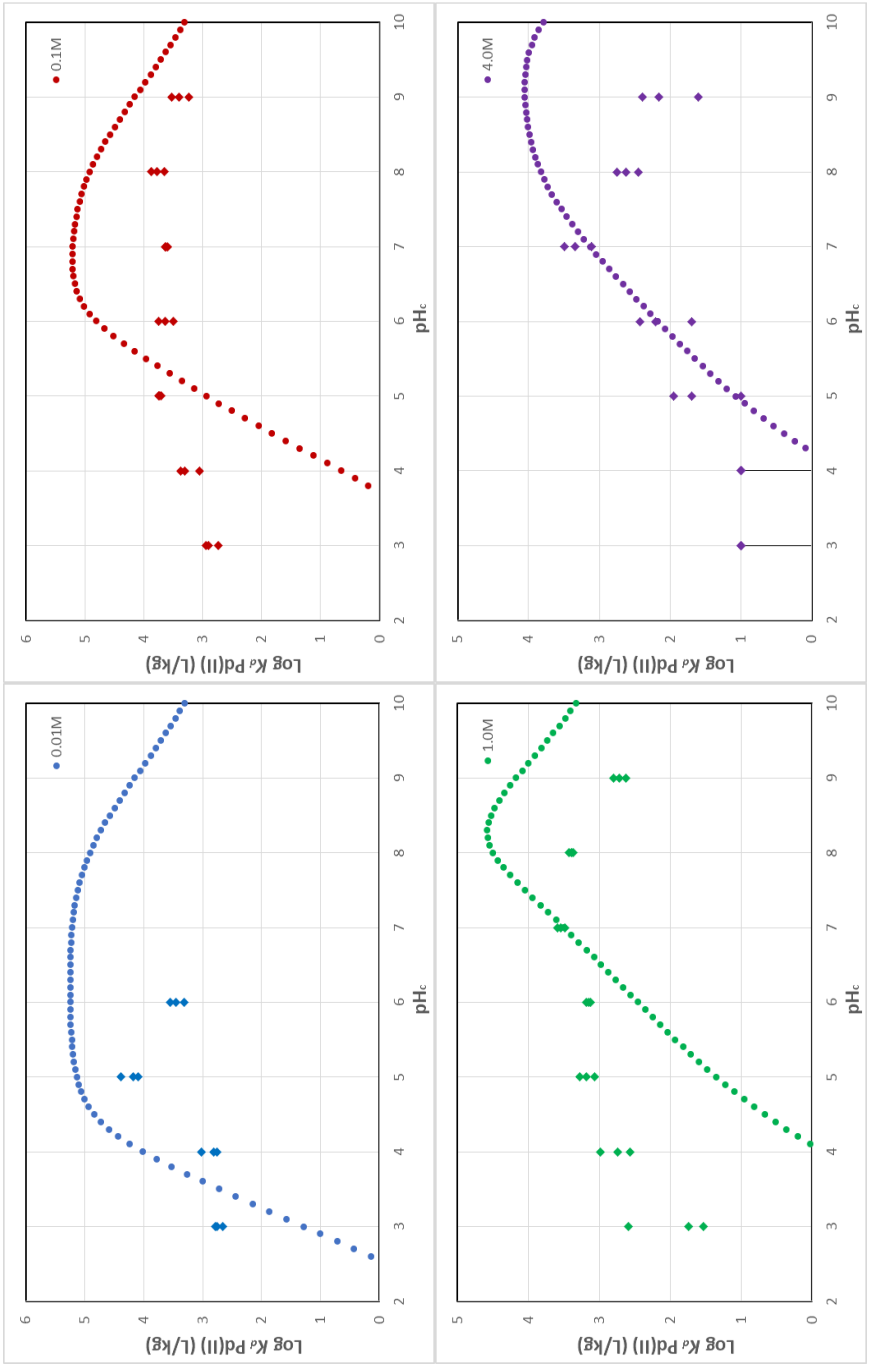

Figure 5.14: Sorption modelling results for Pd(II) onto montmorillonite using the two metal binding surface species recommended in Bradbury (2005b), the third proposed in Vilks (2017), and the addition of all ternary chloride species with formation reaction constants for the respective aqueous species contained in the JAEA TDB. The JAEA TDB was used with the SIT and Davies computational method.

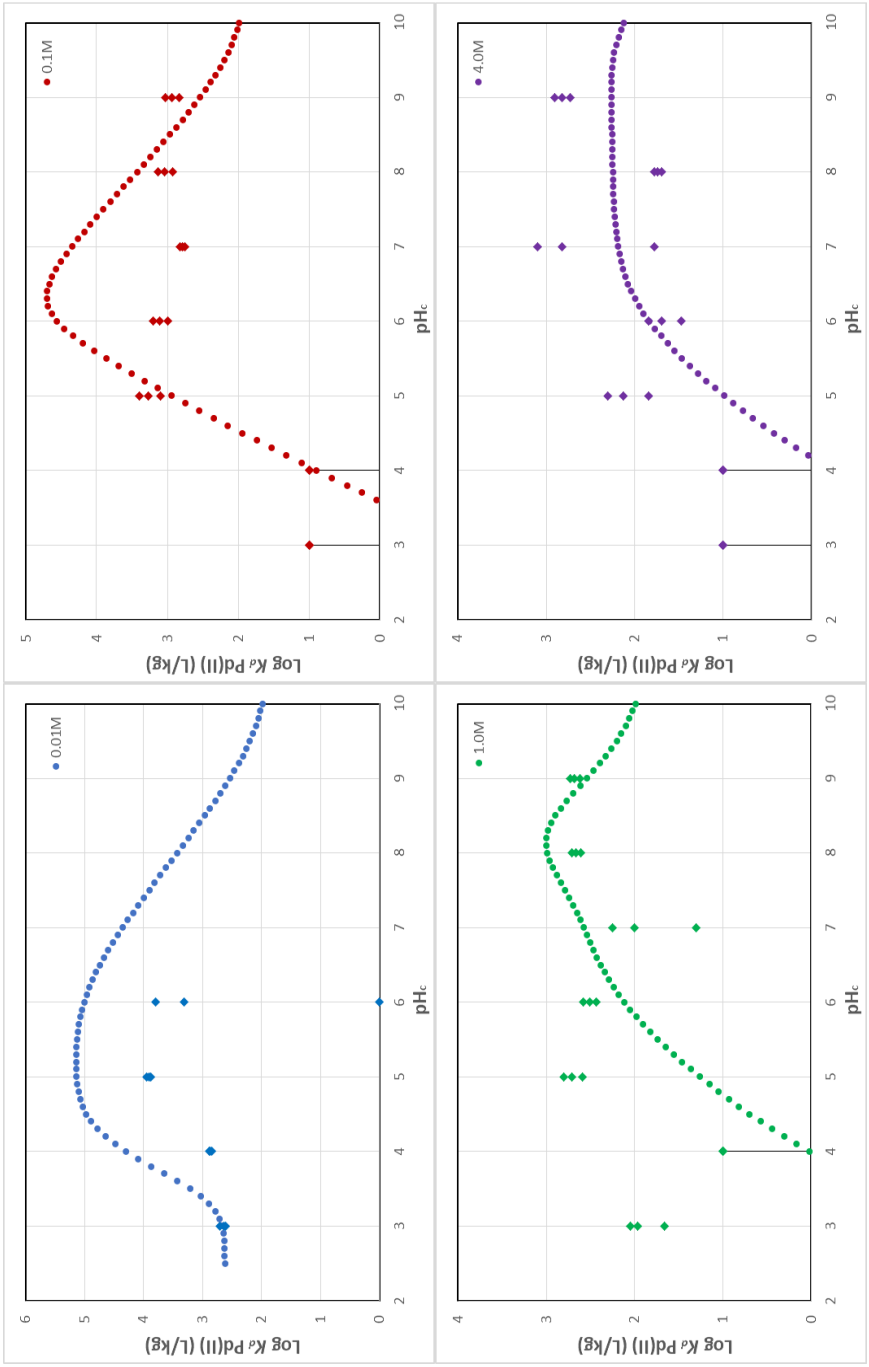

Figure 5.15: Sorption modelling results for Pd(II) onto illite using all surface complexation constants with the addition of the cation exchange species. The JAEA TDB was used with the SIT and Davies computational method.

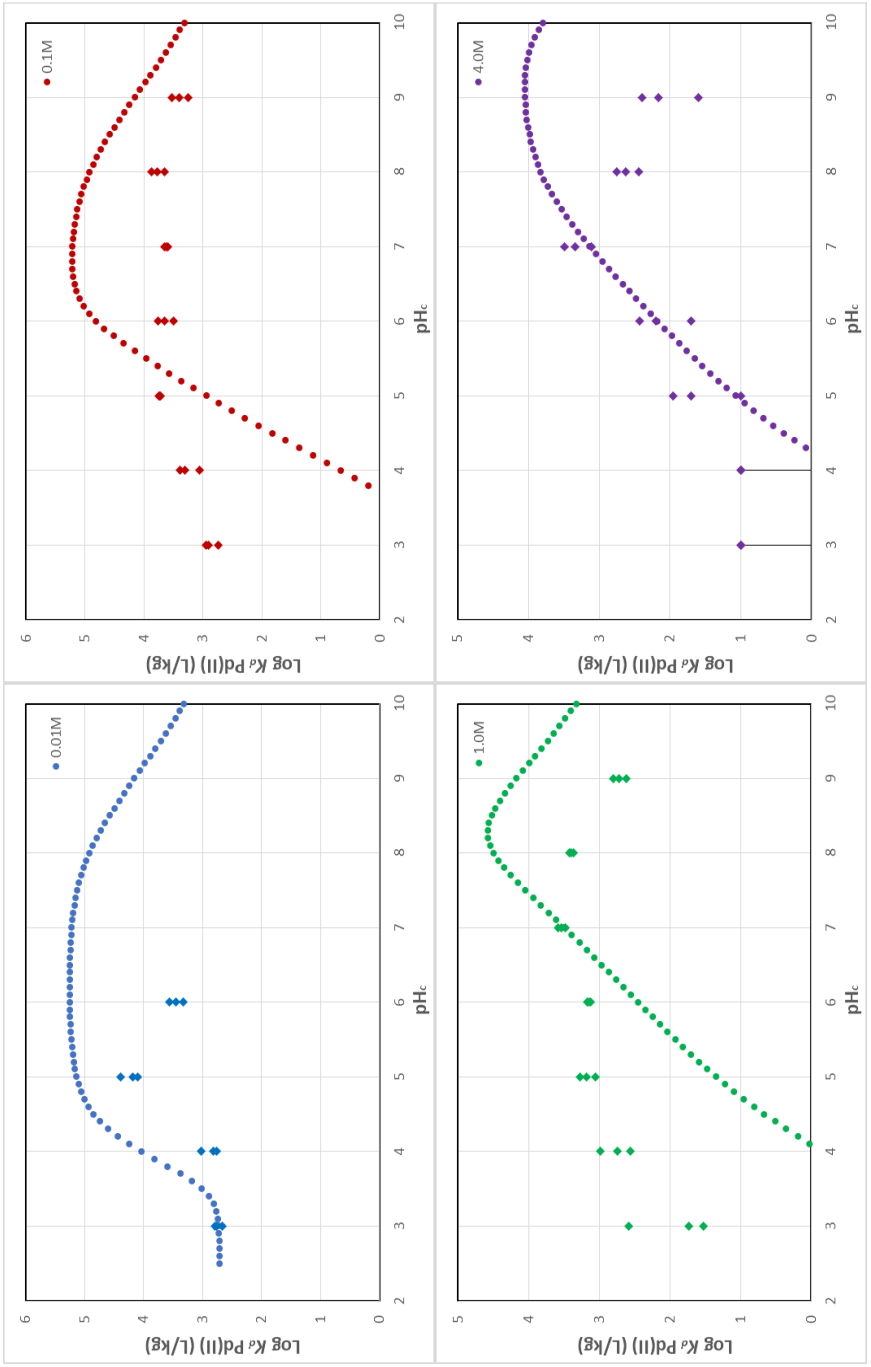

Figure 5.16: Sorption modelling results for Pd(II) onto montmorillonite using all surface complexation constants with the addition of the cation exchange species. The JAEA TDB was used with the SIT and Davies computational method.

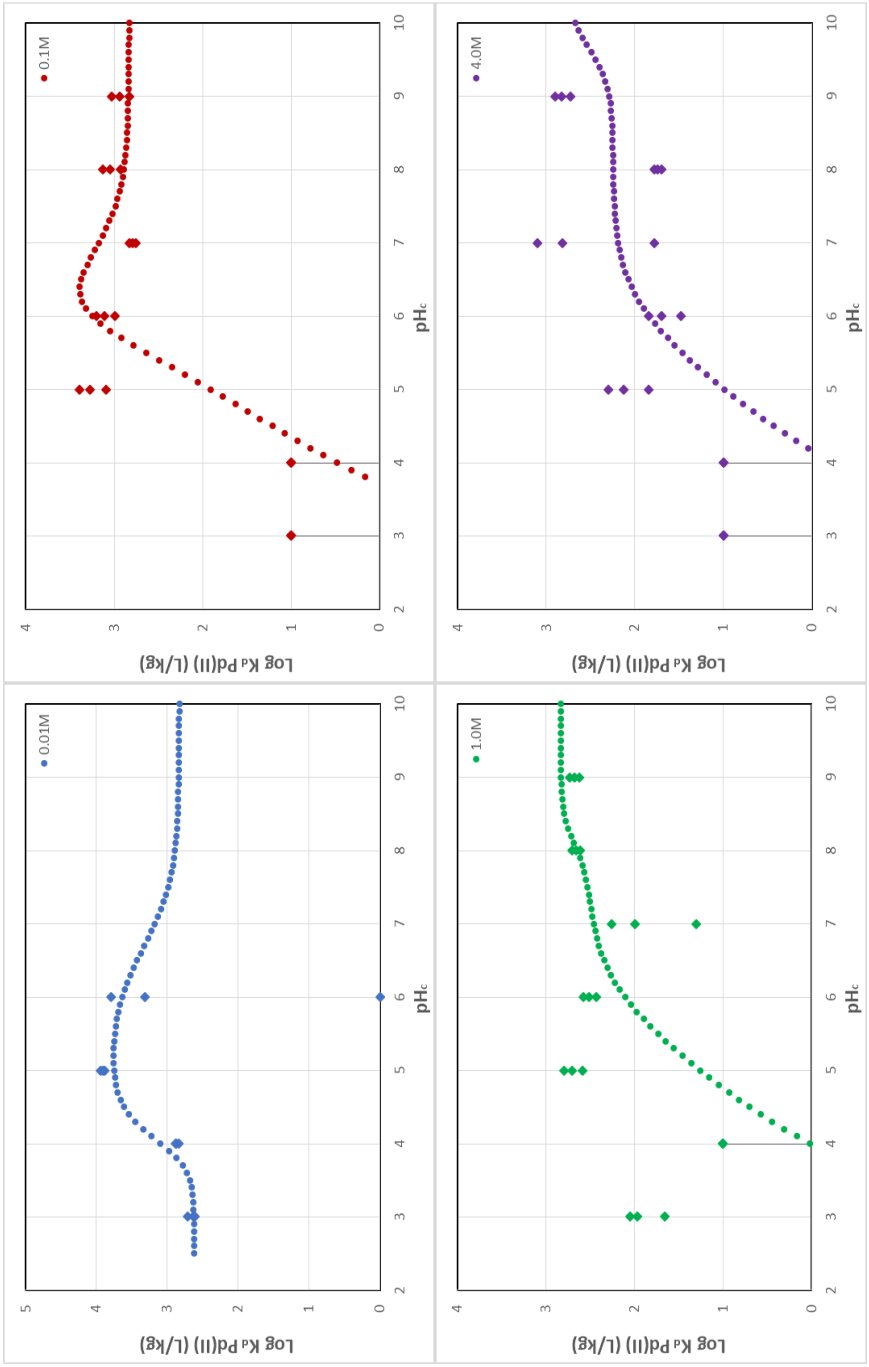

Figure 5.17: Sorption modelling results for Pd(II) onto illite using optimized surface complexation constants for metal-binding surface species, unadjusted constants for ternary chloride surface species, and unchanged cation exchange selectivity coefficients. The JAEA TDB was used with the SIT and Davies computational method.

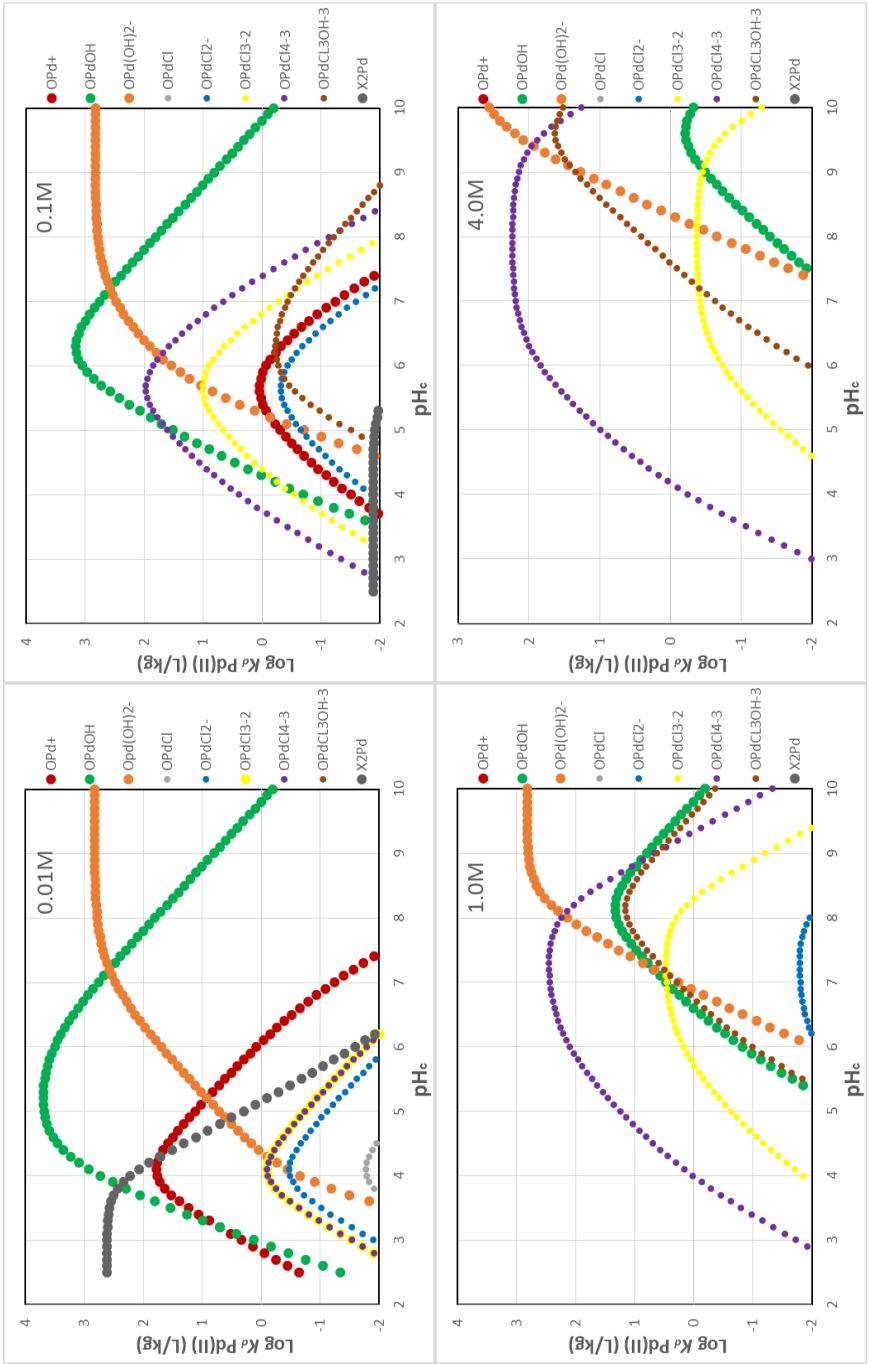

Figure 5.18: Contribution of each species to sorption for Pd(II) onto illite with optimized surface complexation constants and selectivity coefficients. The JAEA TDB was used with the SIT and Davies computational method.

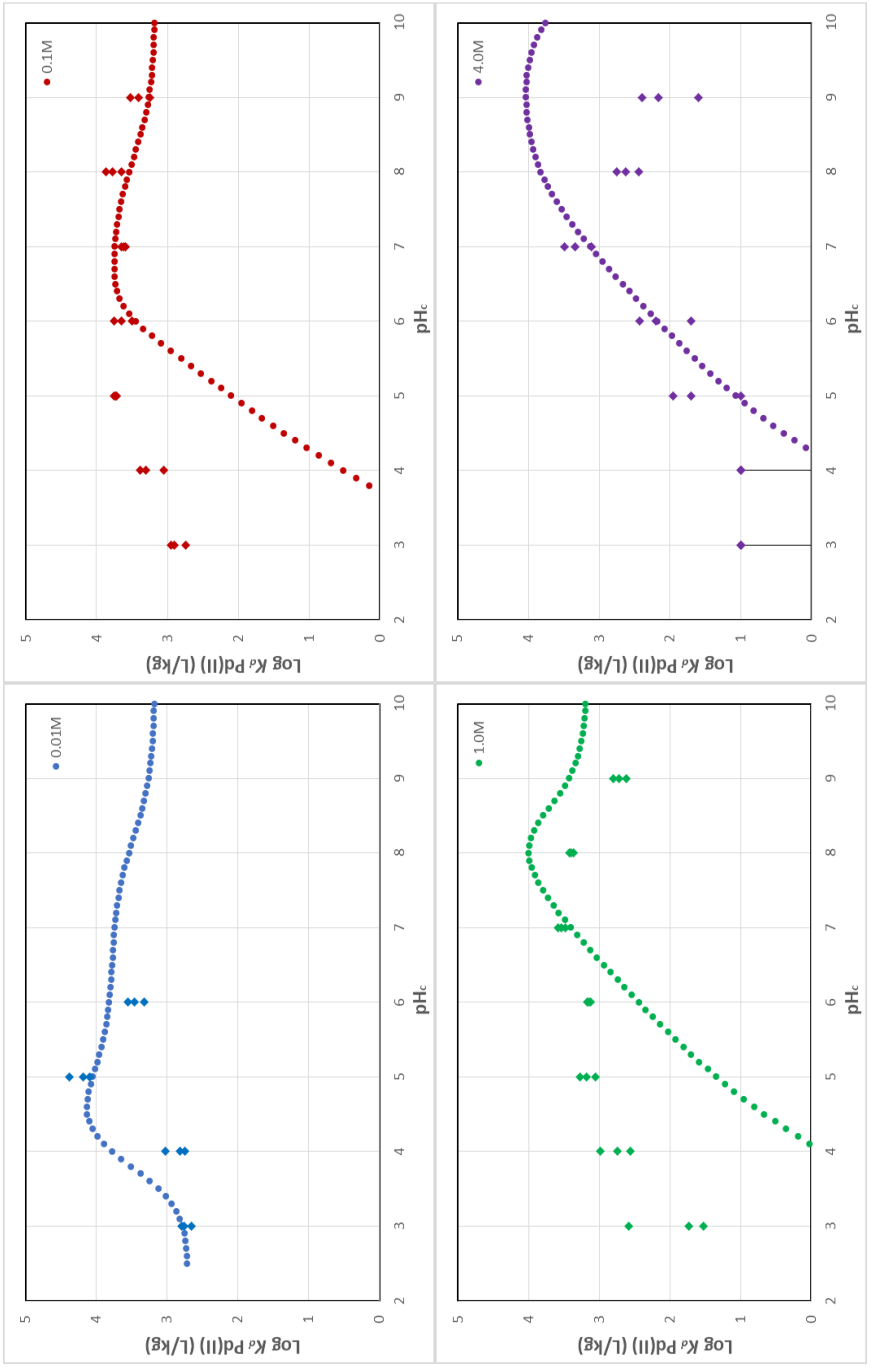

Figure 5.19: Sorption modelling results for Pd(II) onto montmorillonite using optimized surface complexation constants for metal-binding surface species, unadjusted constants for ternary chloride surface species, and unchanged cation exchange selectivity coefficients. The JAEA TDB was used with the SIT and Davies computational method.

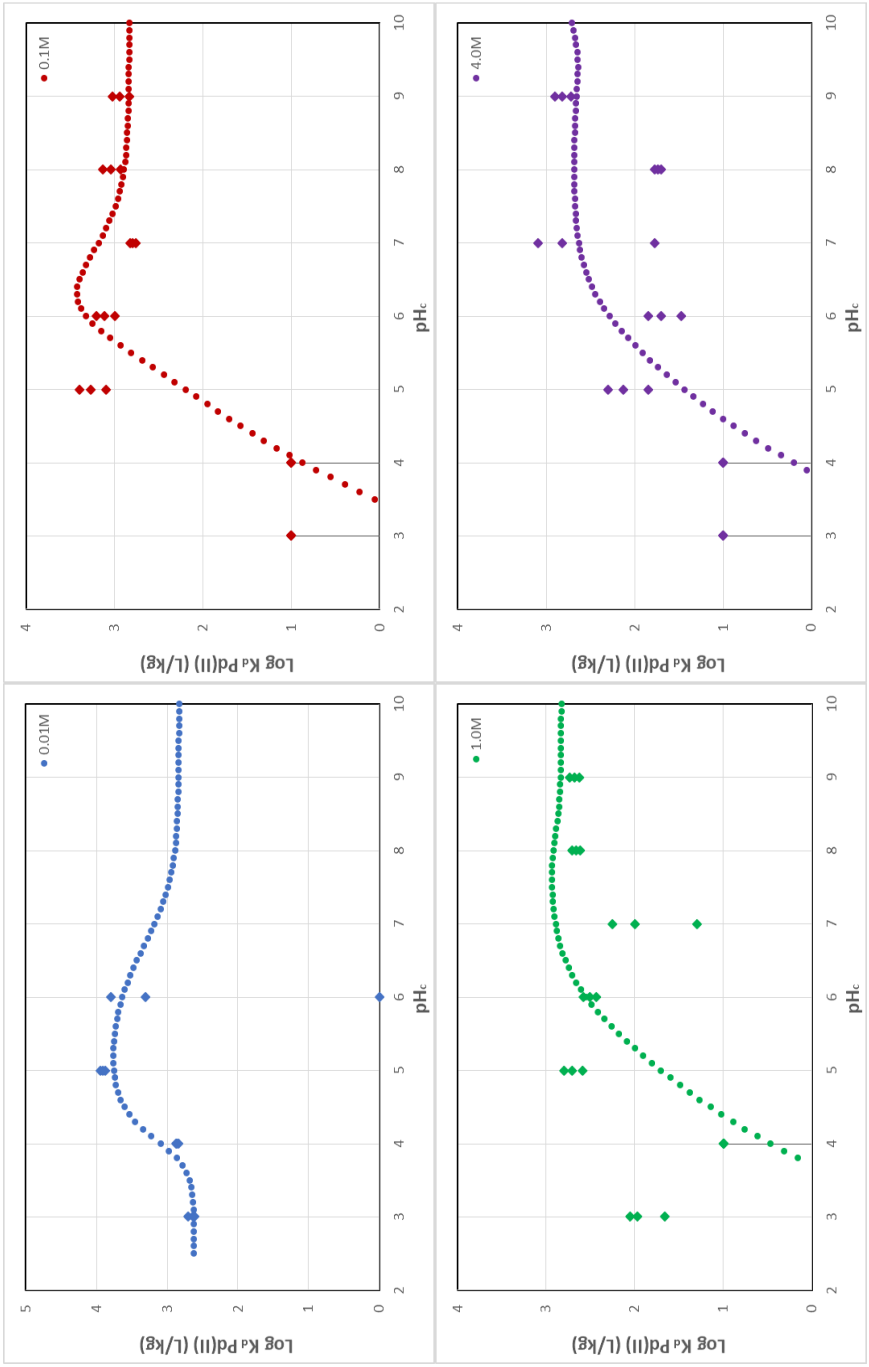

Figure 5.20: Sorption modelling results for Pd(II) onto illite using optimized surface complexation constants for metal-binding surface species, increased complexation constant for the *S-OPdCl*$_4^{-3}$ surface species from 13.05 to 13.50, and unchanged cation exchange selectivity coefficients. The JAEA TDB was used with the SIT and Davies computational method.

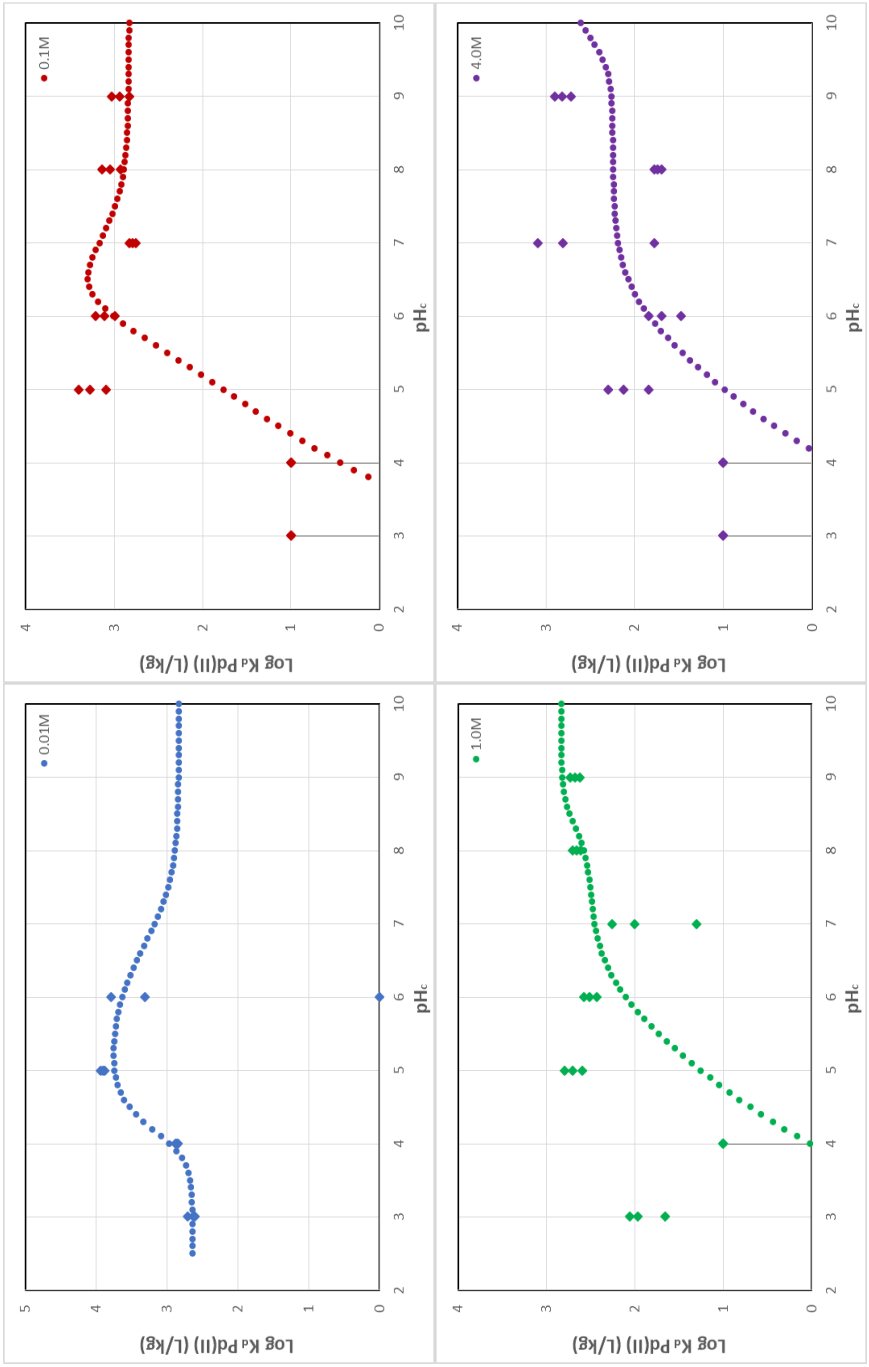

Figure 5.21: Sorption modelling results for Pd(II) onto illite using re-optimized surface complexation constants for metal-binding surface species, increased complexation constant and aqueous species formation reaction constant in JAEA TDB for the *S-OPdCl*$_4^{-3}$ surface species from 13.05 to 13.50, and re-optimized cation exchange selectivity coefficients. The JAEA TDB was used with the SIT and Davies computational method.

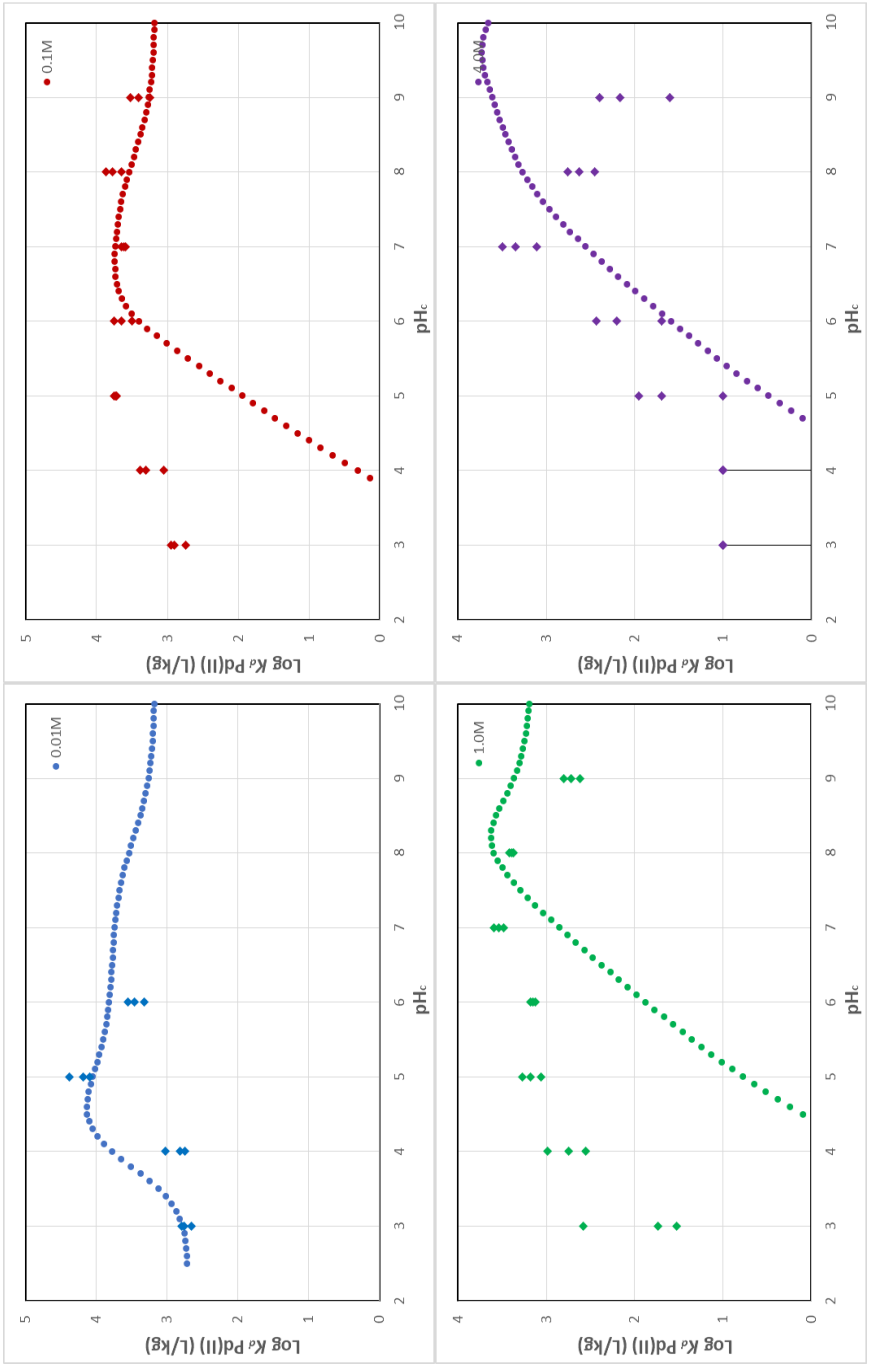

Figure 5.22: Sorption modelling results for Pd(II) onto montmorillonite using optimized surface complexation constants for metal-binding surface species, reduced complexation constant for the *S-OPdCl*$_4^{-3}$ surface species from 13.05 to 12.46, and unchanged cation exchange selectivity coefficients. The JAEA TDB was used with the SIT and Davies computational method.

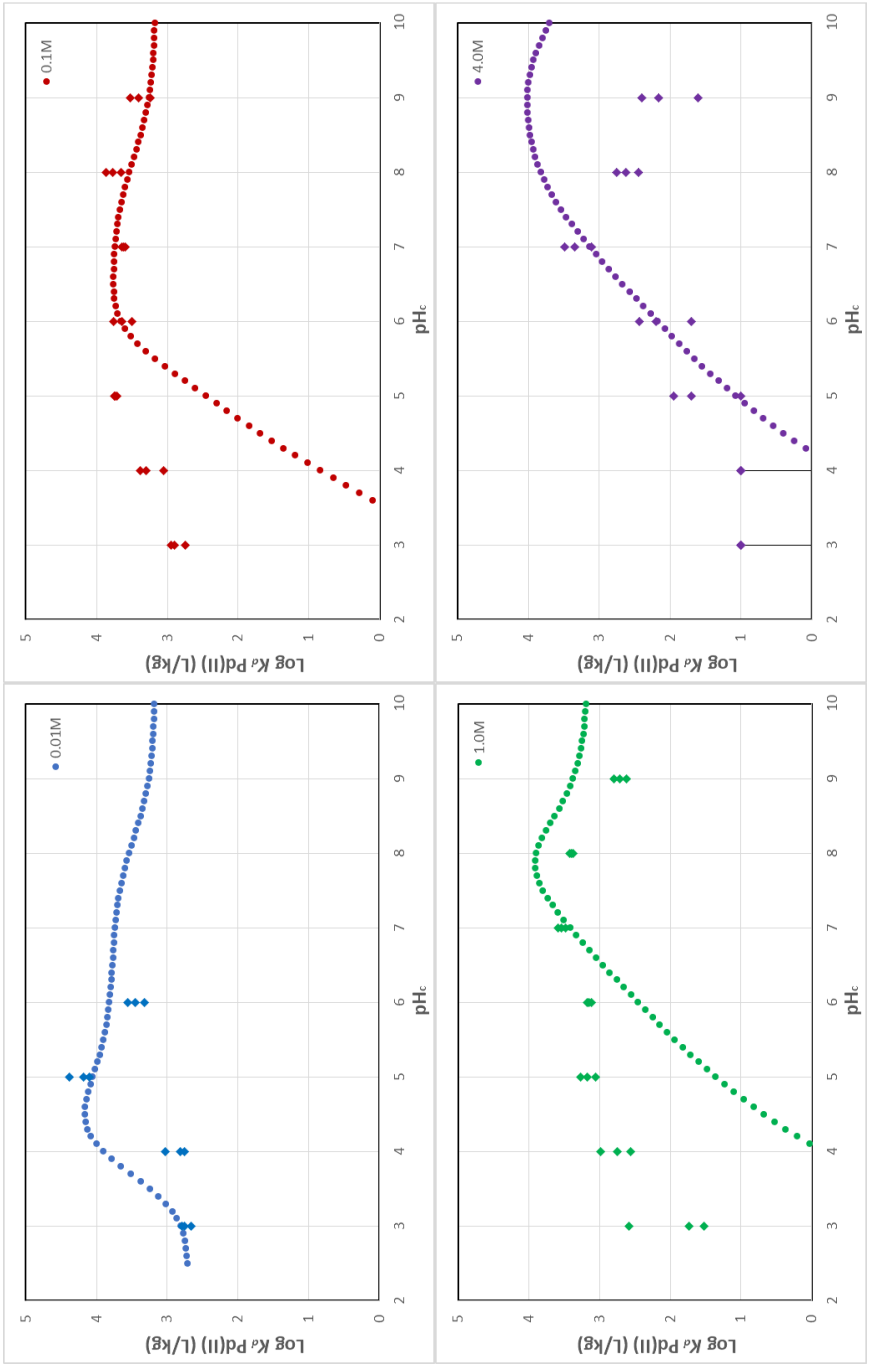

Figure 5.23: Sorption modelling results for Pd(II) onto montmorillonite using re-optimized surface complexation constants for metal-binding surface species, reduced complexation constant and aqueous species formation reaction constant in JAEA TDB for the *S-OPdCl*$_4^{-3}$ surface species from 13.05 to 12.46, and re-optimized cation exchange selectivity coefficients. The JAEA TDB was used with the SIT and Davies computational method.

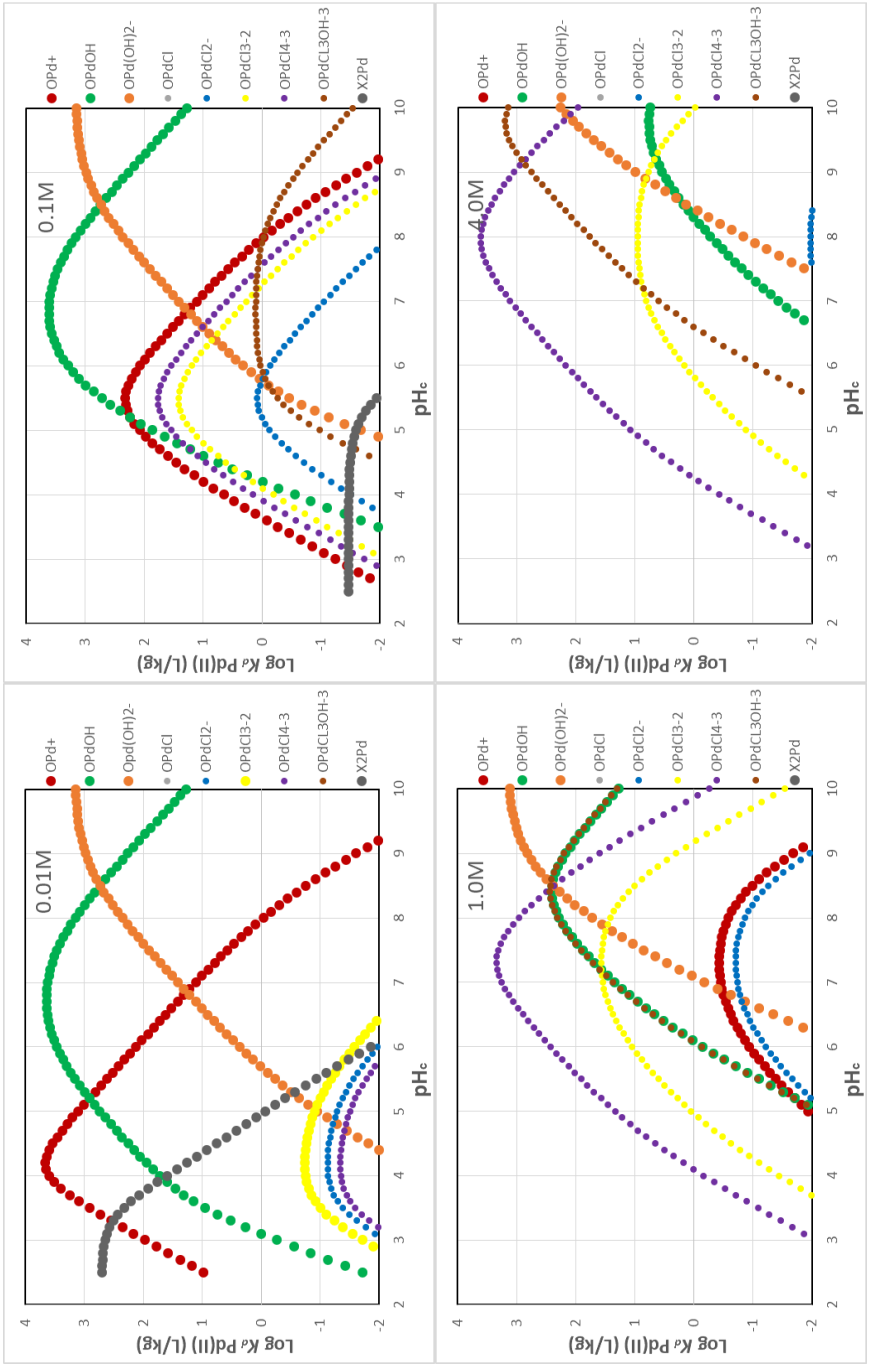

Figure 5.24: Contribution of each species to sorption for Pd(II) onto montmorillonite with optimized surface complexation constants and selectivity coefficients. The JAEA TDB was used with the SIT and Davies computational method.

5.3.3 Np(IV) Sorption Using the 2SPNE SC Model

Np(IV) was first modelled by 2SPNE SC using the R07 THEREDA (2013), and the surface complexation reaction constants obtained from Banik (2016), for illite and Bradbury (2005b), for montmorillonite (Table 4.18). These models were plotted with experimental K_d values obtained from Nagasaki (2017), for 0.1, 4.0, and 6.0 M *Na-Ca-Cl* solutions, which can be seen in Table 5.7 below.

Table 5.7: Referenced K_d data for Np(IV) sorption modelling.

IS (M)	pH_C	K_d - Illite (m^3/kg)	Error (m^3/kg)	pH_C	K_d - Bentonite (m^3/kg)	Error (m^3/kg)
0.1	3.1	89.8	2.8	3.0	99.2	10.3
0.1	4.2	178.6	37.2	3.9	187.4	17.9
0.1	5.0	240.2	21.8	5.0	250.7	4.1
0.1	5.8	210.0	0.0	5.8	220.0	0.0
0.1	7.2	219.9	13.7	7.2	238.5	20.6
0.1	8.2	205.0	0.0	8.2	200.0	0.0
0.1	9.1	232.9	28.2	9.1	242.5	83.9
0.1	10.1	226.3	10.2	9.9	259.8	60.1
4.0	3.3	84.8	3.4	3.2	147.7	14.9
4.0	4.2	83.6	14.2	3.9	111.6	4.9
4.0	5.1	145.7	23.2	5.1	189.6	18.6
4.0	6.2	114.0	14.8	6.2	149.0	8.7
4.0	7.1	116.0	9.1	7.1	131.0	14.6
4.0	8.0	110.0	9.1	8.1	148.0	13.2
4.0	9.0	114.0	6.7	9.1	172.0	7.4
4.0	9.9	113.0	7.2	10.0	149.0	17.0
6.0	3.2	78.0	12.7	3.3	92.6	8.7
6.0	4.1	141.8	23.9	3.9	149.3	5.2
6.0	5.2	103.8	2.5	5.2	173.8	13.3
6.0	6.1	152.0	27.4	6.1	138.0	40.4
6.0	7.1	155.0	19.7	7.0	144.0	10.9
6.0	8.1	123.0	6.4	8.0	131.0	14.7
6.0	8.9	136.0	6.9	9.1	167.0	7.1
6.0	10.4	149.0	15.0	10.0	170.0	13.0

Without the use of the Pitzer parameters contained in the THEREDA, PHREEQC uses the Davies and WATEQ Debye-Hückel equations to compute the activity coefficients. Sorption of Np(IV) was modelled with and without the use of the Pitzer parameters (Table 4.5 & Table 4.6) and computational method, which can be seen for both illite and montmorillonite in Figure 5.25 below. All three of the values of *I* were modelled with the use of the Pitzer parameters, but the Davies equation is only effective at calculating sorption up to a maximum of 0.5 M (Raton, 1986), and was therefore only plotted with the 0.1 M experimental data. Little difference is seen between the two computational methods for 0.1 M *I*, but the Pitzer computational method has the additional capability of accurately modelling at higher *I*.

The models were then modified to fit the experimental data, first with the addition of the ternary chloride species shown in Table 4.18 (having no visible effect on the sorption edge), then with the addition of the missing metal-binding surface species for each soil, and lastly, with the optimization of the surface complexation constants for all strongly-bound metal-binding species. Optimization of the $S\text{-}ONp^{+3}$ surface species (strong and weak), was not required for the optimization of either clay, as the contribution to sorption peaks at a pH less than 2 for 0.1 M *I*, and up to a pH of 3 for 6.0 M *I* for both clays where there is no experimental data to fit to. Instead, the LFER Equations 4.2 and 4.3 for strong, and 5.4 below for weak (Bradbury, 2005b), were used with the corresponding hydrolysis constants in the THEREDA to calculate the surface complexation constants, which can all be seen in Table 5.8 below. Equations 4.2 and 4.3 were also used to calculate the range of surface complexation constants that could still be described by the LFER with the use of the hydrolysis constants contained in the THEREDA. These values can be seen in Table 5.9. Of the four Np metal-binding surface species that were modified to fit the sorption edge to the experimental data ($S\text{-}ONpOH^{+2}$, $S\text{-}ONp(OH)_2^{+}$, $S\text{-}ONp(OH)_3$, & $S\text{-}ONp(OH)_4^{-}$), ranges of values consistent with the LFER could only be calculated for the first three as there is

no formation reaction constant in the THEREDA for $Np(OH)_5^-$. Of the remaining three sorption reactions, two of the reaction constants fall outside the range of values that follow the LFER for both clays: $S\text{-}ONpOH^{+2}$ and $S\text{-}ONp(OH)_3$. Despite the addition of the $S\text{-}ONp^{+3}$ surface species to the optimized model, seen in Figure 5.26 for illite and Figure 5.28 for montmorillonite, it can be seen in Figure 5.27 for illite and Figure 5.29 for montmorillonite that it (along with $S\text{-}ONpCl^{+2}$), does not significantly contribute to the sorption edge. Figure 5.27 and Figure 5.29 show the contribution of each Np surface species to the total sorption in units of L kg^{-1} for illite and montmorillonite respectively. As seen in Figure 5.27 and Figure 5.29: the $S\text{-}ONpOH^{+2}$ surface species dominates sorption up to pH 4 for illite and 4.5 for montmorillonite; $S\text{-}ONp(OH)_2^+$ dominates for pH 4 – 6 for illite, and 4.5 – 5.5 for montmorillonite; $S\text{-}ONp(OH)_3$ dominates at a pH of 5.5 – 6.5 for illite, and for pH 5.5 – 8 for montmorillonite; and $S\text{-}ONp(OH)_4^-$ dominates for pH values above 6.5 for illite, and 8 for montmorillonite.

$$\mathrm{Log}^{\mathrm{W1}}K_M = 6.2 \pm 0.8 + (0.98 \pm 0.09)\,\mathrm{Log}^{\mathrm{OH}}K \tag{5.4}$$

A reasonable fit was obtained for illite and montmorillonite. However, the fit shows that the experimental K_d values slightly decrease with increasing I, whereas the modelled values slightly increase with increasing I between the pH of approximately 4 and 7 for both clays. For illite, the surface complexation constants for the $S\text{-}ONp(OH)_2^+$, $S\text{-}ONp(OH)_3$, and $S\text{-}ONp(OH)_4^-$ surface species obtained from Banik (2016), were all too high and, in particular, the $S\text{-}ONp(OH)_2^+$ surface species, which dominates sorption between a pH of 4 and 6 for all I, had to be lowered in order to reduce the hump in the sorption edge in the same pH region. The $S\text{-}ONpOH^{+2}$ surface species that was added to the illite model is necessary to increase the sorption edge below a pH of 4.5 – 5.0, where there is a steep decline in the K_d values, in order to get a better fit to the experimental K_d values at pH 3

and 4. As *I* increases, the contribution of the $S\text{-}ONpOH^{+2}$ surface species to the sorption edge at low pH decreases, but this is matched by the decrease in the experimental K_d values for pH 3and 4. For montmorillonite, the most significant contribution to the model is with the addition of the $S\text{-}ONp(OH)_4^-$ surface species, which allows for accurate results for sorption in alkaline conditions. Of the three surface complexation constants for metal-binding species obtained from Bradbury (2005b), that were optimized to fit the experimental data ($S\text{-}ONpOH^{+2}$, $S\text{-}ONp(OH)_2^+$, & $S\text{-}ONp(OH)_3$), the $S\text{-}ONpOH^{+2}$ surface species was raised from 8.5 to 9.8 (in order to increase the total sorption around a pH of 3 for all ionic strengths), and the $S\text{-}ONp(OH)_2^+$ and $S\text{-}ONp(OH)_3$ were both decreased to lower the sorption edge between a pH of 5 – 8. Sorption of Np(IV) was found to be slightly dependent on *I* and mostly independent of pH above 6.5 for both illite and montmorillonite.

Table 5.8: Optimized surface complexation constants used for Np(IV) sorption modelling.

Surface Complexation Reaction	$Log^S K_I$	$Log^S K_M$	$Log^{W1} K_M$
Metal Binding:			
$S\text{-}OH + Np^{+4} \leftrightarrow S\text{-}ONp^{+3} + H^+$	8.36	8.1	6.7
$S\text{-}OH + Np^{+4} + H_2O \leftrightarrow S\text{-}ONpOH^{+2} + 2H^+$	9.5	9.8	-
$S\text{-}OH + Np^{+4} + 2H_2O \leftrightarrow S\text{-}ONp(OH)_2^+ + 3H^+$	5.4	5.3	-
$S\text{-}OH + Np^{+4} + 3H_2O \leftrightarrow S\text{-}ONp(OH)_3 + 4H^+$	-0.1	-0.3	-
$S\text{-}OH + Np^{+4} + 4H_2O \leftrightarrow S\text{-}ONp(OH)_4^- + 5H^+$	-6.4	-8.2	-
Ternary:			
$S\text{-}OH + Np^{+4} + Cl^- \leftrightarrow S\text{-}ONpCl^{+2} + H^+$	1.5	1.5	-

*Reaction constants highlighted in grey fall outside of the range of the LFER.

Table 5.9: Range of surface complexation constants that follow the LFER based on the aqueous species formation reaction constants contained in the THEREDA for Np(IV).

Surface Complexation Reaction	$Log^S K_I$	$Log^S K_M$	$Log^{W1} K_M$
$S\text{-}OH + Np^{+4} \leftrightarrow S\text{-}ONp^{+3} + H^+$	7.95 – 8.77	8.28 – 8.91	5.89 – 7.59
$S\text{-}OH + Np^{+4} + H_2O \leftrightarrow S\text{-}ONpOH^{+2} + 2H^+$	7.78 – 8.60	8.12 – 8.72	-
$S\text{-}OH + Np^{+4} + 2H_2O \leftrightarrow S\text{-}ONp(OH)_2^+ + 3H^+$	5.12 – 6.03	5.22 – 5.94	-
$S\text{-}OH + Np^{+4} + 3H_2O \leftrightarrow S\text{-}ONp(OH)_3 + 4H^+$	0.44 – 1.58	0.16 – 1.10	-

To compare additional computational methods, Np(IV) was first modelled with the optimized surface complexation constants in Table 5.8 without the use of the Pitzer parameters for 0.1 M, and can be seen in Figure 5.30 below. Np(IV) was then modelled with the use of the SIT and epsilon parameters contained in the JAEA TDB shown in Table 4.4, but with the same aqueous species formation reaction constants contained in the THEREDA, and not those contained within the JAEA TDB. When modelling with the JAEA TDB with the SIT, the surface complexation constants for the $S\text{-}ONpOH^{+2}$ surface species had to be adjusted from 9.5 to 9.1 for illite, and from 9.8 to 9.7 for montmorillonite, as the sorption edge around pH 3.5 to 5.5 was slightly higher than when using the THEREDA and other computational methods. SIT has only been shown to be accurate when computing the mass-action equations for solutions up to an I of 4.0 M (Grenthe, 1997), so sorption models were only plotted against the experimental data for 0.1 and 4.0 M, which can be seen for illite and montmorillonite in Figure 5.31 below.

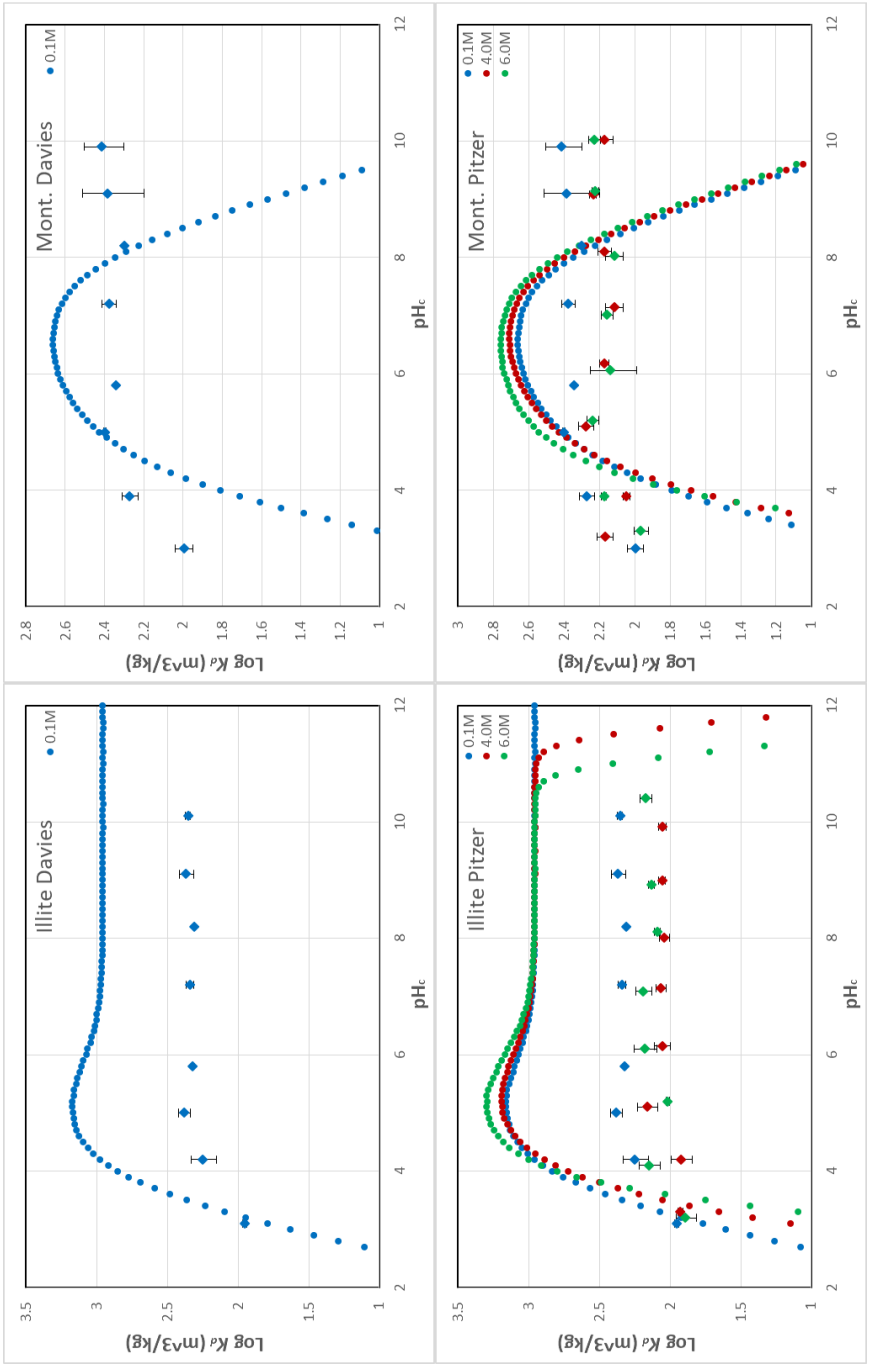

Figure 5.25: Sorption modelling results for Np(IV) onto illite and montmorillonite using surface complexation constants from Banik (2016), and Bradbury (2005b), respectively, and experimental results from Nagasaki (2017). The R07 THEREDA (2013), was used with the Davies and the Pitzer computational method.

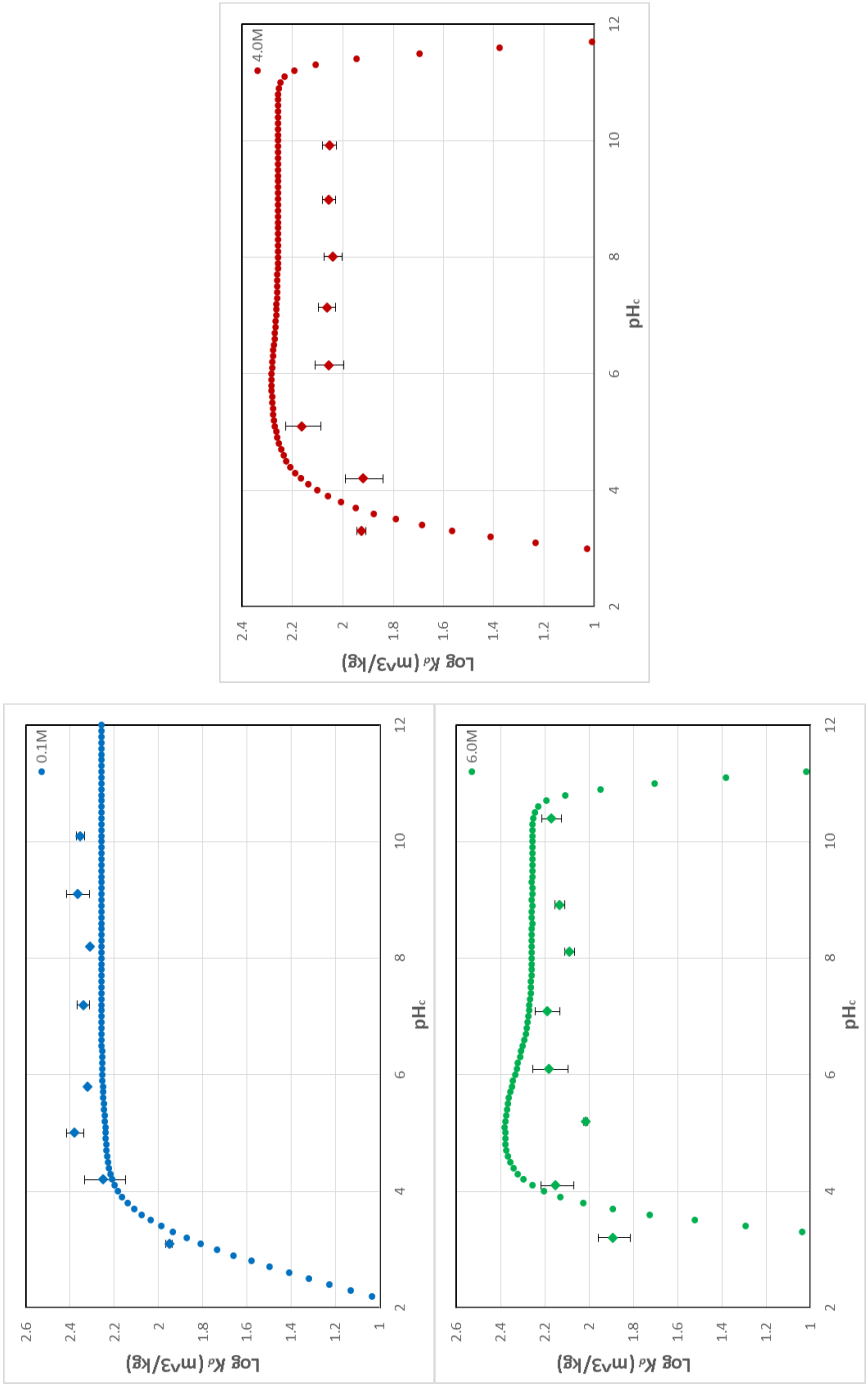

Figure 5.26: Sorption modelling results for Np(IV) onto illite with optimized surface complexation constants, and experimental results from Nagasaki (2017). The R07 THEREDA (2013), was used with the Pitzer parameters and computational method.

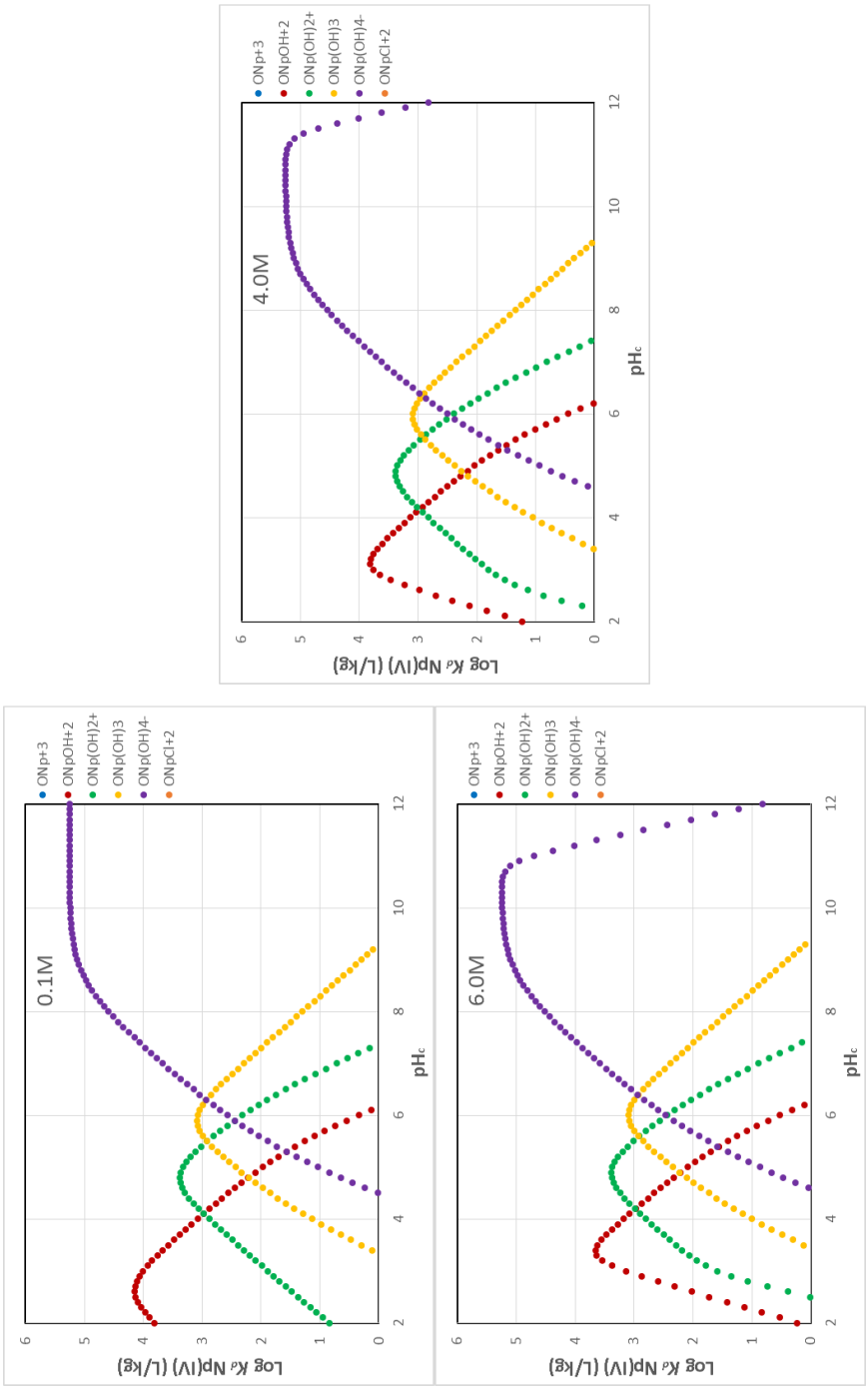

Figure 5.27: Surface species' contribution to sorption for Np(IV) onto illite with optimized surface complexation constants, and experimental results from Nagasaki (2017). The R07 THEREDA (2013), was used with the Pitzer parameters and computational method.

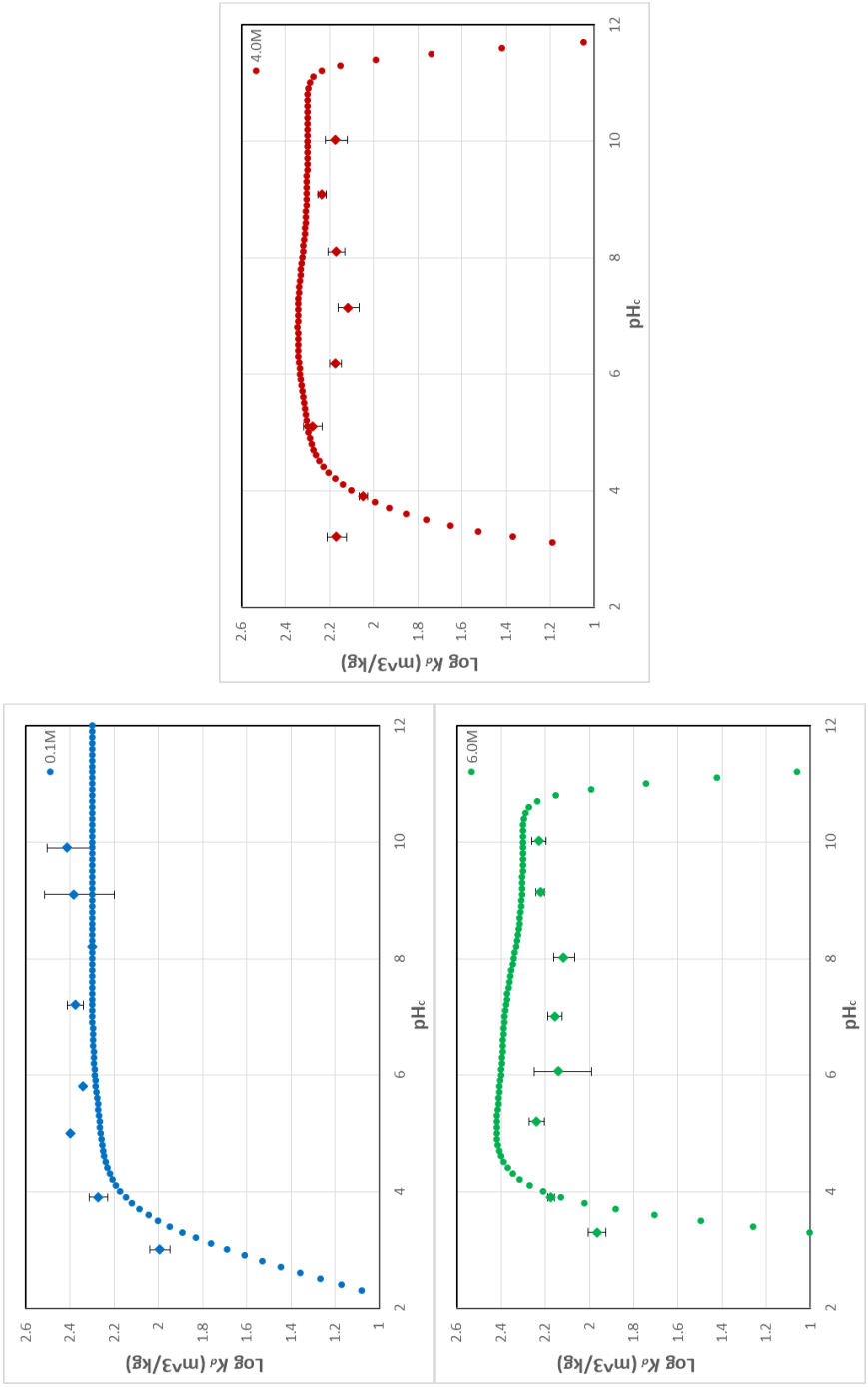

Figure 5.28: Sorption modelling results for Np(IV) onto montmorillonite with optimized surface complexation constants, and experimental results from Nagasaki (2017). The R07 THEREDA (2013), was used with the Pitzer parameters and computational method.

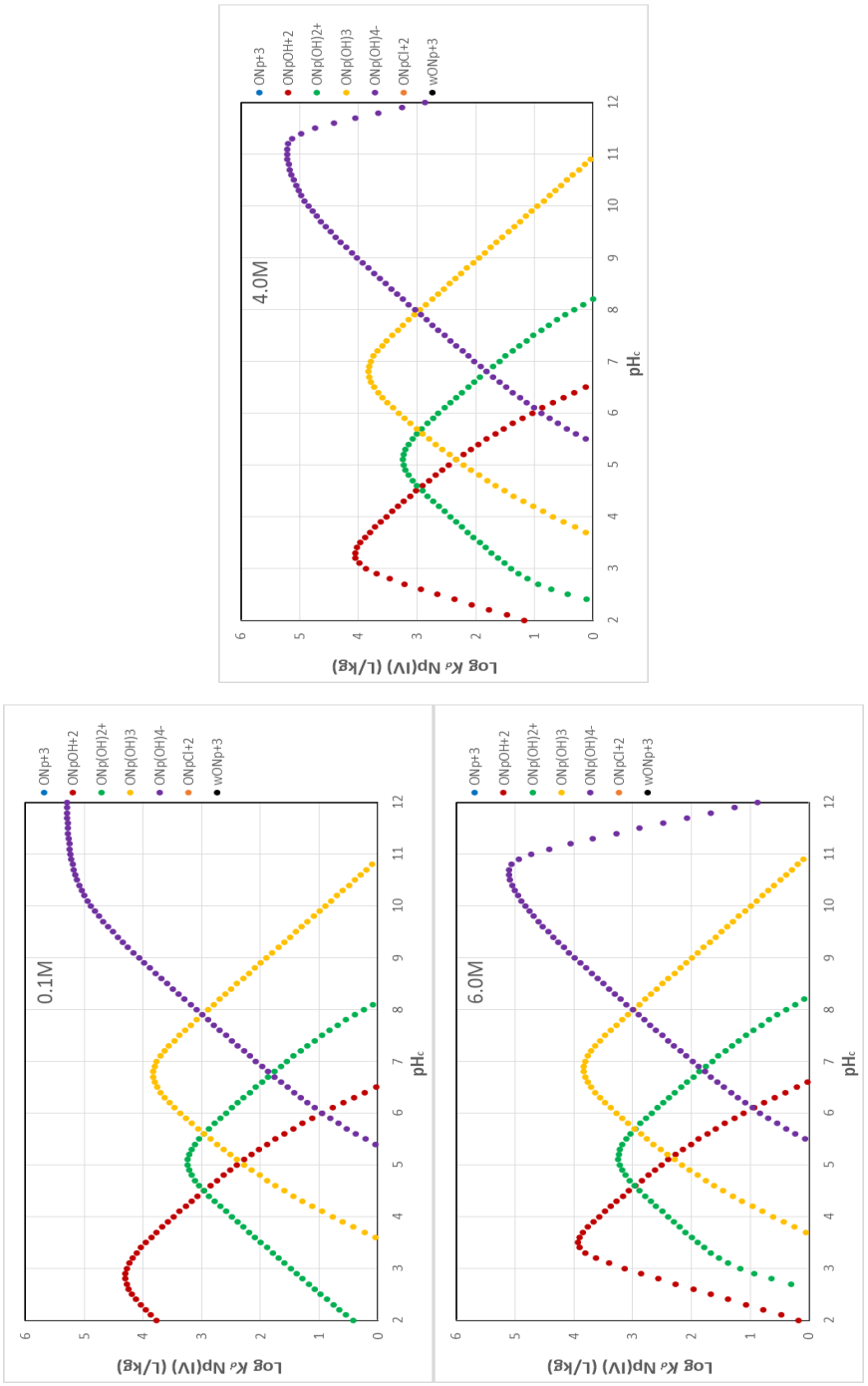

Figure 5.29: Surface species' contribution to sorption for Np(IV) onto montmorillonite with optimized surface complexation constants, and experimental results from Nagasaki (2017). The R07 THEREDA (2013), was used with the Pitzer parameters and computational method.

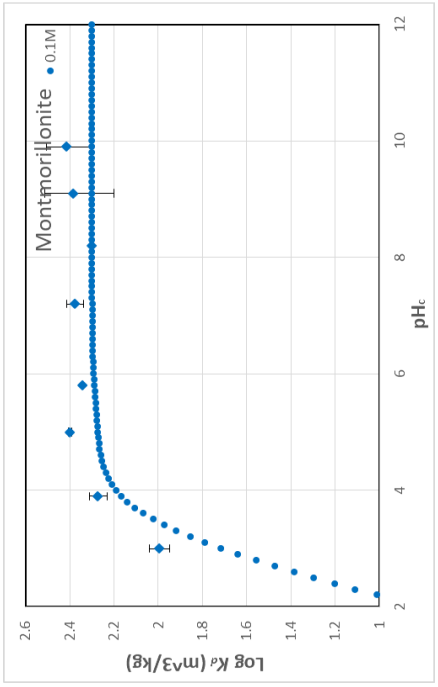

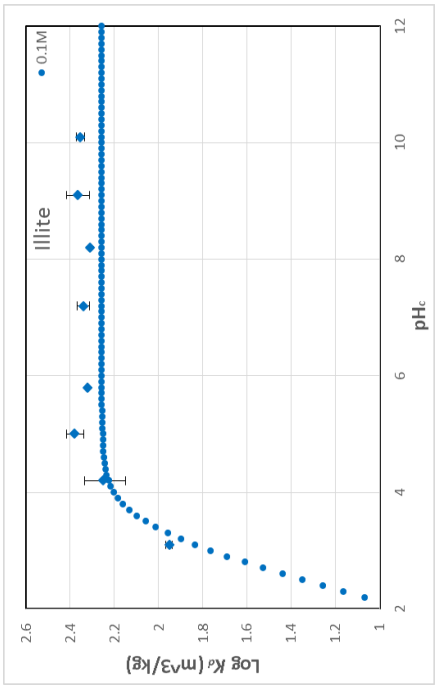

Figure 5.30: Sorption modelling results for Np(IV) onto illite and montmorillonite with optimized surface complexation constants, and experimental results from Nagasaki (2017). The R07 THEREDA (2013), was used without the Pitzer parameters and computational method (defaulting to the Davies and WATEQ Debye-Hückel computational methods).

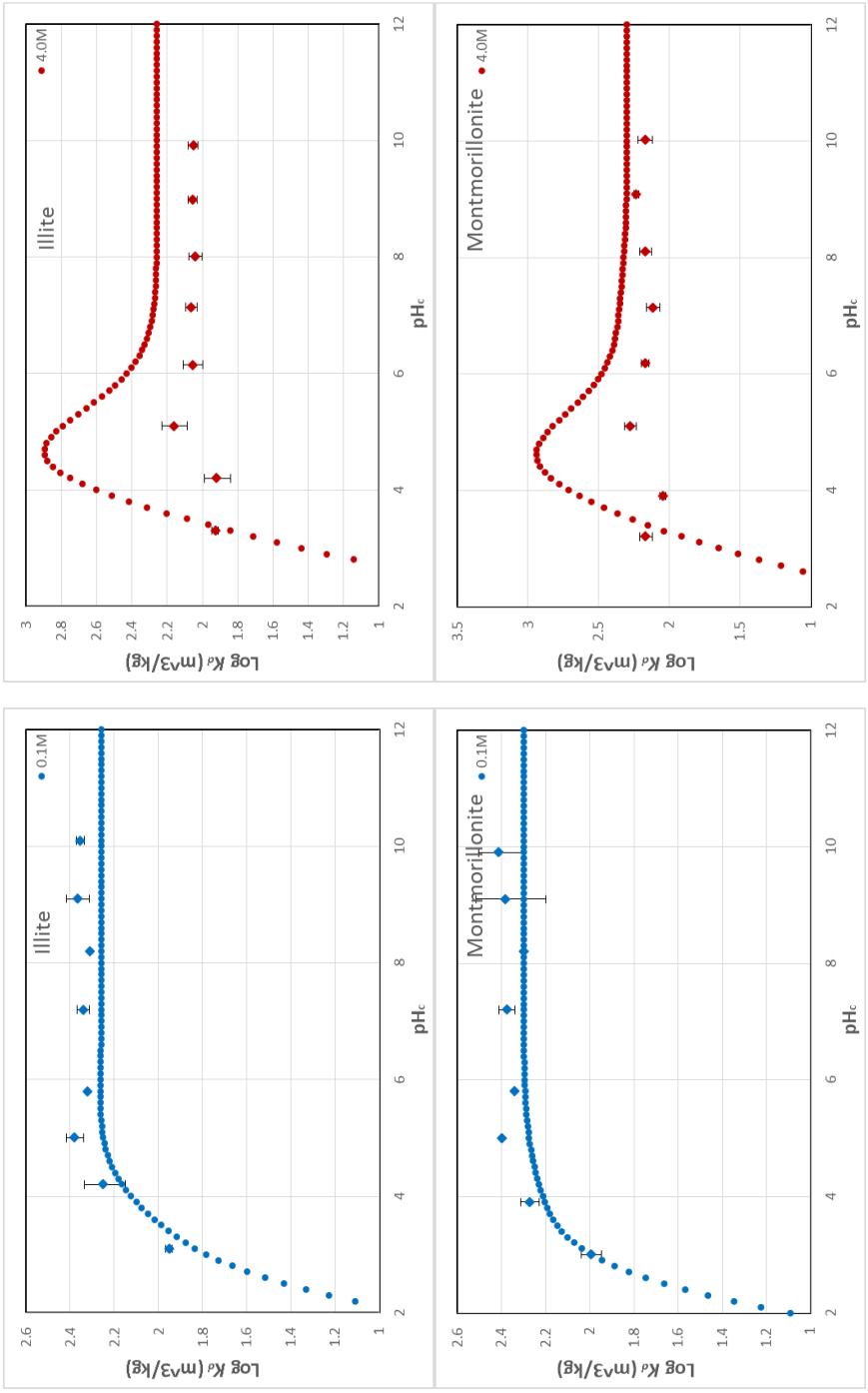

Figure 5.31: Sorption modelling results for Np(IV) onto illite and montmorillonite with optimized surface complexation constants, and experimental results from Nagasaki (2017). The JAEA TDB was used with the NEA formation reaction constants, SIT computational method, and epsilon values contained in the database.

5.3.4 Np(V) Sorption Using the 2SPNE SC Model

Np(V) was modelled by 2SPNE SC using the R04 THEREDA (2015) (modified to include Ca^{+2} to the solution master species), and the surface complexation reaction constants obtained from Gorgeon (1994), and Bradbury (2005b), for illite and montmorillonite (Table 4.19), and can be seen in Figure 5.32 below. These models were plotted with experimental K_d values obtained from Nagasaki (2015), for 4.6 M *Na-Ca-Cl*, which can be seen in Table 5.10 below. Since the experimental sorption tests of Np(V) being modelled were in a solution with an *I* of 4.6 M, the only computational method used was Pitzer. It was found in Nagasaki (2015), that the K_d values for sorption of Np(V) onto illite and montmorillonite were independent of *I* at least between 1.0 – 4.6 M (0.10 – 4.6 M for illite), but preliminary testing of the model did not produce K_d values independent of *I*, so all models were conducted in 4.6 M *I*.

Table 5.10: Referenced Kd data for Np(V) sorption modelling.

***IS* (M)**	**pH$_C$**	**K_d - Illite (L/kg)**	**Error (L/kg)**	**pH$_C$**	**K_d - Bentonite (m^3/kg)**	**Error (m^3/kg)**
4.6	6.24	34.66	4.79	6.23	46.26	7.02
4.6	7.22	40.38	5.32	7.24	70.44	5.18
4.6	7.77	50.18	3.94	8.26	133.65	18.06
4.6	7.65	56.18	2.82	9.08	159.70	34.88
4.6	8.23	57.99	6.30	9.01	176.08	26.21
4.6	9.20	88.11	5.53	9.28	227.06	18.10
4.6	9.71	96.40	7.92	9.73	268.65	38.62

The surface complexation constants were then optimized for both clays to fit the experimental data, which can be seen in Table 5.11 below. The optimized plots for both clays can be seen, along with speciation graphs to show the contribution of each Np surface species to the total sorption in units of L kg^{-1}, in Figure 5.33 below. Sorption of Np(V) was found to be moderately dependent on pH for illite (and highly dependent below 6.5), and

independent of pH above 8 for montmorillonite. Equations 4.2 and 4.3 were also used to calculate the range of surface complexation constants that could still be described by the LFER with the use of the hydrolysis constants contained in the THEREDA, which can be seen in Table 5.12 below. Of the two Np metal-binding surface species that were modified to fit the sorption edge to the experimental data (*S-ONpO₂* & *S-ONpO₂OH⁻*), one of the reaction constants fall outside the range of values that follow the LFER for both clays: *S-ONpO₂OH⁻*.

Table 5.11: Optimized surface complexation constants used for Np(V) sorption modelling.

Surface Complexation Reaction	$Log^S K_I$	$Log^S K_M$
$S\text{-}OH + NpO_2^+ \leftrightarrow S\text{-}ONpO_2 + H^+$	-1.55	-2.25
$S\text{-}OH + NpO_2^+ + H_2O \leftrightarrow S\text{-}ONpO_2OH^- + 2H^+$	-10.5	-11.5

*Reaction constants highlighted in grey fall outside of the range of the LFER.

Table 5.12: Range of surface complexation constants that follow the LFER based on the aqueous species formation reaction constants contained in the THEREDA for Np (V).

Surface Complexation Reaction	$Log^S K_I$	$Log^S K_M$
$S\text{-}OH + NpO_2^+ \leftrightarrow S\text{-}ONpO_2 + H^+$	-2.11 – -0.85	-2.60 – -1.54
$S\text{-}OH + NpO_2^+ + H_2O \leftrightarrow S\text{-}ONpO_2OH^- + 2H^+$	-12.56 – -10.82	-13.91 – -12.37

A good fit was able to be obtained for illite and a reasonable fit was obtained for montmorillonite. For illite, the surface complexation constant obtained from Gorgeon (1994), for the *S-ONpO₂* surface species was too low and was raised from -2.0 to -1.55 to fit the experimental data in the pH range where the surface species dominates sorption: up to 9. The surface complexation constant for the *S-ONpO₂OH⁻* surface species was too high and had to be lowered from -10.3 to -10.5 to slightly lower the modelled sorption edge in the region of dominance above a pH of 9. Although the optimized surface complexation constant for this surface species falls outside of the allowable range for the LFER, the original constant obtained from Gorgeon (1994), falls outside of this range as well. For

montmorillonite, the surface complexation constants obtained from Bradbury (2005b), for the *S-ONpO$_2$* and *S-ONpO$_2$OH$^-$* surface species were too low, and were raised from -2.8 to -2.25 and -12.8 to -11.5 respectively, in order to fit the experimental data in the pH range where the surface species dominates sorption (up to 10 for the former, and above 10 for the latter). Although the surface complexation constant for the *S-ONpO$_2$OH$^-$* surface species fell outside of the allowable range of the LFER after optimization, the reaction constant for the *S-ONpO$_2$* surface species originally proposed in Bradbury (2005b) was brought back into the allowable range of the LFER post-optimization, as it originated outside of the range.

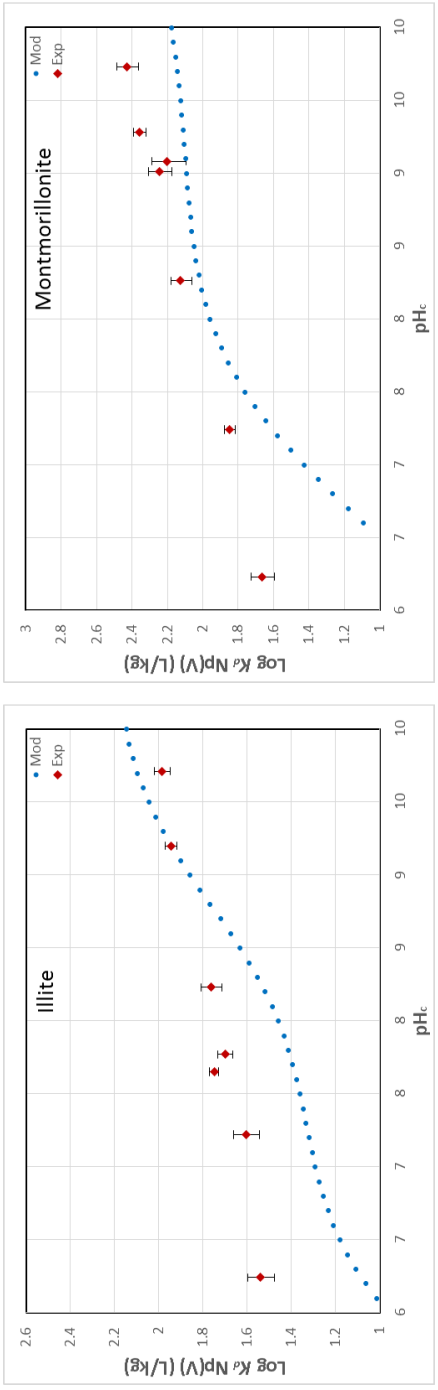

Figure 5.32: Sorption modelling results for Np(V) onto illite and montmorillonite using surface complexation constants from Gorgeon (1994), and Bradbury (2005b), respectively, and experimental results from Nagasaki (2015). The R04 THEREDA (2015) was used with the Pitzer parameters and computational method.

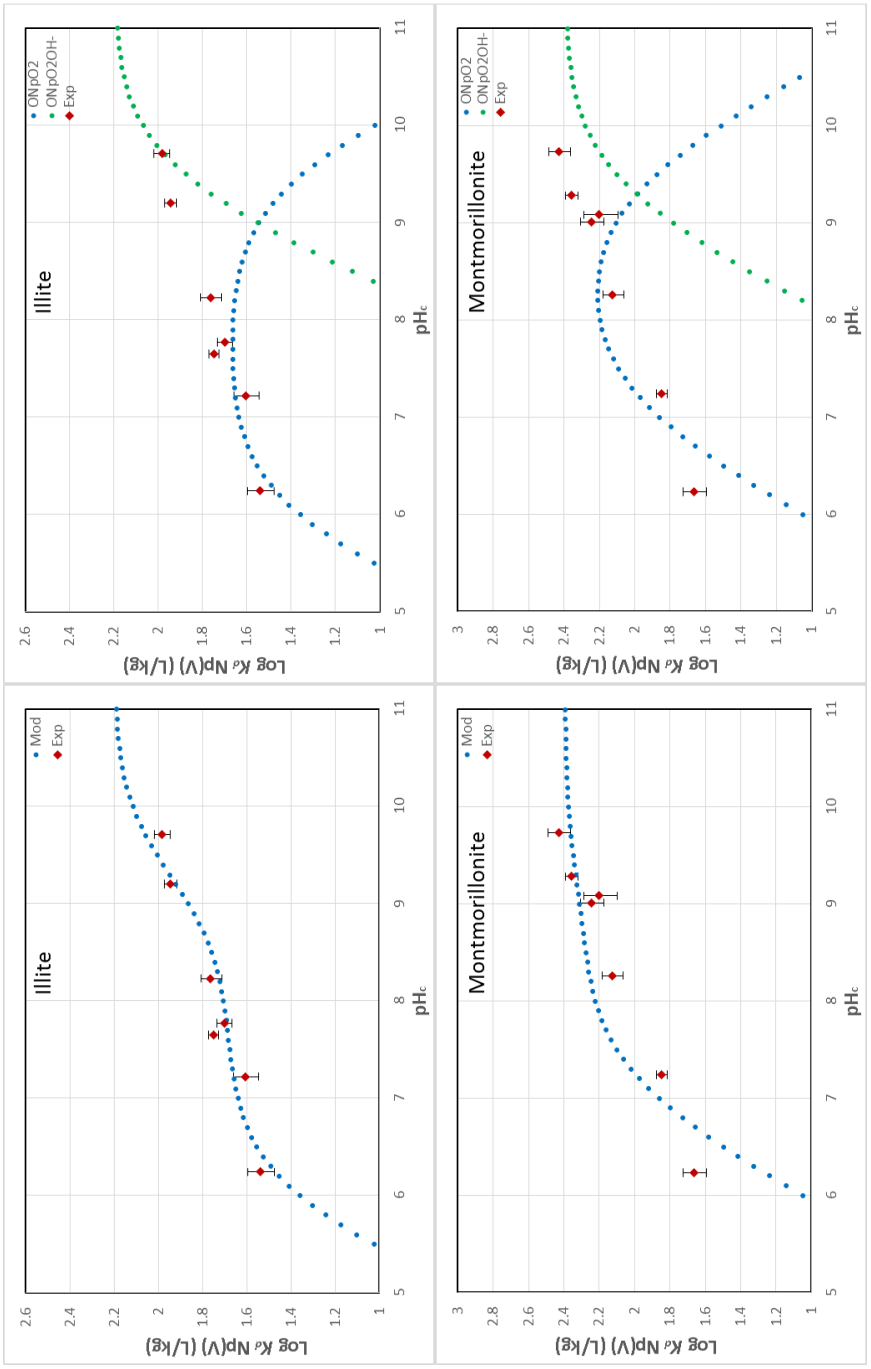

Figure 5.33: Sorption modelling results for Np(V) onto illite and montmorillonite with optimized surface complexation constants, and experimental results from Nagasaki (2015). The R04 THEREDA (2015) was used with the Pitzer parameters and computational method.

Chapter 6

Discussion

6.1 pH Calibrations for *Na-Ca-Cl* Solutions

According to Thermo Fisher Scientific (2014), pH electrodes take measure of the hydrogen ion activity (pH_M), and not the hydrogen ion concentration (pH_C). This is a problem for measuring the pH of solutions with high *I* because ion mobility is decreased in these solutions despite the concentration of ions remaining the same or possibly even increasing. A second problem associated with solutions of high *I* is that they change the liquid junction potential, resulting in bias and instability in probe readings. These effects could be seen as the correction factor between pH_M and pH_C increased proportionally with the *I* of the *Na-Ca-Cl* solution. The probe instability increasing with *I* contributes to a greater error in the pH_M at higher *I*, which when measuring the effect of pH on sorption may result in greater error when plotting K_d values against pH_C, thus affecting the sorption edge and optimized surface complexation constants fitted to those values. To account for this discrepancy arising between the pH_M and pH_C, the equations shown in Table 5.1 were

used in the process of adjusting the pH of sorption samples to the correct pH_C, and for accurately reporting the actual pH of samples from recorded pH_M values for all *I*.

In Riddoch (2016), it was found when modelling the sorption edge of Pd(II) onto illite and montmorillonite that there appeared to be a pH discrepancy between the experimental data and the modelling results. Following the same experimental procedures as in Riddoch (2016), and using the same laboratory equipment in this work some investigation was done into the potential source of this discrepancy. After the conversion formulas in Table 5.1 were used in the experimental procedures, a test was done to find the internal offset of the titrator and the methodology for the derivation of the correction factor formulas by running DI water through the same testing procedure. The result of this test was the last conversion formula listed in Table 5.1, seen in Equation 6.1 below. To correct for this offset, the pH_C in Equation 6.2 has to be subtracted from the other formulas listed in Table 5.1. These corrected conversion formulas can be seen in Table 6.1 below.

$$pH_{C\,(DI)} = 1.02 \times pH_M + 0.01 \tag{6.1}$$

$$pH_O = 0.02 \times pH_M + 0.01 \tag{6.2}$$

Table 6.1: Corrected pH_C & pH_M conversion formulas for aqueous *Na-Ca-Cl* solutions.

Ionic Strength (M)	Adjustment Equation
0.01	$pH_C = 1.02 \times pH_M + 0.01$
0.1	$pH_C = 0.99 \times pH_M + 0.10$
1.0	$pH_C = 0.93 \times pH_M + 0.80$
4.0	$pH_C = 0.95 \times pH_M + 0.94$
6.0	$pH_C = 0.98 \times pH_M + 1.02$

It can be seen from the corrected conversion formulas in Table 6.1 above that the original set of conversion formulas shown in Table 5.1 were overcorrecting the difference

between pH_M and pH_C, resulting in the pH-adjusted Pd samples being adjusted to a slightly lower pH than intended. In addition to this offset being too small to account for the pH-shift discussed in Riddoch (2016), the offset is in the wrong direction (exacerbating the discrepancy). This indicates that the pH-offset found in Riddoch (2016), is unlikely due to the titrator's internal errors when developing the pH conversion formulas. In Riddoch (2016), the y-intercept of the linear regression was ignored in the derivation of the pH conversion formulas for 0.1, 1.0, and 4.0 M *I*. In this work, the y-intercept on the pH_C-pH_M plot was not ignored, resulting in conversion formulas that vary drastically with those presented in Riddoch (2016), which can be seen in Table 6.2 below.

Table 6.2: pH_C & pH_M conversion formulas for *Na-Ca-Cl* solutions in Riddoch (2016).

Ionic Strength (M)	Adjustment Equation
0.1	$pH_C = 1.003 \times pH_M$
1.0	$pH_C = 1.060 \times pH_M$
4.0	$pH_C = 1.012 \times pH_M$

Taking the range of pH_C values that Pd samples were adjusted to in the sorption experiments (3 – 9), the conversion formulas derived in this work, and the conversion formulas presented in Riddoch (2016), were used to determine the offset of the conversion used for the Pd(II) K_d sorption data in Riddoch (2016), which can be seen in Table 6.3 below. With the exception of the two greyed-out rows for 1.0 M *I* at a pH_M of 8 and 9, the differences between the pH_C values calculated using the conversion formulas obtained in this work and those presented in Riddoch (2016), are all positive. Thus, in the sorption experiments conducted in Riddoch (2016), it is possible that the sample solutions were being under-adjusted. If this is true, then the K_d values presented in Riddoch (2016), were actually adjusted to a pH of higher value than the intended pH_C assuming the conversion formulas presented in this work are more accurate. Correcting for this would result in the

experimental K_d values being shifted to the right on a pH plot, or to a higher pH. Generally speaking, the discrepancy between the higher *I* solutions is greater than that for the lower *I* solutions. For 1.0 and 4.0 M, the discrepancy is also greater for lower values of pH. These two trends correspond with the pH-discrepancies between the experimental K_d values and the modelled results presented in Riddoch (2016), as there was a greater pH discrepancy at lower values of pH, and at higher *I*. Although these differences may account for some of the discrepancies in Riddoch (2016), it was indicated that the offset was approximately equal to a pH of 2; however, the largest offset shown in Table 6.3 is only 0.74 for an *I* of 4.0 M at a pH of 5, as there is no experimental data for a pH of 3 or 4 presented in that work. In addition to this, there was little-to-no pH-discrepancy between the experimental K_d values and the modelled sorption edge for 0.01 M *I*, as all experimental results for that concentration of *Na-Ca-Cl* were obtained in this work only, and was therefore unaffected by the offset in the pH-adjustments conducted in Riddoch (2016).

Table 6.3: pH_C & pH_M conversion difference with Riddoch (2016).

0.1 M pH_C			
pH_M	**Riddoch (2016)**	**Goguen (2017)**	**Δ = G - R**
5	5.015	5.160	0.145
6	6.018	6.170	0.152
7	7.021	7.180	0.159
8	8.024	8.190	0.166
9	9.027	9.200	0.173
1.0 M pH_C			
pH_M	**Riddoch (2016)**	**Goguen (2017)**	**Δ = G - R**
5	5.300	5.560	0.260
6	6.360	6.510	0.150
7	7.420	7.460	0.040
8	8.480	8.410	-0.070
9	9.540	9.360	-0.180

4.0 M pH_C			
pH_M	Riddoch (2016)	Goguen (2017)	Δ = G - R
5	5.060	5.800	0.740
6	6.072	6.770	0.698
7	7.084	7.740	0.656
8	8.096	8.710	0.614
9	9.108	9.680	0.572

*K_d values at pH 3 and 4 were not presented in Riddoch (2016).

Some other experimental sources of error that could account for a portion of the pH discrepancy between the experimental data and the modelling results include: the range of pH that the sample solutions were measured to be within when adjusted (+/- 0.05); the inaccuracies of the probe when measuring the sample solution pH (+/- 0.005), and the accuracy of the pH probe calibration using 3 buffer solutions of differing pH; as well as the drift in pH over the duration of the sorption period between each day of pH re-adjustment. Experimental sources of error that lead to inaccurate K_d values may also give the appearance that discrepancies are a result of a shift in the pH value, and not in the K_d value itself. Factors that could affect the final calculated K_d values include: the range of mass that the soil and salts were measured to be within (+/- 1 mg), leading to an error in the L/S ratio, the Na/Ca molar ratio, and the *I* of the sample solutions; inaccuracies within the mass scale when measuring out the masses of soils and salts (+/- 0.5 mg); the volume of DI used for the 50 mL batches of Pd (+/- 0.05 mL), affecting the concentration of Pd and *I*; the volume of sample solution for each 8 mL sample (+/- 0.01 mL), affecting the L/S ratio; the error in the C_i of Pd(II) in each sample solution (+/- 0.002×10^{-7} M), and the C_i used in calculating the K_d values, obtained from ICP-MS stability measurements (+/- 0.05×10^{-7} M); the change in sample solution volume during the pH adjustment process (+/- 0.25 mL); error(s) in the dilution process after centrifugation; the inaccuracy of the Pd solutions used to calibrate the ICP-MS; and all errors internal to the ICP-MS during concentration measurements.

6.2 Ionic Strength & pH Effects on Pd(II) Sorption

K_d was found to be dependent on I from 4 to 6 M for at least bentonite, and potentially illite and shale. K_d is seen to increase by almost an order of magnitude for bentonite between an I of 4.0 and 5.0 M, as seen in Figure 5.3. For illite, the K_d values increased slightly between 4.0 and 5.0 M, but have a large spread of values for 3.0 and 4.0 M (obtained from Riddoch, 2016). Due to the uncertainty in the K_d values for illite at 4.0 M I, it is unknown whether K_d is independent of I between 4.0 and 6.0 M. K_d values slightly decrease from 4.0 to 5.0 M for shale, but when the values for 4.0 M are shown in relationship to those for 3.0, 5.0, and 6.0 M, and given that the relative spread of K_d values for that I are much greater, there is a possibility that the spike in K_d at 4.0 M is due to measurement error. If the K_d values reported in Riddoch (2016), for shale at 4.0 M I are inaccurate, then it is possible that sorption of Pd(II) is constant between an I of 3.0 and 6.0 M. It is also possible that there is a discrepancy in the experimental procedures between the K_d values obtained in this work, and those presented in Riddoch (2016), as all K_d values for 5.0 and 6.0 M I are much closer together than those presented in Riddoch (2016). However, the range of values for each soil at a given I are much closer together in this work, indicating that there may have been greater consistency in experiments for this work. Despite any potential changes in K_d values between an I of 4.0 and 5.0 M, the values were constant between 5.0 and 6.0 M, so pH experiments were only conducted at 4.0 and 6.0 M in this work, and 5.0 M was ignored. Ionic strength dependence tests were not conducted for 0.01 M I, but pH-dependence tests were conducted for this I, and the resulting sorption edge showed a dependence on I between 0.01 and 0.1 M.

Looking at the contribution of each species to sorption in Figure 5.18 for illite, the $S\text{-}OPd^+$ surface species never dominates across the spectrum of pH and I, as the surface complexation constant never had to be optimized from the value proposed in Vilks (2017).

The *S-OPdOH* surface species dominates from a pH of just below 3 to just above 7 at 0.01 M *I*, but reduces significantly for 0.1 M *I*, and only dominates between a pH of 5.25 and 7.25. For 1.0 and 4.0 M *I*, *S-OPdOH* doesn't dominate sorption for illite in any region of the pH spectrum. Above a pH of about 7.25, the $S\text{-}OPd(OH)_2^-$ surface species dominates for both 0.01 and 0.1 M *I*, which moves up to beginning at a pH of 8 for 1.0 M, and almost 9.5 for 4.0 M. Beginning at 0.1 M *I*, the $S\text{-}OPdCl_4^{-3}$ surface species dominates the pH region of sorption below 5, and rapidly moves up to 8 for 1.0 M, and above 9 for 4.0 M. The $S\text{-}O_2Pd$ cation exchange species that was added to the model only dominates in 0.01 M *I* below a pH of about 3.75.

For the contribution of each species to sorption on montmorillonite seen in Figure 5.24, the $S\text{-}O_2Pd$ cation exchange species that was added to the model only dominates in 0.01 M *I* up to a pH of about 3.25, where the $S\text{-}OPd^+$ surface species begins to dominate until just above a pH of 5. This species continues to dominate in an *I* of 0.1 M up to a pH of approximately 5 as the contribution to sorption from the $S\text{-}O_2Pd$ cation exchange species severely drops off beyond this point. The *S-OPdOH* surface species dominates from a pH of just above 5 to of about 8.5 at 0.01 M *I*, but reduces for 0.1 M *I* to the pH region between 5.25 and 8.5. For 1.0 and 4.0 M *I*, *S-OPdOH* does not dominate sorption for montmorillonite in any region of the pH spectrum. Above a pH of about 8.5, the $S\text{-}OPd(OH)_2^-$ surface species dominates for both 0.01 and 0.1 M *I*, which moves up to beginning at a pH of 8 for 1.0 M, and almost 9.5 for 4.0 M. The $S\text{-}OPdCl_4^{-3}$ surface species dominates sorption for both 1.0 and 4.0 *I* below a pH of about 8.5 and 9 respectively. The only region of sorption dominance for the $S\text{-}OPdCl_3OH^{-3}$ surface species is at 4.0 M beyond a pH of about 9.

The modelling results show for both clays that the cation exchange and metal-binding hydroxyl surface species contribute most to sorption at lower *I*, whereas the ternary

and largely chloride species dominate at higher *I*. This is expected for the cation exchange species as the cation exchange capacity for electric double layers on clay increases to approach the total surface charge as *I* approaches that of pure water (Stumm, 1996). The ion exchange species also dominate at low pH as the aqueous concentration of Pd^{+} sharply drops off above a pH of 4, which exerts a greater influence on sorption through this mechanism than the positive correlation between the cation exchange capacity and pH (Stumm, 1996). The transition from metal-binding to ternary surface species-dominated sorption is also expected as the aqueous hydroxyl palladium species dominate in solution at lower *I*, and the aqueous chloride species dominate in solution at higher *I* as confirmed in Riddoch (2016).

Two large contributors to the measure of *I* are the solution concentrations of the cations Na^{+} and Ca^{+2}. Since Pd(II) is also a cation, the higher the *I*, the more salt cations are in solution competing with the aqueous palladium species for sorption. This likely has the effect of reducing overall sorption of palladium for higher ionic strength solutions. Also consistent with the findings in Riddoch (2016), is that the K_d values for sorption of Pd(II) onto shale for 6.0 M *I* were found to be much larger than the K_d values for the sorption onto illite: up to more than a factor of 10. In Vilks (2017), it is stated that shale is approximately made up of about 60% illite, which contributes to the vast majority of sorption on shale. Due to this, it would be expected that illite would have greater K_d values than shale. However, as this was not found to be the case from the results in this work or in Riddoch (2016), it remains a possibility that there is some impurity in the Queenston shale that is contributing to the higher sorption.

K_d values were found to have a strong dependence on pH for all clays, which is consistent with the findings in Riddoch (2016). Sorption tests in 0.01 M *I* showed an increase in sorption on illite and multiple overlapping K_d values for bentonite when

compared against those at 0.1 M *I*. These sorption tests showed a similar trend for illite and bentonite at pH 5 and 6 as the 0.1 M *I* experiments in Riddoch (2016): a decrease in sorption for an increasing pH. Sorption for all values of *I* at a pH between 3 and 5 (for both illite and bentonite), show a trend of increasing K_d values with increasing pH, resulting in a local maximum for the two clays at a pH of 5 across all *I* up to 6.0 M for illite and 4.0 M for bentonite.

6.3 Pd(II) Sorption Using the 2SPNE SC/CE Model

The initial 2SPNE SC model used the *S-OPdOH* and *S-OPd(OH)*$_2^-$ surface species recommended in Bradbury (2005b), with the JAEA TDB, SIT, and surface complexation constants calculated using the LFER. Pitzer parameters were not used for modelling Pd(II) sorption as there is no THEREDA release for palladium, or parameters found anywhere else in the existing literature. For sorption onto illite, the model under-predicted the K_d values at a pH of 3, and over-predicted the values between a pH of 4 and 6 for 0.01 M *I*. For 0.1 M *I*, the model under-predicted the K_d values at a pH of 5 and 9, and over-predicted them for a pH of 6 to 8. For 1.0 M *I*, the model under-predicted the K_d values below a pH of 7, and was close for pH values from 7 to 9. For 4.0 M *I*, the model greatly under-predicts all K_d values across the pH spectrum of experimental data. For montmorillonite, the model under-predicted the K_d values for a pH of 3 in 0.01 M *I*, < 5 for 0.1 M *I*, < 7 for 1.0 M *I*, and < 8 for 4.0 M *I*, and over-predicted all other experimental data. It was clear from this model that these surface species are not sufficient in modelling the experimental sorption data obtained in this work, and Riddoch (2016). In addition to the model not containing enough sorption species, it is possible that the LFER for both clays is not sufficient for predicting the surface complexation constants for metal-binding species.

Following the use of the *S-OPdOH* and *S-OPd(OH)*$_2^-$ surface species alone, the *S-OPd*$^+$ surface species was added to the model using the recommended surface complexation constant in Vilks (2017). The results of this addition was not shown graphically in Chapter 5 as the surface complexation constants were not high enough for either soil to influence the modelled sorption edge. There was also a recommended complexation constant for the *S-OPd(OH)*$_3^{-2}$ surface species in Vilks (2017), however, this was not added to the model as it mostly affects the alkaline region of the sorption edge at a pH greater than the available experimental data.

Once the ternary chloride surface species were added to the model for each aqueous species in the JAEA TDB (in order to account for the chloride species that form in solution), the model predicted the K_d values much more accurately for higher *I* (1.0 & 4.0 M), and lower pH (< 8). This can be primarily attributed to the *S-OPdCl*$_4^{-3}$ surface species, which is largely the only dominant ternary species contributing to sorption. The sorption edges at 0.01 and 0.1 M *I* were not observably effected by this addition to the model, and although the output is much more accurate for 1.0 M *I* below a pH of 7, the model stull under-predicts the K_d values for a pH of 3, 5, and 6 for illite. For 4.0 M *I* on illite, the K_d values fluctuate between different pH values and the modelled sorption edge appears to roughly follow an average within this fluctuation. For montmorillonite, the K_d values at a pH of 7 are no longer being under-predicted with this addition to the model, though all K_d values at a lower pH are. For 4.0 M *I* the model predicts the K_d values very well at pH values of 7 and below, but over-predicts for pH 8 and 9. Despite the model being greatly improved at high *I* for both clays, it is unknown as to whether or not the correlation for Type B ternary surface complexes for organic ligands (Fein, 2002), was correctly applied to Type A for inorganic ligands.

Before modifying any of the surface complexation constants, the 2SPNE SC model was changed to the 2SPNE SC/CE model with the addition of the cation exchange component of the model. Since the *S-O₂Pd* exchange species is only dominant at low *I* and low pH, there were only two sets experimental K_d values to fit the sorption edge to (0.01 M *I*, and pH 3 & 4), which introduced some degree of error into the optimization of the respective selectivity coefficient. To improve the accuracy of this proposed constant, more sorption experiments would need to be conducted either at a lower pH (~2) or at a lower *I* (< 0.01 M). In spite of these limitations, the addition of the cation exchange species allowed for the predicted K_d values to be in agreeance for 0.01 M *I* at pH 2 and 3. Despite the accurate fit of the predicted K_d values by the model, the proposed selectivity coefficients are approximately 5.5 orders of magnitude more than those in existing literature for divalent elements on illite (Marques Fernandes, 2015), and up to 5 orders of magnitude larger than those for montmorillonite (Bradbury, 2005b). The more common method of determining the selectivity coefficient of a certain exchange species is through calculation using the Gaines-Thomas convention (1953), which is also the computational method used in PHREEQC (Appelo, 1999). Following the Gaines-Thomas convention, the selectivity coefficient for a given reaction shown in Equation 6.3 below can be calculated using Equation 6.4 below, where ${}^{B}R_d$ is the distribution ratio of metal *B*, as shown in Equation 5.3 (Bradbury, 2005b), CEC is the cation exchange capacity of the soil, *z* is the charge of the ion, and γ is the aqueous phase activity coefficient. Applying these two equations to Pd(II), we get the respective formulas shown in Equation 6.5 and Equation 6.6 below.

$$z_B A^{Z_A} - clay + z_A B^{Z_B} \leftrightarrow z_A B^{Z_B} - clay + z_B A^{Z_A} \tag{6.3}$$

$${}^{B}_{A}K_c = \left({}^{B}R_d\right)^{Z_A} \cdot \frac{(z_B)}{(CEC)^{Z_A}} \cdot [A]^{Z_B} \cdot \frac{(\gamma_A)^{Z_B}}{(\gamma_B)^{Z_A}} \tag{6.4}$$

$$2Na^{+} - clay + Pd^{+2} \leftrightarrow Pd^{+2} - clay + 2Na^{+} \tag{6.5}$$

$${}^{Pd}_{Na}K_c = \left({}^{Pd}R_d\right) \cdot \frac{2}{(CEC)} \cdot [Na^{+}]^2 \cdot \frac{(\gamma_A)^2}{(\gamma_B)} \tag{6.6}$$

In order to accurately calculate the selectivity coefficient, it would require accurate values of the aqueous concentration of Na^{+} ions and the aqueous phase activity coefficients of both sodium and palladium, specific to the sample solution being tested. Accurately obtaining experimental measurements of these values was outside of the scope of this work, but could be done in the future to obtain values that could be compared against those proposed in this work. For a rough estimate of selectivity coefficient values to expect, Equation 6.6 was used for illite at a pH of 5.0, and an *I* of 0.01 M, which corresponds to a Log R_d value of approximately 3.9 (from the experimental K_d values), a CEC value of 0.21 eq/kg, a [Na^{+}] value of approximately 4.7×10^{-3} M (from PHREEQC output file), and a γ value of 4.2×10^{-3} for sodium, and 1.5×10^{-8} for palladium (also from PHREEQC output file). When used in equation 6.6, the Log of the selectivity coefficient calculated is equal to approximately 3.3. This value is much smaller than the value obtained for illite through optimization by fitting the modelled sorption edge to the experimental results by approximately 3.5 orders of magnitude, but approximately 2 orders of magnitude larger than K_c values for comparable elements of interest with a divalent charge (Marques Fernandes, 2015). One of the challenges with cation exchange is that K_c values can be assumed to be constant only at trace concentrations of the sorbtive (Bradbury, 2005b). It is likely though that the K_c value would have to be re-calculated for every pH and *I* as the R_d, $[Na^{+}]$, γ_{Na}, and γ_{Pd} values would likely all change for each case.

With the 2SPNE SC model complete, the optimized K_c values were held constant and the metal-binding surface complexation constants were optimized. For illite, this greatly improved the model for 0.01 M *I*, almost perfectly predicting the K_d values for pH

3 – 6. The K_d values for 0.1 M *I* were only slightly over-predicted for a pH of 7, and under-predicted for a pH of 5. The peak in the sorption edge appears to occur at a pH approximately one pH higher than what is showed by the experimental data obtained from Riddoch (2016), but correctly predicts that the K_d values for a pH of 3 and 4 are below 10 L/kg. As discussed earlier, there were some inaccuracies in the pH conversion formula used in Riddoch (2016), that could result in a shift in the experimental data to a higher pH than where it was reported. However, as seen in Table 6.3, at a pH of 5 in 0.1 M *I* the pH shift would only be approximately 0.15; not enough to account for the sorption edge peak discrepancy. For 1.0 M *I*, the K_d values were able to be accurately predicted for a pH of only 8 and 9, since the acidic region of the sorption edge is not dominated by the metal-binding surface species. For montmorillonite, the K_d values at a pH of 4 and 6 were still over-predicted, but accurately predicted at 5. For 1.0 M *I*, the K_d values at a pH of 6 – 9 were accurately predicted, but the sorption edge drops off at a much faster rate than the experimental data does, and the model under-predicts the K_d values in the acidic region at a pH less than 6. Since the dominant surface species in the acidic region, $S\text{-}OPd^{+}$, has a contribution to sorption that peaks at a pH of 7.5 in 0.1 M *I*, there is no known sorption species that could raise this area of the sorption edge such that the K_d values are not under-predicted without greatly over-estimating the neutral and alkaline regions. For 1.0 M *I*, the sorption edge was only reduced in the alkaline region, but still over-predicted the K_d values at a pH of 8 and 9. Sorption edges in 4.0 M *I* were not affected by the optimization for either soil.

With the model accurately predicting the K_d values for 0.01 M *I* and no other known species that could be modified to improve the prediction for 0.1 M *I*, the ternary chloride species were looked to for improvement at 1.0 and 4.0 M *I*. Dominating sorption in these regions of the sorption edge is the $S\text{-}OPdCl_4^{-3}$ surface species, whose surface complexation constant needed to be slightly increased for illite and slightly decreased for

montmorillonite. If it was incorrectly reported in Vilks (2017), that the sorption of chlorine directly onto shale and bentonite without a metal does not occur, then it may be the case that the inorganic ligand-surface complex reaction constant ($Log\ K_{S\text{-}L}$) is a non-zero term when calculating the ternary surface complexation constant ($Log\ K_T$). This means that it is possible that the $Log\ K_T$ value could be different from the $Log\ K_{M\text{-}L\ (aq)}$ value, and therefore optimized independently. Since there are no findings to invalidate Vilks (2017), it was assumed that the $Log\ K_T$ value had to be modified with the $Log\ K_{M\text{-}L\ (aq)}$ value in the TDB. When the formation reaction constant for the $PdCl_4^{-2}$ aqueous species was modified within the stated error in the JAEA TDB, the K_c values also had to be re-optimized, but it is not clear as to why this was required looking at Equation 6.6 above, as the $S\text{-}OPdCl_4^{-3}$ surface species does not dominate sorption at a pH or *I* where the $S\text{-}O_2Pd$ exchange species dominates. It is possible that the aqueous phase activity coefficients for various Pd species are affected by this change in the TDB. After all of these changes were made, the model was no longer over-predicting the K_d values for 0.01 M *I* at a pH of 4, but was beginning to under-predict the K_d values at 0.1 M *I* at a pH of 6, so the modification was not adopted. For montmorillonite, the model was over-predicting the K_d values at an *I* of 1.0 M and pH of 8 less and under-predicting the K_d values for 0.1 M *I* at a pH of 6 less, but over-predicting the K_d values in 0.01 M *I* at a pH of 4 more. These changes are taken to be a net-benefit and the new values were adopted for montmorillonite. Despite the modifications to the $Log\ K_{M\text{-}L\ (aq)}$ value for the $PdCl_4^{-2}$ aqueous species being made within the stated error in the JAEA TDB, this value is independent of the soil being used and should be the same for both sets of models. Due to this constraint it is possible that the original $Log\ K_{M\text{-}L\ (aq)}$ value for the $PdCl_4^{-2}$ aqueous species stated in the JAEA TDB of 13.05 produces the best sorption curves, both clays considered.

The optimized surface complexation constants in Table 5.5 are consistent with those proposed in Riddoch (2016), for the $S\text{-}OPd(OH)_2^-$ illite surface species, and the *S-OPdOH*

montmorillonite surface species, but inconsistent for all others. These discrepancies could be partially attributable to the different values used in Riddoch (2016), for the specific surface area (SSA) of montmorillonite and illite. The SSAs used in Riddoch (2016), were from those proposed in Macht (2011), but were for an illite from Hungary and a Ca-bentonite from Germany. The clays used in experiment in this work and in Riddoch (2016), consisted of an illite sample from the Le Puyen-Velay (Haute-Loire), region in France and a Na-bentonite sample from Wyoming. For illite, the SSA used in Riddoch (2016), should have been 70.0 m^2/g instead of 83.0 m^2/g, and for montmorillonite 26.2 m^2/g should have been used instead of the 346.0 m^2/g. This over-estimated clay surface area used in the sorption models in Riddoch (2016), is likely a contributing factor to why many of the optimized surface complexation constants for the metal-binding surface species in this work are larger than those in Riddoch (2016); if the surface area is smaller, then the reaction constants need to be larger. For illite, the proposed SCC for the *S-OPdOH* surface species is 3.2, whereas a value of 3.0 was proposed in Riddoch (2016). For montmorillonite, the proposed SCCs for the $S\text{-}OPd^+$ and $S\text{-}OPd(OH)_2^-$ surface species are 8.2 and -5.5 respectively, whereas in Riddoch (2016), no value was proposed for $S\text{-}OPd^+$ (Log $K = 0$), and a value of -5.66 was proposed for $S\text{-}OPd(OH)_2^-$.

Given that five of the six surface complexation constants for the metal-binding surface species falling outside the error range of the LFER, as stated earlier, it is possible that the LFER is not sufficient for predicting the SCCs from the $Log^{OH} K_{(aq)}$ values. Some reasons for this insufficiency are that the LFER was developed using experimental data from sorption at low I (< 0.1 M), using different experimental procedures in Bradbury (2005a). As noted in Riddoch (2016), it is possible that the LFER can't be applied to sorption of Pd(II) in high ionic strength conditions.

Some of the additional ways that this model could be improved would be with the addition of epsilon values for the interaction of certain aqueous ion species that had to be calculated using the Davies equation, such as H_2O, $CaOH^+$, $HClO$, $HClO_2$, ClO^-, ClO_2^-, $PdCl_2$, and $Pd(OH)_2$ to the JAEA TDB. Another option would be to determine the much more difficult Pitzer parameters in order to use the more accurate Pitzer computational method, which would also be able to model the experimental results at 6.0 M *I*. More accurate titration and pH-adjustment techniques would also lead to a reduction in error in the experimental K_d values. The addition of the weak sites for the 2SP component of the model did not appear to have any impact on the modelled sorption edges, but the addition of weak-bonding surface site species could also help to improve the model. However, little is known about these sorption species for Pd(II) and no data was able to be found in the existing public literature. The non-electrostatic model (NEM) was used for all calculations, but preliminary investigation into the addition of the double-layer model (DLM), indicated that the acidic region of the sorption edge could be raised even at high *I* with the simple removal of the *-no_edl* flag in the *SURFACE* data block. This does, however, raise the K_d values of the sorption edge at the lower *I* in the acidic region, but the metal-binding surface complexation constants and selectivity coefficients could be reduced to account for this portion of the sorption edge. The results of these preliminary findings were not presented in this work, as the validity of the implementation could not be verified prior to publication. However, this holds a possible avenue of improvement for future research, though the thickness of the electrostatic layer would be required for the model. Triple-layer models (TLMs) also exist, but not investigation into this has been done at the time of this work.

6.4 Np(IV) Sorption Using the 2SPNE SC Model

Cation exchange was not included in the 2SPNE SC model for Np(IV) sorption onto illite and montmorillonite due to experimental results obtained from Nagasaki (2017), only being available for 0.1, 4.0, and 6.0 M *I* solutions and not for 0.01 M *I* at a low pH where exchange species dominate sorption. In addition to this, cation exchange reactions are considered to be irrelevant for tetravalent metal ions (Bradbury, 2009b). The R07 THEREDA (2013), was used for containing the most complete and comprehensive available set of Pitzer parameters for use with the Pitzer computation method. The first set of surface complexation reactions and constants used were obtained from Banik (2016), for illite and Bradbury (2005b), for montmorillonite, as these were the most current available sources for referenced values. Modelling with and without the use of the Pitzer parameters at 0.1 M *I* shows the consistency between using the Davies & WATEQ Debye-Hückel set of mass-action computations and the Pitzer computational method. For illite, the K_d values were over-estimated by almost one order of magnitude, but the shape of the sorption edge is very close to the experimental results. This indicates that the sorption surface species proposed in Banik (2016), are likely sufficient in accounting for the dominant sorption processes (the $S\text{-}ONp(OH)_2^+$, $S\text{-}ONp(OH)_3$, and the $S\text{-}ONp(OH)_4^-$ surface species), but that the values of the constants proposed are likely too high. For montmorillonite, the constants proposed in Bradbury (2005b), resulted in an under-prediction of the K_d values in the acidic region below a pH of 5, and over-prediction between a pH of 5 and 8, and an under-prediction again in the alkaline region above a pH of 8. The large drop-off in K_d values for montmorillonite where the sorption edge was over-predicting K_d values for illite indicated that the set of reactions and proposed complexation constants in Bradbury (2005b), is insufficient in describing sorption across the pH spectrum and requires additional surface complexes in the model.

Optimization of the surface complexation constants for both clays was difficult as the experimental K_d values decrease from 0.1 to 4.0 M *I* and remain relatively constant from 4.0 to 6.0 M *I*, whereas the model is independent of *I* between a pH of 7 and 10.5, the K_d values increase with *I* from a pH of about 4.5 to 7, and they decrease with increasing *I* below a pH of about 4. To compromise, the SCCs were modified for illite such that the model largely under-predicts the K_d values at 0.1 M *I* (except pH = 4), over-predicts in 4.0 M *I* (except pH = 3), and slightly over-predicts for 6.0 M *I* (except pH = 3). It is possible that despite the use of the more rigorous Pitzer computational method, that the model is not sufficient at modelling sorption at high *I* and that the sorption edge should have been optimized to fit the 0.1 M K_d values, but this approach was taken instead (possibly resulting in lower K_d values). The SCCs were modified for montmorillonite such that the model largely under-predicts the K_d values at 0.1 M *I* (except pH = 8 - 9), slightly over-predicts in 4.0 M *I* (except pH = 3 - 5), and over-predicts for 6.0 M *I* (except pH = 3 - 4). The SCC for the $S\text{-}ONp^{+3}$ surface species could not be optimized (due to its contribution to sorption being so low), and therefore none were proposed in this work. The results from using the LFER set of equations for both strong and weak-binding surface sites were used instead. In order to determine these reaction constants, experimental sorption results must be obtained at a pH and *I* where the species dominates the sorption process which, for the solutions of *I* tested, would require K_d values at a pH below 2 for 0.1 M *I*, and slightly above a pH of 2 for 4.0 and 6.0 M *I*. The SCCs for the $S\text{-}ONpCl^{+2}$ surface species were not modified as its contribution to sorption was too low for the formation reaction constant of the aqueous $NpCl^{+3}$ species to have a significant effect on sorption by adjusting it within a reasonable range (no error provided in the THEREDA). The SCCs could be modified without changing the thermodynamic data in the THEREDA, but this would no longer agree with the relationship analogously followed for ternary reactions in Fein (2002).

Of the three surface species that were optimized and had formation reaction constants in the TDB (*S-ONpOH*$^{+2}$, *S-ONp(OH)*$_2^+$, and *S-ONp(OH)*$_3$), the *S-ONpOH*$^{+2}$ and *S-ONp(OH)*$_3$ surface species both had surface complexation constants that fell outside of the LFER for both clays (Table 5.9). These findings add to those for the Pd(II) sorption that the LFER may not be sufficient for modelling sorption at high *I*. Unlike sorption of Pd(II), the metal-binding Np(IV) hydroxyl surface species dominate sorption at every *I* and pH modelled. Since the LFER purports to account for sorption of metal-binding hydroxyl surface species, then it should also account for the SCCs used to describe sorption at high *I*. Since the modelled sorption edge generally follows the same shape as the experimental data, the SCCs for the *S-ONpOH*$^{+2}$ surface species are above the allowable range of the LFER, and the SCCs for the *S-ONp(OH)*$_3$ surface species fall below, the optimized SCCs could not be brought into the allowable range of the LFER by simply increasing or decreasing them for all surface species and clays and still closely predict the K_d values of the experimental data. Raising the values of the surface complexation constants for all surface species and both clays would exacerbate the over-prediction of K_d values at high *I* (4.0 & 6.0 M), and lowering them all would further exacerbate the under-prediction of K_d values at low *I* (0.1 M). Due to this, it is unclear that the LFER is able to account for sorption of Np(IV) at as low of *I* as 0.1 M.

The optimized surface complexation constants were then used to compare the Pitzer computational method to the Davies and WATEQ Debye-Hückel again at 0.1 M *I*, which resulted in sorption edges that look visually identical. This confirms again the internal consistency of the two computational methods at low *I*. To further compare computational methods, the JAEA TDB was modified so that the formation reaction constants of the relevant aqueous species were the same as those contained in the R07 THEREDA (2013), so that the SIT computational method could be used. The JAEA TDB greatly over-predicted the K_d values between a pH of 3.5 and 5.5 (but no other region of the sorption

edge), so in order to make the sorption edges between the two computational methods and databases more comparable, the SCC for the *S-ONpOH*$^{+2}$ surface species had to be reduced from 9.5 to 9.1 for illite, and from 9.8 to 9.7 for montmorillonite. This modification made the sorption edges at 0.1 M *I* much more comparable, but the modelled K_d values for 4.0 M *I* were still much greater than the predicted K_d values using the R07 THEREDA (2013), and Pitzer parameters over the same pH range (3 – 6.5), for both clays. This discrepancy for 0.1 M *I* is likely a result of the two different TDBs, as sorption of Pd(II) onto the same clays was shown to be consistent between the SIT computational method and that of the Davies and WATEQ Debye-Hückel when using the JAEA TDB. It is possible that using the same formation reaction constants in the two TDBs is not sufficient enough to make them comparable. It could also be the case that there is an error in one of the SIT values contained in the JAEA TDB for the aqueous species related to the surface species that dominates sorption in the pH range; the $Np(OH)_3^+$ aqueous species, and corresponding *S-*$ONp(OH)_2^+$ surface species. Once the SCCs were modified to correct the discrepancies at 0.1 M *I*, the remaining discrepancies at 4.0 M *I* between the JAEA TDB and SIT, and the R07 THEREDA (2013), with Pitzer parameters could point to a difference in the accuracy of the two computational methods in higher *I* conditions. Given that the Pitzer computational method is considered to be more rigorous than the SIT computational method, the differences in the predicted K_d values are likely due to inaccuracies of the SIT in high *I* solutions, which would contradict the claim in Grenthe (1997), that SIT is accurate up to 4 M *I*.

6.5 Np(V) Sorption Using the 2SPNE SC Model

Cation exchange was not included in the 2SPNE SC model for Np(V) sorption onto illite and montmorillonite due to experimental results obtained from Nagasaki (2015), only being available for 4.6 M *I* solutions and not for 0.01 M *I* at a low pH where exchange species dominate sorption. In addition to not having experimental data to fit the Np(V)-dominated portion of the sorption edge to in order to obtain an experimentally-derived fit, it was proposed in Gorgeon (1994), that the Log K_c value for the $S\text{-}ONpO_2$ exchange species is zero for Na-illite in 0.1 M $NaClO_4$. The R04 THEREDA (2015), was used for modelling even though it had to be modified to include the Ca^{+2} ion, and therefore might not be accurate for use in ionic solutions containing aqueous Ca^{+2} ions. The R07 THEREDA (2013), used for modelling Np(IV) sorption is a more complete TDB as it was tested for use with aqueous solutions containing Ca^{+2} ions, but it was not used for modelling Np(V) as it was not explicitly stated in the R07 (2013), release notes that it is a valid database for Np(V) despite the R07 (2013), containing the formation reaction constants for the NpO_2OH and $NpO_2(OH)_2$ aqueous species. However, the R04 THEREDA (2015), is a newer database, as it was released in 2015, whereas the R07 THEREDA (2013), was released in 2013.

The surface complexation constants proposed in Gorgeon (1994), for illite under-predicted the K_d values between a pH of 6 – 9, but accurately predicted the K_d values for the experimental results at a pH_C of 9.20 and over-predicted at a pH_C of 9.71. For montmorillonite, the SCCs from Bradbury (2005b), under-predicted all experimental K_d values. Once the SCCs were optimized the model accurately predicted all experimental data from Nagasaki (2015), with the exception of K_d values at a pH_C of 7.65 and 9.71, which were under- and over-predicted respectively. For montmorillonite, the model under-predicted the K_d values at a pH_C of 6.23, over-predicted at a pH_C of 7.24 and 8.26, and

accurately predicted at a pH_C of 9.01 – 9.73. Empirically-fitting the SCCs in the SCM is difficult due to there only being two surface species to optimize to the data. Given that the model didn't perfectly predict the K_d values for montmorillonite, there is a possibility that the model is incomplete. Since the K_d values were accurately predicted for illite, it's possible that the soil properties of the montmorillonite being modelled are slightly different than the bentonite used in Nagasaki (2015).

Again, the optimized surface complexation constants for the $S\text{-}ONpO_2OH^-$ surface species for both clays were found to fall outside of the allowable range of the LFER. However, the SCCs are both above the range of the LFER (and only by a maximum of 0.87), and therefore there could be a mere vertical translation offset due to either errors in the model or measured K_d values from Nagasaki (2015). Since the predicted K_d values of the model were so accurate for illite, it is unlikely that there was an error in the optimization process. However, the SCC for the $S\text{-}ONpO_2OH^-$ illite surface species only falls outside the allowable range of the LFER by 0.32, which is a minor deviation when compared to other deviations from the LFER.

Chapter 7

Conclusions

Relationships between the pH_C and pH_M of *Na-Ca-Cl* solutions of varying *I* were determined and conversion formulas were established. These conversion formulas were found to have discrepancies with those proposed in Riddoch (2016), which may partially account for the pH-offset discussed in the work between the predicted K_d values and the experimental results obtained in the work.

The dependence of Pd(II) sorption onto illite, bentonite, and shale on ionic strength at high *I* was determined experimentally and compared to existing data on K_d values from Riddoch (2016). Pd(II) sorption samples with an unadjusted pH in 5.0 and 6.0 M *I* produced the same findings as those found in Riddoch; that $K_{d\ shale} > K_{d\ illite} \approx K_{d\ bentonite}$. This further supports the claim in Riddoch (2016), that there must be some impurities in the Queenston shale core sample obtained from the NWMO that is leading to the higher K_d values, as illite should have larger K_d values than shale given that illite is the major clay constituent of shale. K_d values were found to be independent of *I* for 5.0 and 6.0 M when compared with the K_d values obtained from Riddoch (2016), for sorption at 3.0 and 4.0 M *I*. K_d values were found to be dependent on *I* for bentonite and shale between 4.0 and 5.0 M *I*, and

independent between 5.0 and 6.0 M *I*. There was also found to be a strong dependence of K_d on *I* for illite between 0.1 and 0.01 M between a pH of 3 – 6. The K_d values for bentonite were found to be relatively independent of *I* in the same pH range. However, for the pH-adjusted samples the K_d values were found to be less for 6.0 than 4.0 M *I* for all pH between 5 – 9 (with the exception of 8), onto illite. For bentonite, the K_d values of the pH-adjusted samples were lower for 6.0 than 4.0 M *I* at a pH_C of 5, 7, and 8, and approximately the same for 6 and 9. For shale, the K_d values for 6.0 M *I* were all larger than those in 4.0 M *I* from a pH of 5 – 9.

The dependence of K_d on pH for sorption of Pd(II) was successfully expanded upon from Riddoch (2016). Sorption on illite and bentonite was found to be highly dependent on pH for 0.01 M *I* between a pH of 3 – 6, and for 0.1, 1.0, and 4.0 M between a pH of 3 and 5, with K_d values increasing with pH. For illite and bentonite, the dependence of K_d values on pH in 6.0 M *I* could not be determined between a pH of 3 – 5, as the K_d values could not be accurately determined below 0.01 m^3/kg. K_d values were found to be highly dependent on pH between a pH of 5 – 9 for Pd(II) on illite, and shale in 6.0 M *I*, but only for a pH of 5 – 6 for bentonite, with K_d values increasing with pH. Between a pH of 6 – 9 the K_d values for bentonite in 6.0 M *I* were found to be relatively independent of pH.

The 2SPNE SC model was confirmed to be accurately implemented for the modelling of Th(IV) sorption in PHREEQC onto illite and montmorillonite using reference models from Bradbury (2009, 2005b), before attempting to model the sorption of Pd(II). Sorption of Pd(II) in PHREEQC onto illite was successfully modelled with the JAEA TDB and SIT using the 2SPNE SC/CE model in 0.01, 0.1, 1.0, and 4.0 M *I* solutions between a pH of 3 – 9 (3 – 6 for 0.01 M *I*). For montmorillonite, the sorption of Pd(II) was successfully modelled for 0.01 M *I* between a pH of 3 – 6, 0.1 M *I* between a pH of 6 – 9, and 4.0 M *I* between a pH of 3 – 7. Cation exchange was successfully added to the model and selectivity

coefficients for the *S-O_2Pd* exchange species with sodium were determined empirically through fitting to the experimental K_d values. The *S-O_2Pd* exchange species was found to dominate sorption at a pH < 4 for illite and < 3.25 for montmorillonite in 0.01 M *I* solutions. For specific chemical sorption, the dominant surface species were found to be *S-OPdOH, S-OPd(OH)$_2^-$, and S-OPdCl$_4^{-3}$* for illite, and *S-OPd$^+$, S-OPdOH, S-OPd(OH)$_2^-$, S-OPdCl$_4^{-3}$* and *S-OPdCl$_3$OH^{-3}* for montmorillonite. All optimized surface complexation constants for the metal-binding hydroxyl species were found to fall outside the allowable range of the LFER proposed in Bradbury (2009b, 2005b), for both clays. Modelling sorption of Pd(II) onto illite and montmorillonite with only the two surface species proposed in Bradbury (2005b), was found to not be sufficient, especially in I > 0.1 M. The surface complexation constant for the *S-OPd$^+$* surface species proposed in Vilks (2017), was found to not be large enough for the species to dominate sorption at any *I* or pH. Adjustments to the SCC of the dominant ternary surface species (*S-OPdCl$_4^{-3}$*), and the FRC for the corresponding aqueous species was found to not improve the predicted K_d values for illite, but reducing both within the stated error in the JAEA TDB was found to slightly improve the fit of the sorption edge to the experimental data for montmorillonite. Of the optimized surface complexation constants, the only ones consistent with those proposed in Riddoch (2016), are for the *S-OPd(OH)$_2^-$* illite surface species, and for the *S-OPdOH* montmorillonite surface species.

Sorption of Np(IV) onto illite and montmorillonite was successfully modelled in PHREEQC with the R07 THEREDA and contained Pitzer parameters using the 2SPNE SC model in 0.1, 4.0, and 6.0 M *I* solutions between a pH of 4 – 10 using experimental K_d values obtained from Nagasaki (2017). Experimental K_d values fell with increasing *I* for both clays, but the model results predicted K_d values that were independent of *I* above neutral pH, resulting in more accurate predicted K_d values for 0.1 M *I* than 4.0 and 6.0 M *I*. Metal-binding hydroxyl surface species were found to dominate sorption for Np(IV) onto

both clays across all pH and *I* modelled, with the *S-ONpOH*$^{+2}$, *S-ONp(OH)*$_2^+$, *S-ONp(OH)*$_3$, & *S-ONp(OH)*$_4^-$ surface species dominating sorption. The surface species and surface complexation constants proposed for illite in Banik (2016), and montmorillonite in Bradbury (2005b), were found to not be sufficient for modelling the sorption of Np(IV) onto either clay. These proposed sorption reactions and reaction constants were tested using two computational methods (Pitzer and Davies & WATEQ Debye-Hückel), which both produced the same findings. More than half of the optimized surface complexation constants were found to fall outside of the allowable range of the LFER, indicating that the LFER is insufficient for sorption in not only high *I*, but also likely in sorption of Np(IV) onto illite and montmorillonite as a whole. The optimized SCCs were modelled at 0.1 M *I* using the R07 THEREDA without the use of the Pitzer parameters, defaulting in PHREEQC to the use of the Davies and WATEQ Debye-Hückel computational methods, producing predicted K_d values that are consistent with those produced using the Pitzer parameters and computational method. The JAEA TDB was also used to model the sorption of Np(IV) onto both clays with the use of the SIT and formation reaction constants contained in the R07 THEREDA for the relevant aqueous species at 0.1 and 4.0 M *I*. The SCCs for the *S-ONpOH*$^{+2}$ surface species had to be adjusted for both clays in order to match the predicted K_d values in 0.1 M *I* to those produced using the R07 THEREDA and the contained Pitzer parameters in order to account for any differences in the two TDBs. Despite this change to improve the fit, the model still greatly over-predicted K_d values in 4.0 M *I* between a pH of 4 – 6 for both clays. This finding indicates that either the SIT isn't capable of accurately predicting K_d values for sorption of Np(IV) up to as high of *I* as 4.0 M (disproving the claim in Grenthe, 1997), or that the JAEA TDB does not have accurate epsilon values for Np(IV).

Sorption of Np(V) onto illite and montmorillonite was also successfully modelled in PHREEQC with the R04 THEREDA and contained Pitzer parameters using the 2SPNE

SC model in 4.6 M *I* solutions between a pH of 6 – 10 using experimental K_d values obtained from Nagasaki (2015). The surface complexation constants for the surface species proposed for illite in Gorgeon (1994), and montmorillonite in Bradbury (2005b), were found to not be sufficient for modelling the sorption of Np(V) onto either soil. No additional surface species were required to be added to the model for either clay in order to obtain a good prediction of the experimental K_d values for illite, or a decent fit to those for montmorillonite from Nagasaki (2015). Preliminary testing of the model found that the predicted K_d values for both clays were not independent of *I* around 4.0 M as shown in the experimental data in Nagasaki (2015). Optimized surface complexation constants were found to fall outside of the allowable range of the LFER again, this time for the *S-*$ONpO_2OH^-$ surface species for both clays. The deviations from the range, however, were not that significant for illite (0.32), and only moderately significant for montmorillonite (0.87).

Bibliography

Agilent Technologies (2013). Agilent 8800 ICP-QQQ Application Handbook. Technical report.

Allison, J.D., Brown, D.S., and Novo-Gradac, K.J. (1991). MINTEQA2/PRODEFA2, a Geochemical Assessment Model for Environmental Systems: Version 3.0 User's Manual. Technical report, U. S. Environmental Protection Agency.

Banik, N.I., Marsac, R., Lützenkirchen, J., Diascorn, A., Bender, K., Marquardt, C.M., and Geckeis, H. (2016). Sorption and Redox Speciation of Plutonium at the Illite Surface. *Environmental Science & Technology 2016,* **50***,* 2092-2098.

Bertetti, F.P. (2016). Determination of Sorption Properties for Sedimentary Rocks under Saline, Reducing Conditions – Key Radionuclides. Technical Report, Nuclear Waste Management Organization.

Bidoglio, G. and Stumm, W. (1994). Chemistry of Aquatic Systems: Local and Global Perspectives. *Eurocourses: Chemical and Environmental Science*, **5**, 534.

Bradbury, M.H. and Baeyens, B. (1997). A mechanistic description of Ni and Zn sorption on Part II: modelling. *Journal of Contaminant Hydrology*, **27**, 223-248.

Bradbury, M.H. and Baeyens, B. (2005a). Experimental measurements and modeling of sorption competition on montmorillonite. *Geochimica et Cosmochimica Acta*, **69**(17), 4187-4197.

Bradbury, M.H. and Baeyens, B. (2005b). Modelling the sorption of Mn(II), Co(II), Ni(II), Zn(II), Cd(II), Eu(III), Am(III), Sn(IV), Th(IV), Np(V) and U(VI) on montmorillonite: Linear free energy relationships and estimates of surface binding constants for some selected heavy metals and actinide. *Geochimica et Cosmochimica Acta*, **69**(4), 875-892.

Bradbury, M.H. and Baeyens, B. (2009a). Sorption modelling on illite. Part I: Titration measurement and the sorption of Ni, Co, Eu, and Sn. *Geochimica et Cosmochimica Acta*, **73**(4), 990-1003.

Bradbury, M.H. and Baeyens, B. (2009b). Sorption modelling on illite. Part II: Actinide sorption and linear free energy relationships. *Geochimica et Cosmochimica Acta*, **73**(4), 1004-1013.

Bretti, C., Foti, C., and Sammartano, S. (2004). A new approach in the use of SIT in determining the dependence on ionic strength of activity coefficients. Application to some chloride salts of interest in the speciation of natural fluids. *Chemical Speciation & Bioavailability*, **16**(3), 105-110.

Ciavatta, L. (1980). The Specific Interaction Theory in Evaluating Ionic Equilibria. *Annali di chimica*, **70**, 551.

Crowe, R., Birch, K., Freire-Canosa, J., Chen, J., Doyle, D., Garisto, F., Giersewski, P. Gobien, M., Hatton, C., Hunt, N., Hirchorn, S., Hobbs, M., Jensen, M., Keech, P., Kennell, L., Kremer, E., Maak, P., Mckelvie, J., Medri, C., Mielcarek, M. Murchison, A., Parmenter, A., Ross, R., Sykes, E., and Yang, T. (2016). Technical Program for

Long-Term Management of Canada's Used Nuclear Fuel - Annual Report 2015. Technical report, Nuclear Waste Management Organization.

Davies, C.W. (1962). Ion Association. Butterworths Pub., Washington, DC.

Debye, P. and Huckel, E. (1923). Zur Theorie der Elektrolyte. I. Gefrierpunktserniedrigung und verwandte Erscheinungen [The theory of electrolytes. I. Lowering of freezing point and related phenomena]. *Physikalische Zeitschrift*, **24**, 185-206.

Fein, J.B. (2002). The effects of ternary surface complexes on the adsorption of metal cations and organic acids onto mineral surfaces. *Water Rock Interactions, Ore Deposits, and Environmental Geochemistry*, (7).

Gorgeon, L. (1994). Contribution à la Modélisation Physico-Chimique de la Retention de Radioéléments à Vie Longue par des Matériaux Argileux. Ph.D. dissertation. Université Paris.

Grenthe, I. and Plyasunov, A. (1997). On the use of semiempirical electrolyte theories for modeling of solution chemical data. *Pure and Applied Chemistry*, **69**(5), 951-958.

Hummel, W., Berner, U., Curti, E., Pearson, F.J., and Thoenen, T. (2002). Nagra/PSI Chemical Thermodynamic Data Base 01/01. Technical Report, National Cooperative for the Disposal of Radioactive Waste.

Golder Associates Ltd. (2011). Environmental Impact Statement, Vol. 1: Main Report. Ontario Power Generation. Retrieved from: http://www.opg.com/generating-power/nuclear/nuclear-waste-management/Deep-Geologic-Repository/Documents/Submission/01.Environmental-Impact-Statement-(Volume-1).pdf.

International Union of Pure and Applied Chemistry (1987). *IUPAC Compendium of Analytical Nomenclature*. Blackwell Scientific Publications.

Itagaki, H., Nakayama, S., Tanaka, S., Yamawaki, M. (1992). Effect of Ionic Strength on the Solubility of Neptunium(V) Hydroxide. *Radiochim Acta*, **58**(59), 61–66.

Itälä, A. and Muurinen, A. (2012). Cation Exchange in Montmorillonite. VTT Technical Research Centre of Finland.

Jenne, E.A. (1977). Trace element adsorption by sediments and soils: sites and processes. In Molybdenum in the Environment (2nd ed.). New York, NY; Marcel Dekker Inc.

Jensen, M. (2017). Canadian Geoscience Research and Development in Support of AMP: an Overview. Presentation, Nuclear Waste Management Organization.

Kitamura, A., Doi, R., and Yoshida, Y. (2014). Update of JAEA-TDB: Update of Thermodynamic Data for Palladium and Tin, Refinement of Thermodynamic Data for Protactinium, and Preparation of PHREEQC Database for Use of the Brønsted-Guggenheim-Scatchard Model. Technical report, Japan Atomic Energy Agency.

Macht, F., Eusterhues, K., Pronk, G.J., and Totsche, K.U. (2011). Specific surface area of clay minerals: Comparison between atomic force microscopy measurements and bulk-gas (N2) and -liquid (EGME) adsorption methods. *Applied Clay Science*, **53**(1), 20-26.

Marques Fernandes, M. *et al.* (2015). Predicting the uptake of Cs, Co, Ni, Eu, Th, and U on argillaceous rocks using sorption models for illite. *Applied Geochemistry*, **59**, 189-199.

Marsac, R., Banik, N.I., Lützenkirchen, J., Marquardt, C.M., Dardenne, K., Schild, D., Rothe, J., Diascorn, A., Kupcik, T., Schafer, T., and Geckeis, H. (2015). Neptunium redox speciation at the Illite surface. *Geochimica et Cosmochimica Acta*, **152**, 39-51.

McMurry, J. and Fay, R. (2003). *Chemistry* (4th ed.). Pearson.

Nagasaki, S., Riddoch, J., Saito, T.S., Goguen, J., Walker, A., and Yang T. (2017). Sorption behaviour of Np(IV) on illite, shale and MX-80 in high ionic strength solutions. *J Radioanal Nucl Chem.*

Nagasaki, S., Saito, T.S., and Yang T. (2015). Sorption behaviour of Np(V) on illite, shale and MX-80 in high ionic strength solutions. *J Radioanal Nucl Chem.,* **308**(1), 143-153.

Neck, V. and Kim, J.I. (2000). Solubility and hydrolysis of tetravalent actinides. *Radiochim. Acta,* **89,** 1-16.

Noronha, J. (2016). Deep Geological Repository Conceptual Design Report, Crystalline / Sedimentary Rock Environment. Technical report, Nuclear Waste Management Organization. Retrieved from: https://www.nwmo.ca/~/media/Site/Reports/2016/06/08/10/03/APM_REP_00440_0015_R001.ashx?la=en.

Nuclear Fuel Waste Act (2002, c. 23). Retrieved from the Justice Laws website: http://laws-lois.justice.gc.ca/PDF/N-27.7.pdf.

Nuclear Waste Management Organization (2016). What Is Used Nuclear Fuel? Retrieved from: https://www.nwmo.ca/~/media/Site/Files/PDFs/2016/11/10/12/38/EN_Backgrounder_UsedNuclearFuel_LowRes.ashx?la=en.

Nuclear Waste Management Organization (2017). Deep Geological Repository. Retrieved from: https://www.nwmo.ca/en/A-Safe-Approach/Facilities/Deep-Geological-Repository.

Parkhurst, D.L. and Appelo, C. A. J. (1999). User's Guide to PHREEQC (Version 2) (Equations on which the program is based). Technical report, U.S. Geological Survey.

Parkhurst, D.L. and Appelo, C. (2013). Description of Input and Examples for PHREEQC Version 3 - A Computer Program for Speciation, Batch-Reaction, One-Dimensional

Transport, and Inverse Geochemical Calculations. *U.S. Geological Survey Techniques and Methods*, book 6, ch. A43.

Parks, G.A. (1967). Aqueous surface chemistry of oxides and complex oxide minerals. *Advances in Chemistry*, **67**, 121-160.

Pitzer, K.S. (1991). Ion Interaction Approach: Theory and Data Correlation. *Activity Coefficients in Electrolyte Solutions* (2nd ed.). Boca Raton: CRC Press, 279-434.

Pivovarov, S. (2004). Physico-chemical modeling of heavy metals (Cd, Zn, Cu) in natural environments. *Encyclopedia of Surface and Colloid Science, 2004 Update Supplement*, **5**, 468-492.

Rai, D., Yui, M., and Kitamura, A. (2012). Thermodynamic Model for Amorphous Pd(OH)2 Solubility in the Aqueous Na+-K+-H+-OH-Cl- -ClO4 -H2O System at 25 C: A Critical Review. *Journal of Solution Chemistry*, **41**(11), 1965-1985.

Riddoch, J. and Nagasaki, S. (2016). Sorption of Palladium onto Bentonite, Illite and Shale Under High Ionic Strength Conditions. MASc. Thesis, McMaster University.

Robinson, R.A. and Stokes, R.H. (1968). Electrolyte Solutions. *Butterworths*, London.

Shannon, R.D. (1976). Revised effective ionic radii and systematic studies of interatomic distances in halides and chalcogenides. *Acta Crystallographica Section A,* **32**(5), 751-767.

Sipos, P. (2008). Application of the Specific Ion Interaction Theory (SIT) for the ionic products of aqueous electrolyte solutions of very high concentrations. *Journal of Molecular Liquids*, **143**, 13-16.

Sposito, G. (2008). *The Chemistry of Soils* (2nd ed.). New York, NY: Oxford University Press.

Stern, O. (1924). Zur theorie der electrolytischen doppelschict. *Zeitschrift für Elektrochemie und angewandte physikalische Chemie*, **30**, 508-516.

Stumm, W. and Morgan, J.J. (1996). *Aquatic Chemistry: Chemical Equilibria and Rates in Natural Waters* (3rd ed.). New York: John Wiley & Sons, Inc.

Tachi, Y., Shibutani, T., Sato, H., and Shibata, M. (1999). Sorption and Diffusion Behavior of Palladium in Bentonite, Granodiorite and Tuff. Technical report, Japan Nuclear Cycle Development Institute.

Tait, J., Gauld, I., and Wilkin, G. (1989). Derivation of Initial Radionuclide Inventories for the Safety Assessment of the Disposal of Used CANDU Fuel. Technical report, Atomic Energy of Canada Ltd.

THEREDA, "READY-TO-USE DATABASES," GRS, KIT-INE, HZDR-IRE, TU-BAF, PSI, [Online]. Available: https://www.thereda.de/. [Accessed August 2017].

Thermo Fisher Scientific (2014). Measuring pH of Concentrated Samples. Technical report, Thermo Fisher Scientific.

Thompson, A. and Goyne, K.W. (2012). Introduction to the Sorption of Chemical Constituents in Soils. *Nature Education Knowledge*, **4**(4):7.

Tinsley, I.J. (2004). *Chemical Concepts in Pollutant Behavior*. John Wiley & Sons, Inc.

Truesdell, A. and Jones, B.F. (1974). WATEQ, A Computer Program for Calculating Chemical Equilibria in Natural Waters. *U.S. Geological Survey Journal of Research*, **2**, 233-248.

Turner, D.R., Pabalan, R.T., and Bertetti, F.P. (1998). Neptunium(V) Sorption on Montmorillonite: an Experimental and Surface Complexation Modeling Study. *Clays and Clay Minerals*, **46**(3), 256-269.

Vilks, P. (2014). Sorption of Selected Radionuclides on Sedimentary Rocks in Saline Conditions – Updated Sorption Values. Technical report, Nuclear Waste Management Organization.

Vilks, P. (2016). Sorption of Selected Radionuclides on Sedimentary Rocks in Saline Conditions – Updated Sorption Values. Technical report, Nuclear Waste Management Organization.

Vilks, P. (2017). Sorption Experiments with Sedimentary Rocks under Saline Conditions. Technical report, Nuclear Waste Management Organization.

Villa-Alfageme, M., Hurtado, S., Castro, M.A., Mrabet, S.E., Orta, M.M., Pazos, M.C., and Alba, M.D. (2014). *Applied Clay Science* **101**(2014), 10-15.

Appendix A

Raw Sample Data

Sample data for the *I*-dependence experiments for the sorption of Pd(II) is shown in Table A.1 and the sample data for the pH-dependence experiments for the sorption of Pd(II) is shown in Table A.2 to Table A.6.

Table A.1: Sample data for *I*-dependence on Pd(II) sorption experiments.

Sample ID	Solid	I (M)	pH_M	E_h (mV)	K_d (m^3/kg)
SRP-IL-I5.0-1	Illite	5.0	5.76	210	0.24
SRP-IL-I5.0-2	Illite	5.0	5.67	191	0.34
SRP-IL-I5.0-3	Illite	5.0	5.49	205	0.43
SRP-IL-I6.0-1	Illite	6.0	5.57	226	0.15
SRP-IL-I6.0-2	Illite	6.0	5.62	231	0.23
SRP-IL-I6.0-3	Illite	6.0	5.59	232	0.31
SRP-MX-I5.0-1	Bentonite	5.0	6.14	218	0.26
SRP-MX-I5.0-2	Bentonite	5.0	6.26	205	0.37
SRP-MX-I5.0-3	Bentonite	5.0	6.26	207	0.47
SRP-MX-I6.0-1	Bentonite	6.0	6.02	216	0.24
SRP-MX-I6.0-2	Bentonite	6.0	6.10	216	0.29
SRP-MX-I6.0-3	Bentonite	6.0	6.12	219	0.34
SRP-SH-I5.0-1	Shale	5.0	5.86	215	0.55
SRP-SH-I5.0-2	Shale	5.0	6.03	216	0.65
SRP-SH-I5.0-3	Shale	5.0	5.96	218	0.74
SRP-SH-I6.0-1	Shale	6.0	5.65	225	0.38
SRP-SH-I6.0-2	Shale	6.0	5.83	223	0.55
SRP-SH-I6.0-3	Shale	6.0	5.93	224	0.72

Table A.2: Sample data for pH-dependence on Pd(II) sorption experiments.

Sample ID	Solid	I (M)	pH_M	E_h (mV)	K_d (m^3/kg)
SRP-IL-I0.01-PH3-1	Illite	0.01	2.93	475	0.41
SRP-IL-I0.01-PH3-2	Illite	0.01	2.98	490	0.43
SRP-IL-I0.01-PH3-3	Illite	0.01	2.96	489	0.51
SRP-IL-I0.01-PH4-1	Illite	0.01	3.96	444	0.70
SRP-IL-I0.01-PH4-2	Illite	0.01	3.93	439	0.74
SRP-IL-I0.01-PH4-3	Illite	0.01	3.98	429	0.76
SRP-IL-I0.01-PH5-1	Illite	0.01	5.09	386	7.59
SRP-IL-I0.01-PH5-2	Illite	0.01	5.13	375	8.13
SRP-IL-I0.01-PH5-3	Illite	0.01	5.03	373	8.82
SRP-IL-I0.01-PH6-1	Illite	0.01	6.08	390	2.05
SRP-IL-I0.01-PH6-2	Illite	0.01	6.05	338	6.21
SRP-IL-I0.1-PH3-1	Illite	0.1	2.92	488	<0.01
SRP-IL-I0.1-PH3-2	Illite	0.1	2.96	492	<0.01
SRP-IL-I0.1-PH3-2	Illite	0.1	2.96	492	<0.01
SRP-IL-I0.1-PH4-1	Illite	0.1	3.85	374	<0.01
SRP-IL-I0.1-PH4-2	Illite	0.1	3.83	393	<0.01
SRP-IL-I0.1-PH4-3	Illite	0.1	3.85	354	<0.01
SRP-IL-I1-PH3-1	Illite	1.0	2.37	477	0.05
SRP-IL-I1-PH3-2	Illite	1.0	2.46	494	0.09
SRP-IL-I1-PH3-3	Illite	1.0	2.37	494	0.11
SRP-IL-I1-PH4-1	Illite	1.0	3.47	397	<0.01
SRP-IL-I1-PH4-2	Illite	1.0	3.26	429	<0.01
SRP-IL-I1-PH4-3	Illite	1.0	3.27	432	<0.01
SRP-IL-I4-PH3-1	Illite	4.0	2.09	457	<0.01
SRP-IL-I4-PH3-2	Illite	4.0	1.99	458	<0.01
SRP-IL-I4-PH3-3	Illite	4.0	1.98	463	<0.01
SRP-IL-I4-PH4-1	Illite	4.0	3.26	426	<0.01

Table A.3: Sample data for pH-dependence on Pd(II) sorption experiments.

Sample ID	Solid	I (M)	pH_M	E_h (mV)	K_d (m^3/kg)
SRP-IL-I4-PH4-2	Illite	4.0	2.97	421	<0.01
SRP-IL-I4-PH4-3	Illite	4.0	2.93	445	<0.01
SRP-IL-I6-PH3-1	Illite	6.0	1.92	453	<0.01
SRP-IL-I6-PH3-2	Illite	6.0	1.93	460	<0.01
SRP-IL-I6-PH3-3	Illite	6.0	1.94	465	<0.01
SRP-IL-I6-PH4-1	Illite	6.0	2.94	425	<0.01
SRP-IL-I6-PH4-2	Illite	6.0	2.80	421	<0.01
SRP-IL-I6-PH4-3	Illite	6.0	2.82	422	<0.01
SRP-IL-I6-PH5-1	Illite	6.0	-	389	<0.01
SRP-IL-I6-PH5-2	Illite	6.0	-	407	<0.01
SRP-IL-I6-PH5-3	Illite	6.0	-	396	<0.01
SRP-IL-I6-PH6-1	Illite	6.0	-	369	<0.01
SRP-IL-I6-PH6-2	Illite	6.0	-	306	0.01
SRP-IL-I6-PH6-3	Illite	6.0	-	316	0.05
SRP-IL-I6-PH7-1	Illite	6.0	-	280	<0.01
SRP-IL-I6-PH7-2	Illite	6.0	-	283	0.02
SRP-IL-I6-PH7-3	Illite	6.0	-	275	0.06
SRP-IL-I6-PH8-1	Illite	6.0	-	238	0.05
SRP-IL-I6-PH8-2	Illite	6.0	-	236	0.08
SRP-IL-I6-PH8-3	Illite	6.0	-	235	0.10
SRP-IL-I6-PH9-1	Illite	6.0	-	213	0.06
SRP-IL-I6-PH9-2	Illite	6.0	-	192	0.08
SRP-IL-I6-PH9-3	Illite	6.0	-	195	0.11
SRP-MX-I0.01-PH3-1	Bentonite	0.01	2.86	363	0.46
SRP-MX-I0.01-PH3-2	Bentonite	0.01	2.93	379	0.57
SRP-MX-I0.01-PH3-3	Bentonite	0.01	2.91	364	0.62
SRP-MX-I0.01-PH4-1	Bentonite	0.01	3.86	310	0.57

Table A.4: Sample data for pH-dependence on Pd(II) sorption experiments.

Sample ID	Solid	I (M)	pH_M	E_h (mV)	K_d (m^3/kg)
SRP-MX-I0.01-PH4-2	Bentonite	0.01	3.95	306	0.66
SRP-MX-I0.01-PH4-3	Bentonite	0.01	4.02	296	1.07
SRP-MX-I0.01-PH5-1	Bentonite	0.01	4.81	293	12.45
SRP-MX-I0.01-PH5-2	Bentonite	0.01	5.08	236	15.29
SRP-MX-I0.01-PH5-3	Bentonite	0.01	5.07	239	24.20
SRP-MX-I0.01-PH6-1	Bentonite	0.01	5.78	232	2.09
SRP-MX-I0.01-PH6-2	Bentonite	0.01	6.00	234	2.09
SRP-MX-I0.01-PH6-3	Bentonite	0.01	5.87	236	3.61
SRP-MX-I0.1-PH3-1	Bentonite	0.1	2.89	376	0.56
SRP-MX-I0.1-PH3-2	Bentonite	0.1	2.97	373	0.79
SRP-MX-I0.1-PH3-3	Bentonite	0.1	2.91	374	0.89
SRP-MX-I0.1-PH4-1	Bentonite	0.1	3.92	332	1.13
SRP-MX-I0.1-PH4-2	Bentonite	0.1	3.95	329	2.02
SRP-MX-I0.1-PH4-3	Bentonite	0.1	3.80	343	2.41
SRP-MX-I1-PH3-1	Bentonite	1.0	2.45	401	0.03
SRP-MX-I1-PH3-2	Bentonite	1.0	2.33	398	0.38
SRP-MX-I1-PH3-3	Bentonite	1.0	2.30	397	0.05
SRP-MX-I1-PH4-1	Bentonite	1.0	3.37	377	0.36
SRP-MX-I1-PH4-2	Bentonite	1.0	3.33	369	0.56
SRP-MX-I1-PH4-3	Bentonite	1.0	3.31	380	0.96
SRP-MX-I4-PH3-1	Bentonite	4.0	2.17	391	<0.01
SRP-MX-I4-PH3-2	Bentonite	4.0	2.25	387	<0.01
SRP-MX-I4-PH3-3	Bentonite	4.0	2.17	382	<0.01
SRP-MX-I4-PH4-1	Bentonite	4.0	3.19	398	<0.01
SRP-MX-I4-PH4-2	Bentonite	4.0	3.12	403	<0.01
SRP-MX-I4-PH4-3	Bentonite	4.0	3.31	394	<0.01
SRP-MX-I6-PH3-1	Bentonite	6.0	2.11	393	<0.01

Table A.5: Sample data for pH-dependence on Pd(II) sorption experiments.

Sample ID	Solid	I (M)	pH_M	E_h (mV)	K_d (m^3/kg)
SRP-MX-I6-PH6-2	Bentonite	6.0	-	323	0.10
SRP-MX-I6-PH6-3	Bentonite	6.0	-	305	0.20
SRP-MX-I6-PH7-1	Bentonite	6.0	-	275	0.16
SRP-MX-I6-PH7-2	Bentonite	6.0	-	269	0.20
SRP-MX-I6-PH7-3	Bentonite	6.0	-	298	0.24
SRP-MX-I6-PH8-1	Bentonite	6.0	-	240	<0.01
SRP-MX-I6-PH8-2	Bentonite	6.0	-	252	0.11
SRP-MX-I6-PH8-3	Bentonite	6.0	-	233	0.25
SRP-MX-I6-PH9-1	Bentonite	6.0	-	220	0.10
SRP-MX-I6-PH9-2	Bentonite	6.0	-	207	0.14
SRP-MX-I6-PH9-3	Bentonite	6.0	-	193	0.18
SRP-SH-I6-PH5-1	Shale	6.0	-	329	0.29
SRP-SH-I6-PH5-2	Shale	6.0	-	324	0.31
SRP-SH-I6-PH5-3	Shale	6.0	-	327	0.32
SRP-SH-I6-PH6-1	Shale	6.0	-	285	0.32
SRP-SH-I6-PH6-2	Shale	6.0	-	285	0.66
SRP-SH-I6-PH6-3	Shale	6.0	-	292	1.01
SRP-SH-I6-PH7-1	Shale	6.0	-	274	0.13
SRP-SH-I6-PH7-2	Shale	6.0	-	286	0.16
SRP-SH-I6-PH7-3	Shale	6.0	-	264	0.19
SRP-SH-I6-PH8-1	Shale	6.0	-	237	0.09
SRP-SH-I6-PH8-2	Shale	6.0	-	234	0.25
SRP-SH-I6-PH8-3	Shale	6.0	-	247	0.40
SRP-SH-I6-PH9-1	Shale	6.0	-	235	0.29
SRP-SH-I6-PH9-2	Shale	6.0	-	212	0.44
SRP-SH-I6-PH9-3	Shale	6.0	-	202	0.59

Table A.6: Sample data for pH-dependence on Pd(II) sorption experiments.

Sample ID	Solid	I (M)	pH_M	E_h (mV)	K_d (m^3/kg)
SRP-MX-I6-PH3-2	Bentonite	6.0	2.16	390	<0.01
SRP-MX-I6-PH3-3	Bentonite	6.0	2.10	391	<0.01
SRP-MX-I6-PH4-1	Bentonite	6.0	3.06	400	<0.01
SRP-MX-I6-PH4-2	Bentonite	6.0	3.16	405	<0.01
SRP-MX-I6-PH4-3	Bentonite	6.0	3.43	382	<0.01
SRP-MX-I6-PH5-1	Bentonite	6.0	-	375	<0.01
SRP-MX-I6-PH5-2	Bentonite	6.0	-	382	<0.01
SRP-MX-I6-PH5-3	Bentonite	6.0	-	390	<0.01
SRP-MX-I6-PH6-1	Bentonite	6.0	-	347	0.01

Appendix B

Example PHREEQC Input File

```
DATABASE C:\Desktop\140331s0.tdb
TITLE Palladium Sorption onto Illite
```

The directory of the database containing the relevant thermodynamic data is defined so that the compiler knows which file to use. The title of the simulation is also named.

```
KNOBS
    -logfile                    true
    -iterations                 100
    -step_size                  100
    -tolerance                  1e-15
    -convergence_tolerance      1e-8
    -diagonal_scale             true
END
```

The "KNOBS" command allows the many parameters of the simulation to be set. When "logfile" is set to true, information about the simulation, such as the number of iterations needed for convergence, is automatically saved to a the log file called "phreeqc.log". The parameter "iterations" sets the maximum number of

iterations that will be used when solving algebraic equations. The parameter "step_size" limits the maximum amount that a species' concentration will change on each iteration of the solver. "tolerance" sets the upper limit for numbers that are treated as zero by the software. By setting it to 1e-15, any number less than 10^{-15} is automatically set to zero. "convergence_ tolerance" changes the point at which equations have been considered balanced. Since it is set to 1e-8, any chemical equations are considered balanced when the calculated number of moles is in agreement with the exact solution to within 10^{-8} times, or 10^{-6} percent of, the exact value. "diagonal_scale" changes the default scaling of the equations for the solver. By setting this to "true", any mole-balance equation with total concentrations of less than 10^{-10} M are automatically scaled by the inverse of the total concentration. END closes the KNOBS command.

```
SURFACE_MASTER_SPECIES
       Ill_s  Ill_sOH
       Ill_w       Ill_wOH
       Ill_wt     Ill_wtOH
```

"SURFACE_MASTER_SPECIES" defines the correspondence between the surface binding-site names and the surface master species. On line 15, the master species "Ill_sOH" is given the binding site name Ill_s. The '_s' and '_w' denote that the binding-sites are strong and weak respectively.

```
SURFACE_SPECIES
# Illite Surface Complexation Reactions
# Surface Sites - A-B
       Ill_sOH = Ill_sOH
              log_k  0.0
       Ill_sOH + H+ = Ill_sOH2+
              log_k  4.0
       Ill_sOH = Ill_sO- + H+
```

```
        log_k  -6.2
    Ill_wOH = Ill_wOH
        log_k 0.0
    Ill_wOH + H+ = Ill_wOH2+
        log_k 4.0
    Ill_wOH = Ill_wO- + H+
        log_k -6.2
    Ill_wtOH = Ill_wtOH
        log_k 0.0
    Ill_wtOH + H+ = Ill_wtOH2+
        log_k 8.5
    Ill_wtOH = Ill_wtO- + H+
        log_k -10.5

# Inner/Outer Sphere Complexes - Metal Binding
    Ill_sOH + Pd+2 = Ill_sOPd+ + H+
        log_k  6.4
    Ill_sOH + Pd+2 + H2O = Ill_sOPdOH + 2H+
        log_k  3.2
    Ill_sOH + Pd+2 + 2H2O = Ill_sOPd(OH)2- + 3H+
        log_k  -4.0

# Ternary Complexes (Type A) - Only One Ternary Surface Complexation
Reaction
    Ill_sOH + Pd+2 + Cl- = Ill_sOPdCl + H+
        log_k  5.00
    Ill_sOH + Pd+2 + 2Cl- = Ill_sOPdCl2- + H+
        log_k  8.42
    Ill_sOH + Pd+2 + 3Cl- = Ill_sOPdCl3-2 + H+
        log_k  10.93
    Ill_sOH + Pd+2 + 4Cl- = Ill_sOPdCl4-3 + H+
        log_k  13.05
    Ill_sOH + Pd+2 + 3Cl- + H2O = Ill_sOPdCl3OH-3 + 2H+
        log_k  3.77
```

"SURFACE_SPECIES" identifies the formation reactions for secondary species, along with their log_k values (k is the equilibrium constant of the reaction). All OH master species need to be defined using an identity reaction with a log_k of zero. Different types of reactions (inner/outer sphere formation, Ternary complexation, etc.) are grouped together for readability.

```
EXCHANGE_MASTER_SPECIES
X      X-
```

"EXCHANGE_MASTER_SPECIES" is used to define the name of an exchange site and an exchange species used as the master species in calculations. The name of the site X is set to correspond to the master species "X−".

```
EXCHANGE_SPECIES
       X- = X-
              log_k  0.0
       X- + Na+ = XNa
              log_k  0.0
       X- + H+ = XH
              log_k  0.0
       X- + K+ = XK
              log_k  1.11
       2X- + Ca+2 = X2Ca
              log_k  1.04
       2X- + Mg+2 = X2Mg
              log_k  1.04
       3X- + Al+3 = X3Al
              log_k  1.0
       2X- + Pd+2 = X2Pd+
              log_k  7.3
END
```

"EXCHANGE_SPECIES" is to "EXCHANGE_MASTER_SPECIES" what "SURFACE_SPECIES" is to "SURFACE_MASTER_SPECIES". It gives formation reactions from the master exchange species, and their log_k values. The END command closes the species defining portion of the code.

```
PHASES
        Fix_H+
        H+ = H+
        log_k 0.0
END
```

"PHASES" defines any gas components or minerals that can be used for speciation, along with the log_k value. In this case, Fix_H+ is the phase name, and it is defined with an identity reaction, with a log_k of zero.

```
SURFACE 1
        Ill_sOH 1.44e-6 70.0 1
        Ill_wOH 2.89e-5
        Ill_wtOH 2.89e-5
        -no_edl
END
```

"SURFACE" opens the surface definition command. The number is a numerical identifier in case there is more than one surface in the simulation. Each line begins by identifying the sites on the surface. The values next to the species identifier denote the surface site concentration, equilibrium phase, specific surface area of the surface, and the mass of surface being used respectively. "-no_edl" indicates that no electrostatic terms are used in the mass-action equations, and that no explicit calculation of the diffuse layer is performed.

```
SOLUTION 5 I = 0.01M
       temp   25
       units  mol/kgw
       density      1
       water  1 # kg
       redox  pe
       pH     6
       pe     -3.378
       Ca     0.001754
       Na     0.004737
       Cl     0.008246
       Pd     1E-07
```

"SOLUTION" defines the temperature and chemical composition of an initial solution. The number next to it identifies individual solutions when there are multiple. "temp" sets the temperature of the solution. "units" sets which units will be used for concentrations (in this case they are mol per kg of water). "density" fixes the mass density of the solution in kg/L. "water" indicates the mass of water present in the solution in kg. "redox" defines the couple used to calculate the pe. pH, pe, Ca, Na, Cl, and Pd all define the initial concentrations for the respective species.

```
EQUILIBRIUM_PHASES 1
       Fix_H+  -6.0 NaOH 10
```

"EQUILIBRIUM_PHASES" indicates the phase assemblage and composition. The first variable name identifies which phase previously defined through the "PHASE" input will be used. The number shows the saturation index for the phase. The next name defines an alternative phase that will be added or removed from the solution in order to attain the target saturation index. The last number is the maximum amount of the alternative phase that will be placed into the solution.

```
EXCHANGE 1
       X  0.00021
       -equilibrate with solution 1
       #-pitzer_exchange_gammas true
Save Exchange 1
```

"EXCHANGE" defines the amount of exchange species used in the solution. "-equilibrate with solution 1" identifies which solution is reacting with the exchange species.

```
SELECTED_OUTPUT
       file PdSCM_Ill_0.01
       reset false
```

"SELECTED_OUTPUT" names a file for the output from the "USER_PUNCH" function to be written to. When set to "true", "reset" resets all other identifiers from true to false, so that they will not be printed with the output file (default is true).

```
USER_PUNCH
       10 FOR i = 2.5 to 10 STEP 0.1
       20 a$ = EOL$ + "USE solution 5" + CHR$(59) + "USE surface 1" +
       CHR$(59) + "USE exchange 1" + EOL$
       30 a$ = a$ + "EQUILIBRIUM_PHASES 5" + EOL$
       40 a$ = a$ + " Fix_H+" + STR$(-i) + " NaOH 10.0" + EOL$
       50 a$ = a$ + "END" + EOL$
       60 PUNCH a$
       70 NEXT i
END
```

"USER_PUNCH" prints strings to the output file defined in selected output. By iterating through multiple values, the pH of the solution can be changed on subsequent

iterations. This is accomplished by increasing "Fix_H" during each iteration. The file will be read by the user, using the "INCLUDE" command.

```
SELECTED_OUTPUT
        -file OutPdSCM.out
        -reset true
        -simulation false
        -state false
        -solution true
        -distance false
        -time false
        -reaction false
        -temperature false
        -alkalinity false
        -charge false
        -percent_error false
        -water false
        -step false
        -molalities  Pd+2  Ill_sOH  Ill_sOH2+  Ill_sO-  Ill_sOPd+  Ill_sOPdOH
        Ill_sOPd(OH)2-  Ill_sOPdCl  Ill_sOPdCl2-  Ill_sOPdCl3-2  Ill_sOPdCl4-3
        Ill_sOPdCl3OH-3 X2Pd+
END
```

"SELECTED_OUTPUT" is once again called. When set to "true", "-reset" sets all outputs to be printed. However, certain parameters were set to "false" so that they will not be saved in the new output file. The "-molalities" command outputs the concentration of the species listed after it.

```
USER_PUNCH
        10
        USER_GRAPH 1 Palladium Sorption onto Illite (I = 0.01M)
                -headings mu kd
                -chart_title "Palladium Sorption onto Illite (I = 0.01M)"
```

```
            -axis_titles "pH" "Kd [m3/kg]"
         -start
          10 GRAPH_X -LA("H+")
          20 GRAPH_Y (SURF("Pd","Ill")/TOT("Pd"))
          -end
        INCLUDE$ PdSCM_Ill_0.01
END

USER_GRAPH 1
     -detach
END
```

"USER GRAPH" displays the data from the simulation in a graph. In this case, the graph is plotting the fractional concentration of Pd sorbed onto illite against the pH of the solution. The "-detach" command opens a new window that displays the graph when the computation and formatting are complete (Parkhurst, 2013).